UNIVERSITY OF CALIFORNIA, SAN DIEGO

Requirements for ER reorganization and proliferation by HMG-CoA Reductase

A dissertation submitted in partial satisfaction of the requirements for the degree
Doctor of Philosophy

in

Biology

by

Christine Marie Federovitch

Committee in charge:

Professor Randolph Y. Hampton, Chair
Professor Scott D. Emr
Professor Douglass Forbes
Professor Vivek Malhotra
Professor Maho Niwa
Professor Robert H. Tukey

2007

The Dissertation of Christine Marie Federovitch is approved, and it is acceptable in quality and form for publication on microfilm:

_____

_____

_____

_____

_____

_____

Chair

University of California, San Diego

2007

Dedication

This work is dedicated to my loving husband, Scott.
I never could have done this without you.

And to friends and family members
who have been so supportive of me on this journey.

Thank you.

If we knew what it was we were doing,
it wouldn’t be called research, would it?
Albert Einstein

Try and fail, but don’t fail to try.
Stephen Kaggwa

Success is going from failure to failure without a loss of enthusiasm.
Winston Churchill

Because I am a woman, I must make unusual efforts to succeed.
If I fail, no one will say, "She doesn't have what it takes."
They will say, "Women don't have what it takes."
Clare Boothe Luce

A great pleasure in life is doing what people say you cannot do.
Walter Bagehot

Love is the triumph of imagination over intelligence.
Henry Louis Mencken

Table of Contents

List of Figures

List of Tables

Acknowledgements

I would like to thank Randy Hampton for allowing me to work on such an interesting project for cultivating my leadership skills in the laboratory. The many undergraduate researchers that he assigned to work with me provided an invaluable experience and was, without a doubt, one of the most rewarding of my graduate career.

These undergraduate researchers, with whom I have had the privilege of training and working with side by side in the laboratory, have taught me a great deal about life and how to become an effective leader. The first was Emily Moyeda, who performed the initial fluorescent co-culture assays that Randy developed. I cannot thank Thomas Cunningham enough for all of his dedication and hard work both as an undergraduate researcher in the laboratory and as a Masters student. His tireless effort in conducting the UV screen for HPE genes was invaluable as was his infectiously positive attitude. Monica Rodriguez continued that screen during a summer with us. She identified the first HPE gene (back then, we called them PIE genes), *SPF1/COD1*, which was critical in providing any hope of continuing that line of inquiry. Shirine Benhenda's insatiable appetite for knowledge was very refreshing and I appreciate her efforts in trying to clone the still elusive *pie1-1* allele. Shuyi Zhao conducted the galactose lethality screen with remarkable persistence and positivity. I am

also indebted to Tuyet Lam, Kevin Mak, Matthew McGee, and Erin Quan all of whom have contributed to the exploration of the various facets of the ER.

The Hampton Lab is composed of a dynamic and diverse set of individuals, all of whom have contributed to my graduate experience. The early members of the Hampton Lab, Nathan Bays and Stephen Cronin were both wonderful resources and I thank them for their time. Omar Bazirgan and Alex Shearer are both excellent critical thinkers and were always eager to share their insights. Renee Garza and I joined the lab at the same time and have traveled this road together. I cannot thank her enough for her friendship, scholarship and strength throughout the years. Elizabeth Long infected the lab with a positive spirit and enthusiasm. I feel grateful for having the opportunity to work with, learn from, and become friends with Isabelle Flury. Brian Sato and Tai Davis both have wonderful senses of humor and I have enjoyed our many conversations. I have enjoyed working with Sarah Carroll and Jarrod Heck, the most recent graduate students in the group. I would particularly like to thank Sarah for keeping a constant supply of coffee during these past few weeks. The most recent lab member, Chandra Theesfeld, has also contributed a tremendous amount of energy into the laboratory during these past few months. Finally, I thank the media makers, diswashers and lab managers/orderers for handling those tasks and helping the lab run more smoothly.

I have had the opportunity to foster many wonderful collaborations with other laboratories and researchers. This dissertation would not have been possible without their contributions. My first collaborations were with Vic Vacquier and Raffi Aroian to utilize sea urchins and C. elegans, respectively, for my rotation project in the Hampton lab. Upon joining the lab, the collaborations have multiplied. Ying Jones of the UCSD NCMIR has been such a pleasure with whom to work. I learned so much about electron microscopy from her and would not have been able to obtain the extraordinary images shown in Chapters 2 and 3 without her. Jacques Corbeil's laboratory in the Biomedical Sciences Department at UCSD was pivotal in conducting our microarray experiments, particularly Roman Sasik. My relationship with the Niwa Lab in the Biology Department, here at UCSD has been tremendous over the years. I am grateful to Jenny DuRose, Aditi Chawla, Arvin Tam, Anna Babour, and particularly Alicia Bicknell for all of their time and energies in teaching me RNA techniques and for insightful scientific discussions. Amy Tong of the Boone lab, at the University of Toronto, generated the yeast haploid array described in Chapter 2, and scored the resulting array for synthetic lethal phenotypes. The NIH's Will Prinz conducted all of the phospholipid composition experiments in Chapter 3. Steve Briggs and Zhouxin Shen are our most recent collaborators, generating a proteomic profile of yeast with and without Hmg2p overexpression. I also thank Steve for sharing his

insights not only about my dissertation project, but also about the biotech industry.

Many other laboratories have been generous in both their contribution of reagents, equipment use, and expertise including the laboratories of Maurice Montal, Jim Kadonaga, Michael David, Scott Emr, Roger Tsien, Vivek Malhotra, Douglass Forbes, Lorraine Pillus, Gentry Patrick, Ben Glick, Guenther Daum, and Robin Wright. I also wish to thank Scott Emr, Douglass Forbes, Vivek Malhotra, Maho Niwa, and Robert Tukey for serving and participating actively on my dissertation committee. They have dually challenged me, and have been unwaveringly supportive during my growth as a scientist here at UCSD. In addition, I am grateful for the support of friendship throughout this endeavor, including Matthew Kinseth, Danielle Huffman, Susy McKay, Alicia Bicknell and many others.

Prior to my time at UCSD, I had many wonderful teachers who truly have inspired me. Among them are: Mr. Speck, who helped me identify myself as a problem-solver, Mr. Engle, Ms Tumey, and Mrs. Chase who brought science to life, Mr. Hoffbeck and Mr. Qualiano, for passing on an appreciation for strategy and literature, and Mr. Guiliano for not only teaching me writing as an art, but for helping me to find value in myself and the courage to not change for others. I am also indebted to Carol Condit, who mentored me in her

laboratory at the University of Nevada, Reno. I never would have thought to apply to graduate school if it wasn't for her.

There are a few other people whom I have not yet mentioned, and are some of the most important to my success. My husband Scott is my pillar and I would not have been able to do this without his enduring support, friendship, and love. Also, my parents taught me not to be afraid to try different things and not to let other people set my limits. They instilled a strong belief that I can do anything to which I put my mind. The final person I wish to acknowledge is my sister, Liz. She reminds me that I need balance in my life.

Chapter 1, in part, is a reprint of the material as it appears in Current Opinions in Cell Biology 2005. Federovitch, CM, Ron D, Hampton RY, Elsevier B.V., 2005. The dissertation author was one of the authors of this paper.

Chapter 2 will be submitted for publication. Ying Jones generated all of the electron micrograph images shown in this chapter. Amy Tong generated the yeast haploid array with *GAL1-10pr*-driven Hmg2p^{s}-GFP*. The dissertation author was the primary investigator and author of this work.

Chapter 3 will be submitted for publication. Will Prinz conducted the phospholipid composition assays, Alicia Bicknell produced the northern blots, and Ying Jones generated the electron micrographs in this chapter. The dissertation author was the primary investigator and author of this work.

Vita

2000 Bachelor of Science, University of Nevada, Reno

2007 Doctor of Philosophy, University of California, San Diego

Honors and Awards

2001-2004 Genetics Training Grant

2000-2002 Cellular, Molecular and Genetics Training Grant

2001 Honorable Mention, NSF Graduate Research Fellowship

Academic Service

2003-2005 Advisory Board Member, UCSD Registration Fee Committee

2002-2004 Graduate Student Representative, UCSD Biology Department

2000-2002 Committee Member, UCSD Biology Graduate Recruitment

Publications

Bicknell, A.A., Babour, A., **Federovitch, C.M.**, Niwa, M. A novel role in cytokinesis reveals a housekeeping function for the unfolded protein response. Journal of Cell Biology. 2007 Jun 18;177(6):1017-27. PMID: 17562790

Federovitch, C.M., Ron, D., Hampton, R.Y. The Dynamic ER: experimental approaches and current questions. Current Opinions in Cell Biology. 2005 Aug;17(4):409-14. PMID: 15975777

ABSTRACT OF THE DISSERTATION

Requirements for ER reorganization and proliferation
by HMG-CoA Reductase

by

Christine Marie Federovitch

Doctor of Philosophy in Biology

University of California, San Diego, 2007

Professor Randolph Y. Hampton, Chair

The largest and most dynamic endomembrane compartment in eukaryotic cells is the endoplasmic reticulum (ER). This organelle is the site of protein folding, lipid synthesis, and drug detoxification, among other vital cellular processes. The size and shape of the ER is continually adjusted to accommodate cellular need. This can be observed under a wide variety of circumstances, ranging from complex cellular

differentiation processes, to simple increases in the expression of single ER membrane proteins. Despite the amenability of this phenomenon to observation, the underlying mechanisms have largely eluded researchers. HMG-CoA reductase (HMGR) catalyzes the rate-limiting step in sterol biosynthesis and is used throughout this work as a model to study ER rearrangement and expansion. By utilizing the Hmg2p isozyme of *S. cerevisiae*, we have identified the features of this protein that are required to reorganize the ER into elaborate, highly structured membrane arrays. Using this information, we designed and executed a screen to identify genes required for Hmg2p-induced ER formation. Our analysis of the effects of Hmg2p on cellular membranes is extended to a biochemical analysis of the abundance and composition of total cellular phospholipids. In this way, we clearly delineate the difference between membrane reorganization and membrane proliferation. Furthermore, we demonstrate the requirement of a phospholipid biosynthetic enzyme, *PSD1*, for the Hmg2p-induced changes in ER structure as well as phospholipid abundance and composition. This is the first analysis to reveal a genetic connection between the ER structures generated by increased expression of Hmg2p, and phospholipid biosynthesis.

Chapter 1:

The dynamic ER

Randy Hampton, David Ron and I wrote a review of the literature regarding ER dynamics and proliferation in 2005. This chapter is, in large part, a reprint of that work. I have updated the information presented to incorporate recent findings that contribute to the understanding of this field.

ER dynamics

All eukaryotic cells have distinct membrane-bound organelles, each having its role to play in maintaining cell viability. It is critical that these organelles maintain proper size, shape and distribution throughout the life cycle of the cell, and that the organelle is able to adapt to changing cellular need. The largest endomembrane compartment in eukaryotic cells it the endoplasmic reticulum (ER).

The ER is an extremely plastic and dynamic organelle. Its size and shape can undergo drastic changes to meet changing demands for ER-related functions, or as a response to drugs or pathogens. Because of the ER's key functions in protein and lipid synthesis, this organelle is a hotbed of detailed molecular analysis.

There are many instances in biology when the size of the ER compartment changes drastically. Some of the most dramatic cases occur when cells differentiate into types that have high demands on the ER as a secretory apparatus [1], a lipid synthetic platform [2,3] or a calcium repository [4,5]. Other examples occur from outside influences that cause or promote the

expression of proteins that alter ER structure, such as hepatitis C virus [6], or treatment with drugs such as statins [7,8] or phenobarbital [9]. Despite the large number of cases where the ER undergoes dramatic changes, there is still little known about the molecular mechanisms that underlie these processes.

Perturbations that cause ER expansion range from increased expression of a single membrane protein to activation of coordinated developmental programs that drive cells down professional secretory lineages such as the plasma B cell. One challenge is to ascertain if common mechanisms are at play in these distinct ways of inducing changes in ER structure and size. Another is to integrate the findings from the extremely active study of signaling pathways that monitor and control ER status, such as the unfolded protein response (UPR) [10], into the various situations that cause changes in ER size and function.

I will focus on two extremes in the range of dynamic ER changes; the acquisition of professional secretory status, and the proliferation of the smooth ER. These examples demarcate the wide territory that covers ER dynamics, which needs to be covered in a unified model of ER plasticity.

Plasma B cells and other professional secretory cells

When B lymphocytes differentiate into plasma B cells, they must undergo changes that allow the synthesis and secretion of prodigious amounts of immunoglobin, in the range of 200-1000 IgM multimers per second, or

roughly their own weight in protein per day! Striking electron micrographs (Figure 1.1a) show that the resulting B cell has a massive, rough ER that appears to fill most of the cytoplasm. This transition can be recapitulated in culture by treating the B cell lymphoma line I.29$^{\mu+}$ with LPS, causing their terminal differentiation into immunoglobin-secreting plasma cells [11]. A number of "professional secretory cells" exist which undergo different routes to their final state however, all seem to have expanded ERs for high capacity secretion of their appropriate proteins. The transition to the plasma B cell is marked by the expansion of the entire ER compartment, including membrane and the lumenal and membrane proteins that dictate the functions and identity of this compartment. The resulting ER is thus the classic "rough ER" that is capable of guiding new protein translocation, folding, assembly and packaging into vesicles, as would be expected. Questions include: What developmental program brings on this onslaught of ER components? How is ER expansion coordinated, to what extent are the processes that cause smooth ER expansions (see below) involved, and how do known or novel signaling pathways control or govern this dramatic functional change?

Crystalloids and other expansions of the smooth ER

There are many examples of cells that undergo similarly dramatic expansions of the ER as they become proficient to synthesize lipids or detoxify drugs, both functions that occur at the ER surface. Cells of the adrenal cortex or

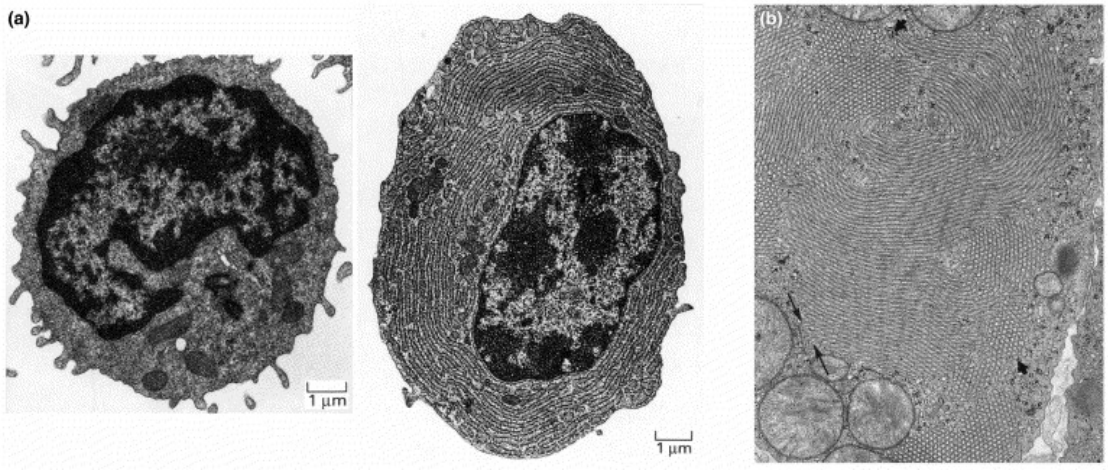

Figure 1.1 Examples of highly proliferated ER.

(a) Massively expanded rough ER in a plasma B-cell (right), compared to an undifferentiated cell (left). Reproduced with permission from [39].
(b) Crystalloid smooth ER in embryonic adrenal cells that produce large amounts of sterols. Courtesy of the authors of [3].

Leydig cells of the testes that synthesize large amounts of sterols have dramatic proliferations of the ER known as crystalloid ER, due to the ordered appearance of membranes [2,3] (Figure 1.1b). Another classic example of smooth ER proliferation is observed in the liver cells of animals treated with phenobarbital [9]. Exposures of as little as a few days result in hepatocytes with impressive increases in their smooth ER, where the integral membrane, drug-detoxifying cytochrome P450 (CYP450) enzymes reside.

Unlike the case of plasma B-cell formation, expansion of the smooth ER can be caused by sufficiently high expression of single proteins, and in all likelihood, the natural cases are due in large part to the high level expression of such a proliferant in those circumstances. For example, cultured cells expressing high levels of HMG-CoA reductase (HMGR), the ER-resident rate-limiting enzyme of sterol synthesis, produce crystalloid ER that are identical in appearance to the proliferations of the sterol-producing Leydig and adrenal cortex cells discussed above [12]. Importantly, these effects of HMGR are not due to increased sterol synthesis caused by the enzyme. In both mammals and yeast cells, the same ER proliferation effects are caused by versions of HGMR that do not possess catalytic activity. Rather, it is purely an effect of increased HMGR protein levels. Similarly, forced expression of CYP450 by molecular biological means will cause proliferation of the smooth ER like that caused by CYP450-inducing drugs. This ER response is broadly conserved, is also

observed in both budding and fission yeast [13,14], and probably reflects an ancient response to increased demand for membranes imposed by integral membrane proteins such as HMGR and CYP450. In fact, examples of membrane proteins inducing the proliferation of bacterial inner membranes have also been noted [15,16], implying that this "capacity control" response may precede the split between prokaryotes and eukaryotes. Important questions remain: What is the signal that various structurally distinct membrane proteins send to trigger ER proliferation? What are the molecular events that underlie the expansion of the ER caused by single-protein proliferants? Are there known or novel ER signaling pathways that play a role in smooth ER proliferation? Does this ancient response play a role in the more elaborate expansion of the ER seen in secretory cells?

The role of the UPR in ER proliferation

The unfolded protein response (UPR) is a conserved signaling pathway that measures unfolded protein levels in the ER and adjusts the production of ER chaperones and degradation factors, via transcription, to allow maintenance of acceptably low levels of misfolded proteins in the lumen [10,17]. The range of genes that are controlled by the UPR includes several enzymes involved in phospholipid synthesis.

One widely-held opinion in the field is that the signaling cascade of the UPR stimulates ER proliferation, although there is very little direct evidence of

this. A recent paper by Bernales and colleagues showed that the ER structure is dramatically altered when the UPR is stimulated [18]. By using optical means of quantitating membranes, a 5-fold or greater expansion of the ER is reported under UPR-induced conditions compared to cells that are not engaging the UPR.

This analysis is a prime example of how the field of membrane proliferation/ER organization is dominated by optical analyses, rather than biochemical techniques. It is impossible to determine if the assembly of membranes observed is from pre-existing membranes recruited from other areas of the cell or if it is a representation of an actual increase in phospholipids that compose the observed membrane arrays. Without a biochemical evaluation of these systems, it remains debatable whether or not true membrane proliferation is occurring.

UPR in formation of a professional secretory cell

Testing the role of the UPR in the formation of specialized cells, such as the B cell, is complex since the resulting increase in secretory protein production would be expected to induce the unfolded protein response, making it hard to parse out cause and effect. Which comes first, UPR or expanded ER? So far, the amassed evidence does not provide a simple answer. Support for a role of UPR in ER expansion comes from several observations. The XPB1 gene, which is induced and spliced into an active form as part of the

mammalian UPR, is required for successful differentiation to a plasma cell [19]. Similarly, mimicking the UPR by simply driving the expression of the spliced form of XBP1 causes increased phosphatidylcholine production and the appearance of intracellular membranes in mammalian cells [20]. A time-series proteomic analysis of the LPS-induced transition of B cell lymphoma I.29$^{\mu+}$ into plasma cells indicates that the UPR may play a late role in this process [11]. When this line goes down the plasma cell pathway, a variety of ER components are strongly induced significantly before the upregulation of UPR occurs. This implies that UPR-independent early events conspire to expand the ER. However, it is important to remember that the UPR in mammals has three distinct branches, numerous effectors and the possibility of elaborate dynamics [21]. When sufficient tools are available, it will be informative to overdrive all three mammalian UPR branches simultaneously by molecular biological means to directly examine the effect on the size and shape of the ER compartment.

UPR in smooth ER proliferation

The involvement of UPR in the simpler case of smooth ER expansion caused by single proliferant proteins is also not completely resolved. However, one thing is clear: there are circumstances when smooth ER proliferation does not require the UPR. Proliferation of the yeast ER by overexpression of HMGR isozymes does not stimulate nor require the UPR pathway [22]. Conversely, it has been reported that high levels of expression of CYP450 does cause

induction of the UPR, in both yeast and mammals [23,24]. I have directly examined whether the UPR is stimulated in response to CYP450 overexpression by assaying for activation of *HAC1* (the yeast XBP1 homolog), as well as upregulation of UPR target genes via the UPRE (transcriptional elements specific to UPR activation) and was not able to detect any UPR activation (Figure 3.4). Hopefully this direct analysis of the induction of the UPR by CYP450 will correct this misinterpretation of previous results [23]. However, both my work and previously published reports agree that, regardless of whether or not CYP450 induces the UPR, the UPR is absolutely not required for formation of CYP450-induced structures or phospholipid increases in yeast. Thus, it is clear that, in yeast, there are UPR-independent pathways involved in the response to single-protein proliferants. Whether these operate in mammalian smooth ER proliferation, or in the synthesis of new ER in secretory cells is still unclear.

Other pathways involved in ER proliferation

Although the above results are complex, the case can be made that there are undiscovered pathways that participate in ER expansion. A separate ER-localized signaling system has been described and termed the "ER overload response" or EOR. It was discovered as a response to high-level expression of viral membrane proteins that often accompanies infection [25]. When the burden of certain ER membrane protein expression is sufficiently high, the

broad-action transcription factor NF-κB is activated. In the expression profiling study mentioned above, expression of CYP450 at ER-inducing levels in mammalian cells caused induction of genes characteristic of both UPR and EOR, lending some credence to the idea that EOR may be involved in some types of ER proliferation [24]. The role of EOR, or the need for NF-κB in the more complex case of ER expansion during secretogenesis has not yet been studied. The ability of membrane proteins to trigger a signaling cascade is compelling for model building, however it is important to remember that some types of membrane proliferation are conserved far more broadly than the NF-κB pathway.

More open-ended genetic and genomic analyses have not revealed a concrete pathway for ER proliferation, but the number of attempts has not been exhaustive. A traditional genetic screen by Koning and colleagues for mutants deficient in formation of stacked ER called “karmellae” by the yeast HMGR isozyme Hmg1p identified a number of genes required for trafficking to vacuole (the yeast lysosome), but surprisingly no ER-resident factors [26]. Whether this reflects a mechanistic interplay between ER and vacuole, or an indirect physiological effect of vacuolar deficiency on ER proliferation has not been determined. The same group performed a search for genes required for cell fitness during expression of proliferation-inducing levels of Hmg1p. Using

null-gene bar coding and microarray analysis, they identified the ER-bound ubiquitin conjugating enzyme Ubc7p as one such factor [27]. This is interesting in that degradation of ER proteins is strongly dependent on this ubiquitin E2 in at least two ER degradation pathways, but how this connects to ER expansion is not clear. It was shown in a follow-up study that although karmellae formation is altered in the *ubc7* null strain, the increased activity of HMGR was found to be necessary to observe the growth defect [28].

Proliferation or rearrangement: lipid status in ER expansion

The many images of ER proliferation in the literature are quite striking (e.g. Figure 1.1). In both the acquisition of secretory capacity and the simpler proliferation of smooth ER, it would appear that more lipids have been synthesized or otherwise amassed as part of this process. But there has been little experimental attention directed towards this idea. Early studies of *in vivo* proliferation of ER in liver indicated that phospholipid synthesis does increase in a manner consistent with increased lipid mass during the formation of membrane structures [29,30]. Similarly, in yeast, bulk phospholipids increase upon expressing ER-proliferating CYP450 by ~ 1.3 fold, without an apparent change in lipid composition [23] Also, as mentioned above, forced expression of the UPR-induced XBP1 in mammalian cells increases the rate of phosphatidylcholine synthesis [20].

Increased synthesis (or decreased degradation) of phospholipids could occur by a variety of mechanisms. It may be that changes in enzyme expression causes an alteration in lipid levels. However, the complete list of genes induced by ER-proliferating levels of CYP450 in mammalian cells does not include rate-limiting enzymes of phospholipid metabolism [24]. Of course, this does not include post-transcriptional mechanisms of enzyme induction. Alternatively, lipid-synthetic enzymes might be activated allosterically in response to membrane protein overexpression or by increased secretory cargo synthesis. Since many of the key enzymes of lipid synthesis are localized to the ER membrane, they would be correctly situated to sense and respond to an impending protein burden. Such a mechanism could either be directly affected by increased flux of proteins into the ER, or harnessed by the regulated production of a "trigger protein" that activates lipid synthesis as part of a signaling pathway such as is used in differentiation of a professional secretory cell. The latter model would explain the role of XBP1 in upregulating enzymes involved in phospholipid biosynthesis. Whatever the mechanism of ER proliferation, it will be important to actually measure the normalized amounts and types of lipids in the various examples of cells with proliferated ER, as has been done in yeast with CYP450 [23], to ascertain if and how lipid quantities are being altered by these fairly simple perturbations. These sorts of analyses

would also allow more detailed comparison of the various descriptive cases of ER proliferation at a more molecular level.

Determinants of ER proliferation

What are the features of single proteins that cause ER proliferation? Perusal of the literature reveals a bewildering array of different features. Usually proliferants are membrane proteins, but certainly not all membrane proteins trigger expansion of the ER. A variety of ER-destined proteins might cause proliferation, if it is a general response to increased membrane occupancy. However, it appears that cytosolic portions of proteins can in some cases be critical as well. The formation of "OSER" (organized stacks of ER) in mammalian cells depends on interactions between cytosolic fusion partners on the membrane-anchored protein [31]. Similarly, in yeast, Hmg1p-induced karmellae also require a multimerizing activity imparted by the C-terminal cytosolic domain of the Hmg1p molecule [32]. It is unclear how or even if multimerization triggers the biochemical changes that lead to increases in ER lipids in these special cases. The multimerization of cytosolic domains anchored to membrane proteins contribute to the rearrangement of the ER, even if these interactions do not confer ER expansions. From the diverse array of proteins that can alter ER structure, it seems likely that common biophysical features of these proteins may determine the capacity to actually increase membranes and even alter phospholipid composition. What these features are

and whether they are harnessed in the more elaborate expansion of the ER observed in secretory lineages is remains elusive.

Reversal of ER proliferation

Very little is known about the turnover or destruction of the proliferated ER. What happens when a signal for increased ER proliferation is eliminated, or when the serum level of a proliferant drug drops? One might imagine that organelle expansion is a permanent cellular state. However, early experiments indicate that the proliferated ER is a dynamic entity that can be disassembled. The mammalian cell line UT-1 overexpresses HMGR to such an extent that the smooth ER is highly proliferated, creating a crystalloid ER almost identical to the natural ones observed in sterol synthesizing cells (e.g. Figure 1.1b). When these cells are treated with sterols, HMGR synthesis drastically decreases concomitantly with in increase in its degradation, leading to a rapid decline in HMGR levels [12,33]. Remarkably, this is associated with an almost simultaneous disassembly of the proliferated ER membranes, indicating that the proliferant provides a continuous signal needed to maintain the expanded ER.

What happens to the proliferated ER? There are hints that autophagy, by which intracellular contents and whole organelles are engulfed and delivered to the lysosome, may provide a route for its destruction. Early studies on the reversal of phenobarbital-induced smooth ER in rat livers showed a drop in smooth ER levels and an increase in autophagic bodies when the drug was

withdrawn [34]. Hamasaki and colleagues have demonstrated that the yeast ER can be degraded by the autophagic pathway [35], indicating this may be a broadly conserved pathway for turnover of the expanded ER. Recent studies in yeast by Bernales and colleagues reported that autophagy counterbalances the ER expansion caused by the UPR, but did not provide a direct measurement of this effect [18]. Thus, it will be interesting to directly examine the role of autophagy in the dynamics of proliferated ER.

The more complex case of secretory cells undergoing downsizing of the ER also has a precedent for a similar mechanism. Many studies have described "crinophagy" in which secretory vesicles and rough ER components are delivered to the lysosome in secretory cells [36,37], and that this process may be used to adjust the size of the ER in less active secretory cells [38]. With the growing knowledge of molecules that mediate the autophagic processes, it will be important to evaluate crinophagy for overlap with the known autophagic pathways conserved between yeast and man.

Redefining proliferations

Until now, the term proliferation has been widely used throughout the field of ER dynamics and, with the exception of OSER, has been applied to any instances where membrane reorganization is observed. This reflects the bias for optical methods in studying these structures. The liberal use of the word "proliferation" in this particular document has been maintained both to conform

to and demonstrate the previous standards. If proliferation means to either grow or multiply by rapidly producing new parts, or to increase or spread, then a requirement should be that demonstration of actual increases be shown. By not examining whether or not proliferation is occurring, and calling the observations such, it provides a false sense of knowledge, which is only speculation. Therefore, to promote a better understanding, and accurate discussion of the phenomena observed, from this point onward, I will refrain from using the term proliferation as a general description of membrane structures unless direct evidence is shown to indicate that there is truly an increase in cellular phospholipids.

Hmg2p as a model for ER dynamics

In this dissertation, I have addressed some of the fundamental questions that have been raised in this introduction. I have selected the model system, *Saccharomyces cerevisiae* to study the effects of the Hmg2p isozyme of HMGR. To this end, I have learned what features of Hmg2p are required to generate its characteristic membrane structures. Based on this analysis, I was able to conduct a genetic screen that identified the first Hmg2p Proliferated ER, or HPE genes. These genes are of particular interest as they include the first known ER resident and phospholipid biosynthetic genes to be involved in ER organization by HMGR. These findings are discussed in Chapter 2.

In Chapter 3, I specifically address the issue of membrane proliferation vs. reorganization. By directly measuring phospholipids per cell, I have demonstrated that not all highly organized arrays of membranes are representative of membrane expansions. This analysis is extended to include effects on phospholipid composition that occur when Hmg2p levels are increased in cells. Lastly, I identify the first role for a phospholipid biosynthetic gene in the role of Hmg2p membrane proliferation.

Acknowledgements:

Chapter 1, in part, is a reprint of the material as it appears in Current Opinions in Cell Biology: Federovitch, CM, Ron D, Hampton RY, Elsevier B.V., 2005. The dissertation author was one of the authors of this paper.

References:

1. Wiest DL, Burkhardt JK, Hester S, Hortsch M, Meyer DI, Argon Y: **Membrane biogenesis during B cell differentiation: most endoplasmic reticulum proteins are expressed coordinately**. *J Cell Biol* 1990, **110**:1501-1511.

2. Sisson JK, Fahrenbach WH: **Fine structure of steroidogenic cells of a primate cutaneous organ**. *Am J Anat* 1967, **121**:337-367.

3. Black VH: **The development of smooth-surfaced endoplasmic reticulum in adrenal cortical cells of fetal guinea pigs**. *Am J Anat* 1972, **135**:381-417.

4. Martone ME, Zhang Y, Simpliciano VM, Carragher BO, Ellisman MH: **Three-dimensional visualization of the smooth endoplasmic reticulum in Purkinje cell dendrites**. *J Neurosci* 1993, **13**:4636-4646.

5. Sorrentino V: **Molecular** determinants **of the structural and functional organization of the sarcoplasmic reticulum**. *Biochim Biophys Acta* 2004, **1742**:113-118.

6. Greive SJ, Webb RI, Mackenzie JM, Gowans EJ: **Expression of the hepatitis C virus structural proteins in mammalian cells induces morphology similar to that in natural infection**. *J Viral Hepat* 2002, **9**:9-17.

7. Singer, II, Scott S, Kazazis DM, Huff JW: **Lovastatin, an inhibitor of cholesterol synthesis, induces hydroxymethylglutaryl-coenzyme A reductase directly on membranes of expanded smooth endoplasmic reticulum in rat hepatocytes**. *Proc Natl Acad Sci U S A* 1988, **85**:5264-5268.

8. Anderson RG, Orci L, Brown MS, Garcia-Segura LM, Goldstein JL: **Ultrastructural analysis of crystalloid endoplasmic reticulum in UT-1 cells and its disappearance in response to cholesterol**. *J Cell Sci* 1983, **63**:1-20.

9. Feldman D, Swarm RL, Becker J: **Ultrastructural study of rat liver and liver neoplasms after long-term treatment with phenobarbital**. *Cancer Res* 1981, **41**:2151-2162.

10. Zhang K, Kaufman RJ: **Signaling the unfolded protein response from the endoplasmic reticulum**. *J Biol Chem* 2004, **279**:25935-25938.

11. van Anken E, Romijn EP, Maggioni C, Mezghrani A, Sitia R, Braakman I, Heck AJ: **Sequential waves of functionally related proteins are expressed when B cells prepare for antibody secretion**. *Immunity* 2003, **18**:243-253.

12. Chin DJ, Luskey KL, Anderson RG, Faust JR, Goldstein JL, Brown MS: **Appearance of crystalloid endoplasmic reticulum in compactin-resistant Chinese hamster cells with a 500-fold increase in 3-hydroxy-3-methylglutaryl-coenzyme A reductase**. *Proceedings of the National Academy of Sciences of the United States of America* 1982, **79**:1185-1189.

13. Lum PY, Wright R: **Degradation of HMG-CoA reductase-induced membranes in the fission yeast, Schizosaccharomyces pombe**. *Journal of Cell Biology* 1995, **131**:81-94.

14. Koning AJ, Roberts CJ, Wright RL: **Different subcellular localization of Saccharomyces cerevisiae HMG-CoA reductase isozymes at elevated levels corresponds to distinct endoplasmic reticulum membrane proliferations**. *Molecular Biology of the Cell* 1996, **7**:769-789.

15. Hurek T, Van Montagu M, Kellenberger E, Reinhold-Hurek B: **Induction of complex intracytoplasmic membranes related to nitrogen fixation in Azoarcus sp. BH72**. *Mol Microbiol* 1995, **18**:225-236.

16. Weiner JH, Lemire BD, Elmes ML, Bradley RD, Scraba DG: **Overproduction of fumarate reductase in Escherichia coli induces a novel intracellular lipid-protein organelle**. *J Bacteriol* 1984, **158**:590-596.

17. Patil C, Walter P: **Intracellular signaling from the endoplasmic reticulum to the nucleus: the unfolded protein response in yeast and mammals**. *Curr Opin Cell Biol* 2001, **13**:349-355.

18. Bernales S, McDonald KL, Walter P: **Autophagy counterbalances endoplasmic reticulum expansion during the unfolded protein response**. *PLoS Biol* 2006, **4**:e423.

19. Reimold AM, Iwakoshi NN, Manis J, Vallabhajosyula P, Szomolanyi-Tsuda E, Gravallese EM, Friend D, Grusby MJ, Alt F, Glimcher LH: **Plasma cell differentiation requires the transcription factor XBP-1**. *Nature* 2001, **412**:300-307.

20. Sriburi R, Jackowski S, Mori K, Brewer JW: **XBP1: a link between the unfolded protein response, lipid biosynthesis, and biogenesis of the endoplasmic reticulum**. *J Cell Biol* 2004, **167**:35-41.

21. DuRose JB, Tam AB, Niwa M: **Intrinsic capacities of molecular sensors of the unfolded protein response to sense alternate forms of endoplasmic reticulum stress**. *Mol Biol Cell* 2006, **17**:3095-3107.

22. Larson LL, Parrish ML, Koning AJ, Wright RL: **Proliferation of the endoplasmic reticulum occurs normally in cells that lack a functional unfolded protein response**. *Yeast* 2002, **19**:373-392.

23. Menzel R, Vogel F, Kargel E, Schunck WH: **Inducible membranes in yeast: relation to the unfolded-protein-response pathway**. *Yeast* 1997, **13**:1211-1229.

24. Szczesna-Skorupa E, Chen CD, Liu H, Kemper B: **Gene expression changes associated with the endoplasmic reticulum stress response induced by microsomal cytochrome p450 overproduction**. *J Biol Chem* 2004, **279**:13953-13961.

25. Pahl HL, Baeuerle PA: **The ER-overload response: activation of NF-kappa B**. *Trends Biochem Sci* 1997, **22**:63-67.

26. Koning AJ, Larson LL, Cadera EJ, Parrish ML, Wright RL: **Mutations That Affect Vacuole Biogenesis Inhibit Proliferation of the Endoplasmic Reticulum in Saccharomyces cerevisiae**. *Genetics* 2002, **160**:1335-1352.

27. Wright R, Parrish ML, Cadera E, Larson L, Matson CK, Garrett-Engele P, Armour C, Lum PY, Shoemaker DD: **Parallel analysis of tagged deletion mutants efficiently identifies genes involved in endoplasmic reticulum biogenesis**. *Yeast* 2003, **20**:881-892.

28. Loertscher J, Larson LL, Matson CK, Parrish ML, Felthauser A, Sturm A, Tachibana C, Bard M, Wright R: **Endoplasmic reticulum-associated degradation is required for cold adaptation and regulation of sterol**

biosynthesis in the yeast Saccharomyces cerevisiae. *Eukaryot Cell* 2006, **5**:712-722.

29. Staubli W, Hess R, Weibel ER: **Correlated morphometric and biochemical studies on the liver cell. II. Effects of phenobarbital on rat hepatocytes**. *J Cell Biol* 1969, **42**:92-112.

30. Young DL, Powell G, McMillan WO: **Phenobarbital-induced alterations in phosphatidylcholine and triglyceride synthesis in hepatic endoplasmic reticulum**. *J Lipid Res* 1971, **12**:1-8.

31. Snapp EL, Hegde RS, Francolini M, Lombardo F, Colombo S, Pedrazzini E, Borgese N, Lippincott-Schwartz J: **Formation of stacked ER cisternae by low affinity protein interactions**. *J Cell Biol* 2003, **163**:257-269.

32. Profant DA, Roberts CJ, Koning AJ, Wright RL: **The role of the 3-hydroxy 3-methylglutaryl coenzyme A reductase cytosolic domain in karmellae biogenesis**. *Molecular Biology of the Cell* 1999, **10**:3409-3423.

33. Orci L, Brown MS, Goldstein JL, Garcia-Segura LM, Anderson RG: **Increase in membrane cholesterol: a possible trigger for degradation of HMG CoA reductase and crystalloid endoplasmic reticulum in UT-1 cells**. *Cell* 1984, **36**:835-845.

34. Feldman D, Swarm RL, Becker J: **Elimination of excess smooth endoplasmic reticulum after phenobarbital administration**. *J Histochem Cytochem* 1980, **28**:997-1006.

35. Hamasaki M, Noda T, Baba M, Ohsumi Y: **Starvation triggers the delivery of the endoplasmic reticulum to the vacuole via autophagy in yeast**. *Traffic* 2005, **6**:56-65.

36. Lenk SE, Fisher DL, Dunn WA, Jr.: **Regulation of protein secretion by crinophagy in perfused rat liver**. *Eur J Cell Biol* 1991, **56**:201-209.

37. Dunn WA, Jr.: **Autophagy and related mechanisms of lysosome-mediated protein degradation**. *Trends Cell Biol* 1994, **4**:139-143.

38. Bernabe A, Gomez MA, Seva J, Serrano J, Sanchez J, Navarro JA: **Light and ultrastructural immunocytochemical study of prolactin cells in**

ovine adenohypophysis. Influence of lactation and weaning. *Cells Tissues Organs* 2001, **168**:264-271.

39. D. Zucker-Franklin: **Atlas of Blood Cells: Function and Pathology** (2nd edition), Lea & Febiger, Milan, Italy (1998).

Chapter 2:

Reorganizing the ER with Hmg2p

Abstract:

The endoplasmic reticulum is the site of protein folding, drug detoxification and lipid biosynthesis. This organelle is highly plastic, and increased expression of single ER-resident membrane proteins, such as HmgCoA reductase (HMGR), can induce a dramatic restructuring of ER membranes into highly organized arrays. By studying Hmg2p, one of the two HMGR isozymes in *S. cerevisiae*, we have determined the features of this protein required to generate these ER structures. Like Hmg1p, Hmg2p required a folded cytoplasmic domain to reorganize ER membranes. Although the multimerization domain of the Hmg2p cytoplasmic domain was not required to make Hmg2p-induced structures, loss of the small, helical N-domain significantly decreases the number of cells in which ER structures are observed. We also clearly demonstrated that the characteristic features of the structures generated by Hmg1p and Hmg2p were determined by the transmembrane region of the proteins. In the case of Hmg2p, we discovered that proper topology of the transmembrane domain is sufficient to maintain discrete localization of Hmg2p and Kar2p, even in the absence of Hmg2p-induced structures.

Based on our understanding of the requirements for Hmg2p-induced structure formation, we engineered a screen to identify genes required for this

process. The genes identified encode both ER resident proteins and proteins involved in phospholipid biosynthesis among others: none of which have previously been implicated in HMGR structure formation. Furthermore, the VPS genes required for Hmg1p-induced ER structures were not recovered from this screen.

Introduction:

The endoplasmic reticulum (ER) is extremely plastic, and boasts the largest endomembrane compartment in most cell types. Protein folding, drug detoxification, phospholipid and sterol biosynthesis are a few of the many processes that occur within the ER or at its surface. As such, the ER must have the capacity to adapt to changing cellular need. For example, when lymphocytes differentiate into antibody producing B cells, the volume of the ER increases by greater than 4-fold [1]. In addition to this and other complex cellular differentiation cascades, elevation of single ER resident proteins such as HMG-CoA reductase (HMGR) or cytochrome P450 (CYP450) can cause profound alterations in ER structure that are conserved from yeast to mammalian cells [2-5]. Despite many studies of ER expansion and reorganization, the molecular mechanisms that underlie these structural changes have remained elusive (for review see [6]). We focused our attention on the single-protein trigger of ER alteration, HMGR, to discern the underlying processes.

HMGR catalyzes the conversion of HMG-CoA to mevalonate, the rate-limiting step in sterol biosynthesis. This protein is composed of three distinct domains: an N-terminal transmembrane region, a linker, and the highly conserved C-terminal domain. The large transmembrane domain spans the ER

membrane eight times and is connected to the cytoplasmic domain via the flexible linker. The cytosolic-facing C-terminal domain is composed of two distinct subregions: the small helical N-domain and the tightly folded multimerization domain, which contains the essential catalytic activity [7].

Many scientists have observed and reported that elevation of HMGR causes a striking structural reorganization of the ER, which is conserved from yeast to mammalian cells. Extensive arrays of smooth ER membranes are prominent features of cells that produce large quantities of sterols [3,8]. Generation of a tissue culture line with HMGR expressed at greater than 500-fold normal levels, recapitulates this cellular phenomenon [9]. Identification of genes required for these ER changes would prove to be a valuable resource in understanding this process.

S. cerevisiae expresses two functional isozymes of HMGR, Hmg1p and Hmg2p [10]. A high level of Hmg1p expression induces the formation of nuclear-associated stacks of membranes, called karmellae [2]. Similarly, increased expression of Hmg2p induces both nuclear-associated stacks, and cytoplasmic whorls and strips of membrane [11]. Superficially these proteins are remarkably similar. Hmg1p and Hmg2p are structurally similar, have the same enzyme activity, and even have similar *in cis* requirements to induce their respective ER structures. However, closer analysis reveals many differences in how cells respond to each of these proteins.

Hmg1p is a stable protein that has been used by the Wright laboratory to examine both structural and genetic aspects of karmellae formation. A detailed examination of the features of Hmg1p has shown that both the transmembrane domain and a large, properly-folded cytoplasmic domain are required to generate karmellae [12-14]. In addition, the Wright group has performed two large-scale genetic analyses of karmellae formation by Hmg1p. The first screen, conducted to identify genes required for karmellae formation, uncovered a large group of VPS (Vacuolar Protein Sorting) genes that are known to be required for vacuolar biogenesis [15]. None of the genes identified affected Hmg2p-induced structures. The second screen was designed to identify mutants that exhibited growth defects when Hmg1p was expressed, thus inducing karmellae. However the genes identified were sensitive to elevated HMGR enzymatic activity, per se, rather than the karmellae-forming determinants [16,17].

The second yeast isozyme, Hmg2p, undergoes HRD1-dependant regulated degradation and has been extensively studied as a substrate for ER associate degradation (ERAD) (for review see [18]). In addition, Hmg2p also forms characteristic membrane structures that are distinct from Hmg1p-induced karmellae in several ways. As mentioned earlier, when Hmg2p levels are elevated in the cell, nuclear-associated stacks of membrane form, in addition to cytoplasmic strips and whorls of membranes. Hmg2p structures also differ from those of Hmg1p in that Kar2p strongly colocalizes with Hmg1p structures

whereas it is excluded from the strips and whorls generated by Hmg2p [11]. Most notably, the fact that the genes required for Hmg1p-induced structure formation, are not required for structures induced by Hmg2p expression suggests that there are fundamental mechanistic differences between these two seemingly similar processes.

Based on the already observed differences between Hmg1p and Hmg2p, we sought to understand Hmg2p in its capacity to stimulate ER structures. As genes have been identified that are relevant to Hmg1p and not Hmg2p, we posited that a reciprocal analysis would uncover genes specific to Hmg2p. We characterized the features of Hmg2p required to form Hmg2p-induced structures, and used this information to design an effective screen. We have confirmed many of the Wright lab's observations and have identified new genes specifically required for formation of Hmg2p-induced structures. Intriguingly, these include genes directly involved in lipid synthesis, and do not include any of the genes previously identified in the screens conducted with Hmg1p.

Results:

Hmg2p as a model for membrane dynamics

Hmg1p and Hmg2p are similar proteins, both structurally and functionally (Figure 2.1A). Although these two isozymes are very similar, they generate different ER membrane arrays [11]. We verified the characteristics of the structures generated by these proteins by immunofluorescence and electron microscopy (Figure 2.1B and C). Furthermore, Hmg2p, unlike Hmg1p, undergoes regulated degradation in response to sterol pathway signal. Mutating K6 to arginine completely prevents Hmg2p degradation ([19] and Figure 2.1A). To facilitate study of the effects of Hmg2p on ER structure, we use the non-degraded stable K6R mutant, referred to as Hmg2p^{s}, throughout this work.

Hmg2p^{s} is expressed at higher levels than Hmg1p

The analysis of Hmg1p has primarily been conducted using the strong, inducible *GAL1-10* promoter (*GAL1-10pr*). It has been previously reported that Hmg1p expressed from the strong, constitutive *TDH3* promoter (*TDH3pr*) does not generate the karmellae as expected. However, when expressed from the same promoter, Hmg2p does generate membrane stacks and whorls [20]. We wondered if this difference was due to differences in protein levels. To determine the relative expression levels of the *TDH3pr* and *GAL1-10pr*, we generated three sets of strains. These all employed integrating plasmids of

Figure 2.1 Hmg1p and Hmg2p^{s} make distinct structures.

(A) Cartoon depicting the three domains of Hmg1p and Hmg2p^{s}. Amino acid positions at domain junctions are indicated, as well as the K6R stabilizing mutation in Hmg2p. Myc tag insertions in both Hmg1p and Hmg2p are indicated by the thick black bars immediately following the linker domain. (B) Representative immunofluorescence images of myc tagged Hmg1p and Hmg2p^{s} expressed at 2 copies per cell. Arrows indicate characteristic structures. (C) Electron micrographs of membrane structures observed when two copies of Hmg1p or Hmg2p^{s} are expressed from the *TDH3pr*. Arrows indicate membrane structures induced by Hmg1p and Hmg2p^{s}. (D) Different expression levels of myc-tagged Hmg1p and Hmg2p^{s} are shown by western blot. Each protein is expressed from either the constitutive *TDH3pr* integrated at one (1x *TDH3*) or two (2x *TDH3*) genomic loci, or from the *GAL1-10pr* integrated at a single locus (1x *GAL1-10*). (E) Quantitation of cells with membrane structures expressing one or two *TDH3pr*-driven copies of Hmg1p or Hmg2p^{s}. In three separate experiments, cells were harvested, prepared for immunofluorescence, and a minimum of 200 cells were counted. Averages and standard deviations are shown.

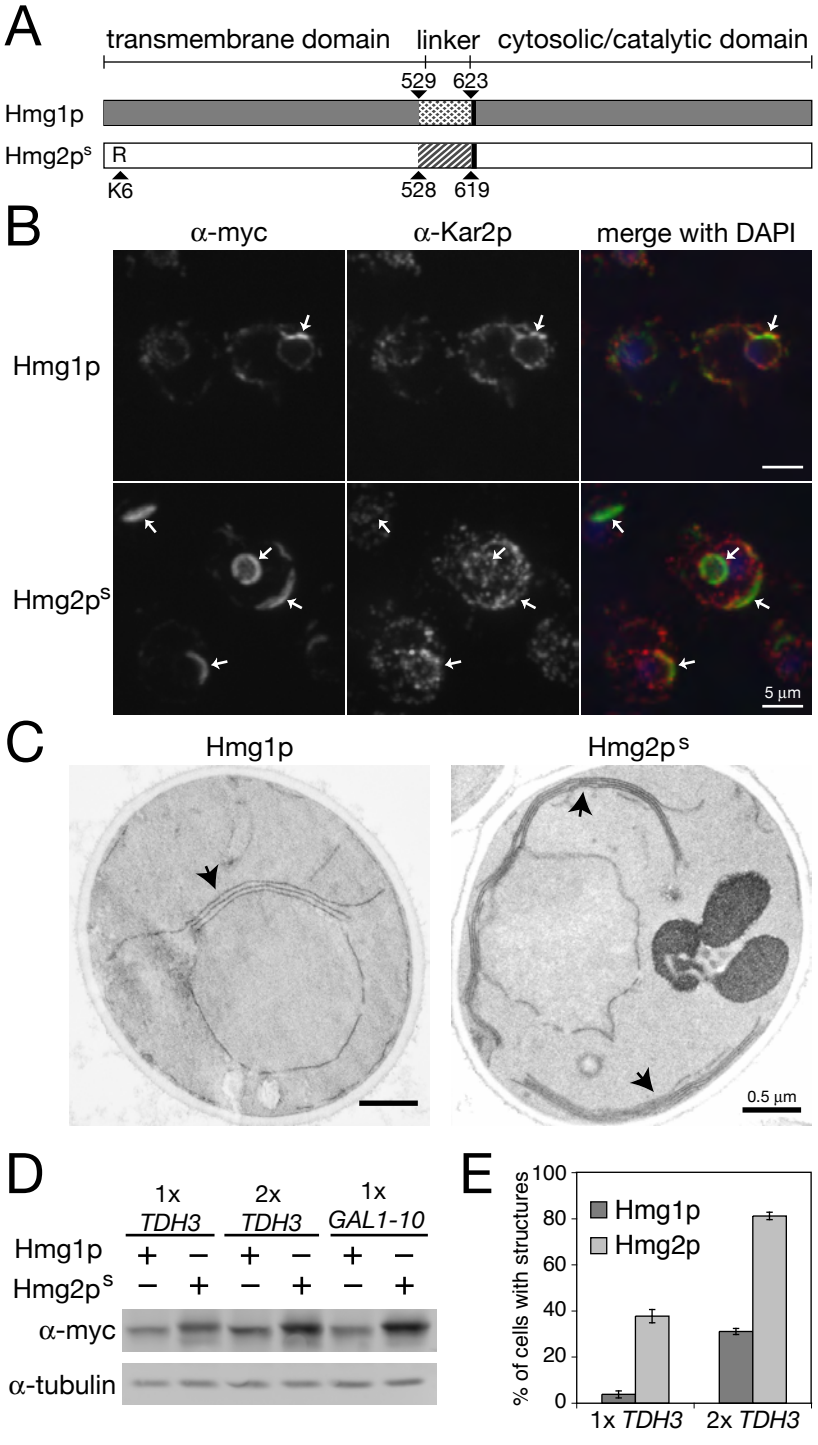
A
transmembrane domain
linker
cytosolic/catalytic domain
529
623
Hmg1p
Hmg2p^s
R
K6
528
619
B
α-myc
α-Kar2p
merge with DAPI
Hmg1p
Hmg2p^s
5 μm
C
Hmg1p
Hmg2p^s
0.5 μm
D
1x TDH3
2x TDH3
1x GAL1-10
Hmg1p
Hmg2p^s
α-myc
α-tubulin
E
% of cells with structures
Hmg1p
Hmg2p
1x TDH3
2x TDH3

either myc-tagged Hmg1p or Hmg2p^{s} expressed by the *TDH3pr* present at one or two copies per cell, or expressed from the inducible *GAL1-10pr* at one copy per cell (Figure 2.1D). Cells expressing the GAL constructs were first grown with raffinose as the carbon source, to eliminate the glucose repression, then galactose was added to 4% for 4 hours to induce expression from the *GAL1-10pr* prior to analysis.

Expression of these HMGR proteins from the *TDH3pr* was about half as strong as the *GAL1-10pr*. Furthermore, expression of Hmg2p^{s} was ~45% higher than Hmg1p in all cases tested. These differences in protein expression levels were reflected when we scored cells for ER membrane organization (Figure 2.1E). Greater than 30% of cells had stacks and whorls of membrane when expressing 1x *TDH3pr*-driven Hmg2p^{s}, whereas less than 10% of cells expressing Hmg1p under the same conditions had karmellae. The number of cells with karmellae increased to slightly more than 30% when a second Hmg1p construct was introduced. These numbers from 2x *TDH3pr*-driven Hmg1p expression were consistent with the Wright lab's observations when expressing Hmg1p from the *GAL1-10pr* [12,13]. The number of cells with stacks and whorls of membranes increased to more than 80% of the cells observed when expressing 2x *TDH3pr*-driven Hmg2p^{s}. We do note that the number of layers of stacked membranes observed in Hmg1p expressing cells are not as numerous as

those reported previously with the *GAL1-10pr*, and may be due to differences in acute versus chronic expression of Hmg1p.

Increased HMGR activity causes a decrease in cellular fitness

Hmg2p, like Hmg1p, catalyzes the rate-limiting step in the mevalonate pathway in addition to restructuring the ER. Large-scale analysis of the growth effects conferred by membrane protein overexpression has been conducted in *S. cerevisiae* and revealed that both Hmg1p and Hmg2p cause a significant decrease in growth when overexpressed [21]. However, it was not determined whether this was due to structure formation or increased HMGR activity. As such, we wanted to evaluate the contribution of each of these components to the overall fitness of the cell. It should be noted that when these strains are grown on plates, no observable difference in growth rate is observed (data not shown). Therefore, a more sensitive assay was required.

We developed a fluorescent-based liquid co-culture assay to measure relative differences in growth rate between two strains (Figure 2.2A and B). Traditionally, liquid co-culture fitness assays are scored by employing strains with reciprocal auxotrophies. Samples of the liquid co-culture are then plated on solid media to enable strain differentiation and quantitation by colony counting (for example see [22]). In our fluorescent assay, the strains are distinguished optically allowing rapid *in vivo* quantitation using a flow cytometer (Figure 2.2B). This method of co-culture analysis is also

Figure 2.2 Elevated HMG-CoA reductase activity causes a significant decrease in cellular fitness.

(A) Illustration of co-culture experiment. Two populations of growing cells in liquid media are added in a ratio of 1:1 and are maintained in log phase growth to determine if one strain has a fitness advantage. (B) Quantitation of populations within co-cultures is achieved using flow cytometry. One strain expresses GFP from the *TDH3pr* to optically distinguish it from the other strain. (C) Graphic representation of co-culture experiment comparing growth of a strain expressing GFP against a strain with an empty vector for 100 culture doublings. (D-G) Co-culture experiments of active and inactive variants of Hmg2p expressed from the *TDH3pr* grown against the GFP expressing strain. Strains grown against GFP strain are: (D) Hmg2p^{s} (myc-tagged Hmg2p with stabilizing K6R mutation), (E) Hmg2p^{si} (myc-tagged Hmg2p with stabilizing K6R mutation and inactivating mutations E711Q and D920N), (F) Hmg2p CD (Hmg2pΔ1-527 which is only the soluble catalytic domain of Hmg2p), and (G) Hmg2p CD^{i} (Hmg2pΔ1-527 with the inactivating mutations E711Q and D920N).

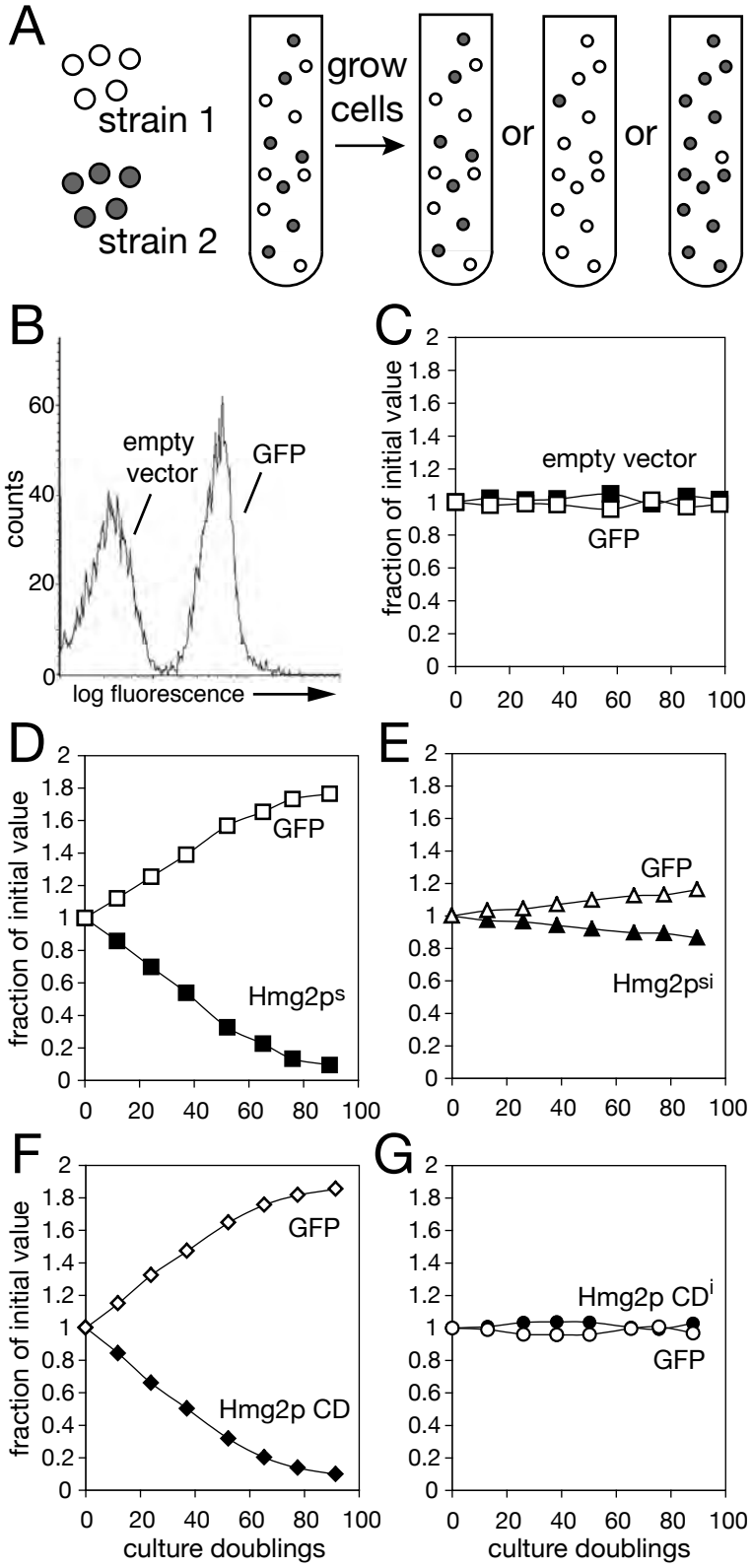
A
strain 1
strain 2
grow cells
or
or
B
counts
empty vector
GFP
log fluorescence
C
fraction of initial value
empty vector
GFP
D
fraction of initial value
GFP
Hmg2p^s
E
GFP
Hmg2p^si
F
fraction of initial value
GFP
Hmg2p CD
culture doublings
G
Hmg2p CD^i
GFP
culture doublings

advantageous in that both strains have identical auxotrophies, thus eliminating any fitness effects due to differences in genetic markers. One strain expresses soluble GFP from the *TDH3pr* integrated at a single locus, and the other strain has a distinct plasmid with the same auxotrophy marker, which is being tested for its effect on growth rate (in Figure 2.2B and C, an empty vector). The ratio of the fluorescent to non-fluorescent cells during the course of many culture doublings are graphically displayed to determine if one strain has a growth disadvantage. The graph in Figure 2.2C demonstrates that the GFP reporter does not confer any observable effects on growth rate when compared to the otherwise identical, non-fluorescent wild type strain.

Using this assay we evaluated the effects of elevated Hmg2p, by expressing various Hmg2p variants from the *TDH3pr*. When we tested Hmg2p^{s} in this assay, we found that there is a clear decrease in cellular fitness, compared to the GFP strain (Figure 2.2D). To determine if this was due to the catalytic activity of the protein, we mutated two critical amino acids E711 and D920 to glutamine and asparagine, respectively, to render the Hmg2p^{s} enzymatically inactive, and verified the effects of these changes (data not shown). When we examined the fitness of the strain expressing this stable, inactive Hmg2p (Hmg2p^{si}) compared to the GFP strain, we found that there was very little effect on growth (Figure 2.2E). To verify that the decreased growth rate of Hmg2p^{s} was due to the catalytic activity, we tested the effect of

expressing the soluble cytoplasmic domain of Hmg2p (deleted amino acids 1-527, Hmg2p CD). The soluble cytosolic domain caused a fitness decrease similar in magnitude to the full-length polytopic Hmg2p^{s}, when grown against the GFP strain (Figure 2.2F). Introducing the same inactivating mutations (E711Q and D920N) into the coding region of the soluble cytoplasmic domain (Hmg2p CD^{i}), completely abrogated the fitness decrease caused by the active soluble enzyme domain (Figure 2.2G). This confirmed that the majority of the growth effects conferred by Hmg2p^{s} overexpression were due to increased HMGR activity per se. It is interesting that the inactive Hmg2p, Hmg2p^{si}, conferred a small growth effect that may be due to ER organization by that protein.

Hmg2p transmembrane domain is not sufficient to generate ER stacks and whorls

Work by the Wright lab has demonstrated that both the transmembrane domain of Hmg1p and a folded cytosolic domain are required for karmellae formation [13]. In contrast, the requirements for the characteristic membrane structures induced by Hmg2p have not yet been evaluated. To better understand the features necessary to generate Hmg2p-induced stacks and whorls, we generated a series of Hmg2p^{s}-based *TDH3pr* expression constructs (Figure 2.3A). We first evaluated expression of these proteins to that of Hmg2p^{s} (data not shown).

Figure 2.3 The transmembrane domain of Hmg2p is not sufficient to organize membranes.

(A) Illustrations of Hmg2p variants examined. *TDH3pr* driven proteins were integrated at one or two loci. Cells were prepared for immunofluorescence and examined for structures. At least 200 cells were counted in three independent experiments; averages and standard deviations are shown. (B) Representative immunofluorescence images of constructs tested, present at two copies per cell. Hmg2p variants were detected with either anti-myc or anti-GFP monoclonal antibodies. Arrows indicate ER membrane structures. (C-E) Electron micrographs of the structures generated by the Hmg2p variants (C) Hmg2p^{sl}, (D) Hmg2p^{s}-GFP, and (E) Hmg2p^{s}-GFP*. Arrows indicate structures.

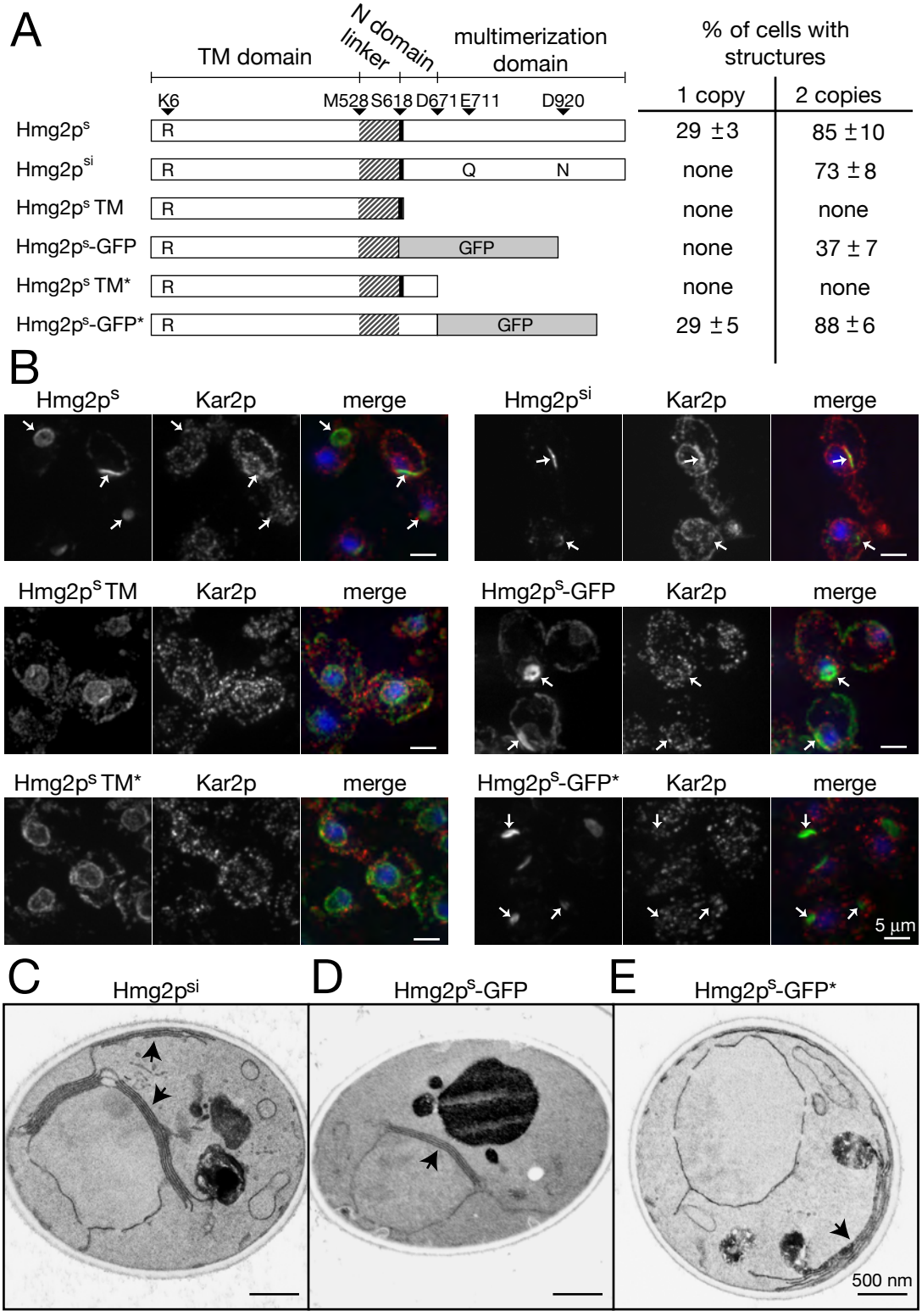
A
TM domain
N domain linker
multimerization domain
K6
M528
S618
D671
E711
D920
% of cells with structures
1 copy
2 copies
Hmg2p^s
R
29 ±3
85 ±10
Hmg2p^si
Q
N
none
73 ±8
Hmg2p^s TM
none
none
Hmg2p^s-GFP
GFP
none
37 ± 7
Hmg2p^s TM*
none
none
Hmg2p^s-GFP*
29 ±5
88 ±6
B
Hmg2p^s
Kar2p
merge
Hmg2p^si
Hmg2p^s TM
Hmg2p^s-GFP
Hmg2p^s TM*
Hmg2p^s-GFP*
5 µm
C
Hmg2p^si
D
Hmg2p^s-GFP
E
Hmg2p^s-GFP*
500 nm

Catalytic activity is not required for Hmg1p-induced karmellae, so we began by determining if the catalytic activity was required to form Hmg2p-induced structures. When we examined the expression level of the inactive version, Hmg2p^{si}, we found that it not as strongly expressed as Hmg2p^{s} (data not shown). At one copy per cell, Hmg2p^{si} did not generate any of the characteristic structures at the light microscopic level. Upon introducing a second expression plasmid, the number of cells with structures increased to ~73%, demonstrating the catalytic activity was not required for generating Hmg2p-induced structures. We confirmed by electron microscopy that these structures were similar in nature to those generated by Hmg2p^{s} (Figure 2.3C).

Next we wanted to test the requirement of a cytoplasmic domain in making Hmg2p-induced structures. We started by completely removing the cytoplasmic domain of Hmg2p (Hmg2p^{s}-TM, Figure 2.3A). This protein has the entire transmembrane (TM) domain and linker region but lacks the C-terminal 425 amino acids. When we examined these cells by immunofluorescence, we were surprised to see that even when two copies were present, no structures were formed. We further confirmed by electron microscopy that no membrane alterations were observable (data not shown). Our protein expression analysis indicated that this protein was expressed at similar levels to Hmg2p^{s}, indicating that the lack of structures was not due to a

corresponding lack of protein. This suggests that the TM domain alone is not sufficient to generate membrane stacks and whorls.

Hmg1p requires a large cytoplasmic domain to generate its characteristic membrane patterns. To determine if this was also the case for Hmg2p, we replaced the entire 425 amino acid cytoplasmic domain with GFP (Hmg2p^{s}-GFP Figure 2.3A). When we expressed this protein in cells, we again did not observe any of the expected structures. However, introducing a second copy induced structures in ~37% of cells. At the level of light microscopy, the structures looked similar to those generated by Hmg2p^{s} (Figure 2.3B), and this was confirmed by electron microscopy (Figure 2.3D). Like Hmg2p^{s} TM, Hmg2p^{s}-GFP was expressed at comparable levels to Hmg2p^{s}, indicating that the decrease in structures observed was not due to decreased protein levels.

To better understand the role of the cytoplasmic domain, we generated a pair of constructs with the first 50 conserved amino acids in the cytoplasmic domain intact. This completely removes the tetramerization and dimerization domains that have been identified by crystallization of huHMGR, but retains the small, helical N-domain [7]. Therefore, we can determine if this multimerization region of the cytoplasmic domain is required to generate Hmg2p structures. One of these proteins is truncated, completely removing the last 375 amino acids of the cytoplasmic domain (Hmg2p^{s} TM*), and the other has the last 375 amino acids of the cytosolic domain replaced with GFP

(Hmg2p^{s}-GFP*, Figure 2.3A). Previous work has shown that replacing the last 375 amino acids of the Hmg2p cytoplasmic domain with GFP allows the characteristic structures to form [11,20]. When we tested the Hmg2p^{s}-GFP* construct, we found that the number of cells with structures was the same as that of Hmg2p^{s}, at both expression levels tested (Figure 2.3A). Examination of these structures by electron microscopy confirmed that they appeared similar to structures that full-length Hmg2p^{s} generates (Figure 2.3D).

When we examined the Hmg2p^{s} TM* protein, we did not observe any structures when expressed at one copy or two copies per cell (Figure 2.3A), and verified the lack of structures by electron microscopy (data not shown). Our protein analysis confirmed that expression of this protein is significantly lower than the others examined. These data suggest that the presence of any cytoplasmic domain – even GFP - stabilizes the TM domain.

The TM domain of Hmg2p does not colocalize with Kar2p

As mentioned earlier, the structures formed by Hmg2p generally do not colocalize with Kar2p. We wanted to test if this was a general feature of the TM domain of Hmg2p or if it was a feature of the structures themselves. To do this, we analyzed all of the mutants tested in Figure 2.3A for localization with respect to Kar2p. Colocalization between the Hmg2p variants and Kar2p was hardly ever observed, regardless of whether or not strips and whorls were

present (Figure 2.3E). These results indicate that there is some feature in the TM domain of Hmg2p that serves to separate its localization from Kar2p.

GFP does not have intrinsic abilities to reorganize membranes

In our analysis of the requirements of Hmg2p to generate membrane strips and whorls, we discovered that Hmg2p might require a cytoplasmic domain. We also wanted to examine the membrane-organizing features of these cytoplasmic domains. Previous reports have indicated that attachment of a multimerizing GFP to a TM domain is sufficient to reorganize membranes [23], so we could not rule out the possibility that multimerization through the cytoplasmic domain was contributing to the structures that we were observing. This is particularly compelling, given the multimerization properties of the HMGR cytosolic domain [7].

To test the effects of various cytoplasmic domains independent of the Hmg2p TM domain, we used the ER-localized Ole1p as our independent anchor. To eliminate any effects from enzymatic function, we used an inactive form of the protein that has histidines 161 and 166 mutated to alanine (Ole1p^{i}). This protein also has a triple myc tag at the N-terminus (Figure 2.4A), which allowed us to compare protein expression levels to Hmg2p^{s} (data not shown). First we verified that overexpression of this protein did not confer any alteration of the ER membranes when expressed at one or two copies per cell from the

Figure 2.4 The ER anchored cytoplasmic domain of HMGR is sufficient to cause membrane reorganization.

(A) Diagrams of Ole1p variants examined. *TDH3pr*-driven triple-myc-tagged Ole1p with the H161A, H166A inactivating mutations was fused to various soluble proteins as indicated. Nomenclature is as follows: Ole1p^{i} – Ole1p with H161A and H166A mutations, Ole1p^{i}-GFP – inactive Ole1p fused to GFP, Ole1p^{i}-GFP* - inactive Ole1p fused to the helical N-domain of Hmg2p and GFP, Ole1p^{i}-Hmg2p CD – inactive Ole1p fused to the cytoplasmic domain of Hmg2p, and Ole1p^{i}-Hmg1p CD – inactive Ole1p fused to the cytoplasmic domain of Hmg1p. Quantitation of cells harboring one or two copies of the expression plasmids are listed on the right. Expression plasmids were integrated at one or two loci. Cells were prepared for immunofluorescence and examined for structures. A minimum of 200 cells was counted in three independent experiments; averages and standard deviations are shown. (B) Representative immunofluorescence of strains with two expression constructs is shown. Arrows indicate ER membrane structures. (C) Electron micrographs of cells with two copies of *TDH3pr*-driven Ole1p^{i}-Hmg2p CD and Ole1p^{i}-Hmg1p CD. Double arrowheads indicate structures.

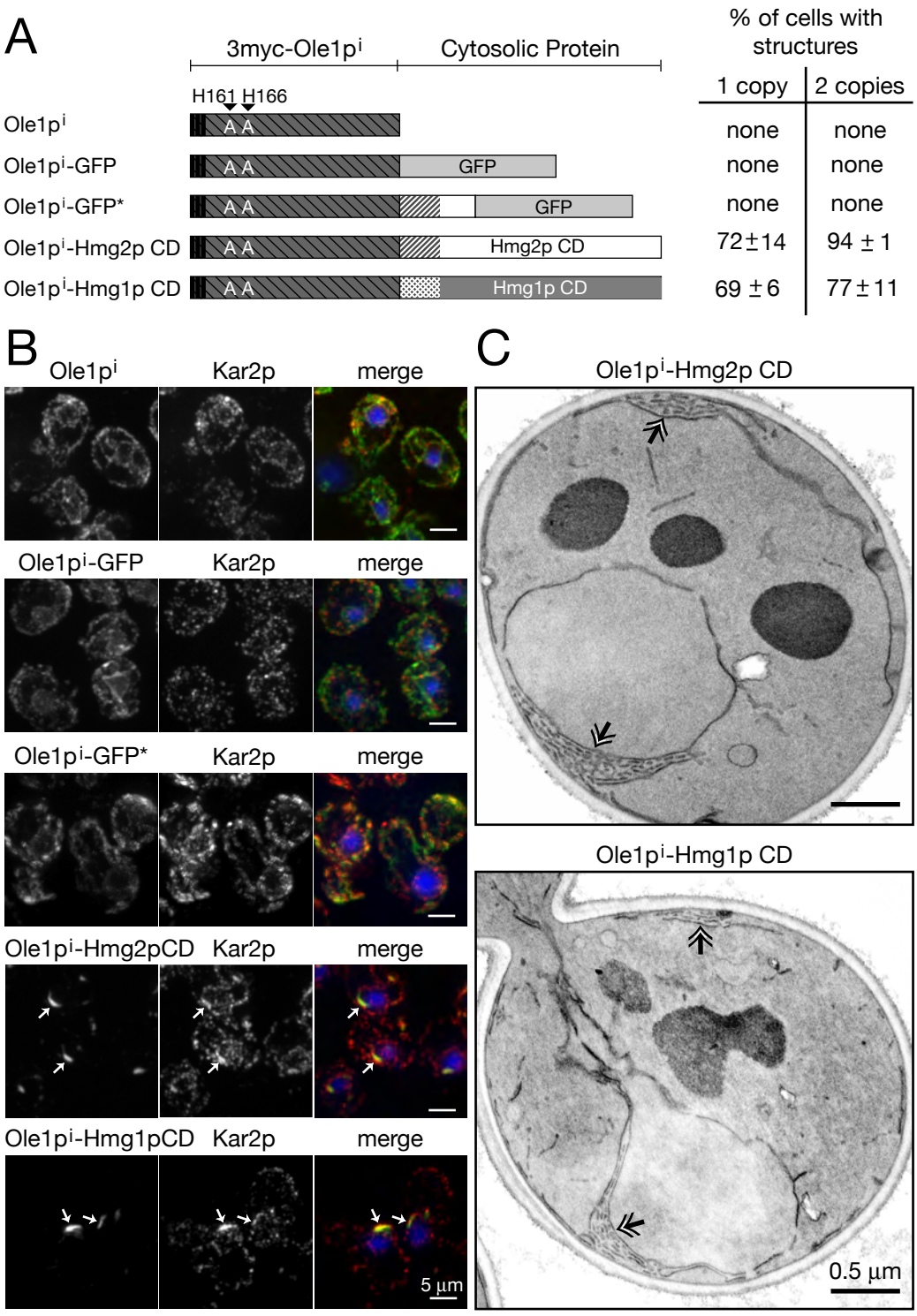
A
3myc-Ole1p^{i}
Cytosolic Protein
H161 H166
Ole1p^{i}
Ole1p^{i}-GFP
Ole1p^{i}-GFP*
Ole1p^{i}-Hmg2p CD
Ole1p^{i}-Hmg1p CD
A A
GFP
Hmg2p CD
Hmg1p CD
% of cells with structures
1 copy
2 copies
none
none
none
none
none
none
72±14
94 ±1
69 ±6
77±11
B
Ole1p^{i}
Kar2p
merge
Ole1p^{i}-GFP
Ole1p^{i}-GFP*
Ole1p^{i}-Hmg2pCD
Ole1p^{i}-Hmg1pCD
5 µm
C
Ole1p^{i}-Hmg2p CD
Ole1p^{i}-Hmg1p CD
0.5 µm

TDH3pr (Figure 2.4B) and confirmed this observation by electron microscopy (data not shown).

Next we generated fusion proteins between the Ole1p^{i} and the various cytoplasmic domains tested in Figure 2.3 (Figure 2.4A). The first fusion that we tested was Ole1p^{i}-GFP. When we evaluated this strain by immunofluorescence and electron microscopy, we did not observe any ER membrane structures (Figure 2.3B and data not shown). This indicated that the GFP used in our analysis of Hmg2p did not contribute to membrane stacking through an intrinsic ability to multimerize. Next we wanted to test if the helical N-domain of the cytoplasmic domain of Hmg2p with GFP could stimulate membrane reorganization (Ole1p^{i}-GFP*). When we tested the Ole1p^{i}-GFP*, we again did not observe any structures when expressed from the *TDH3pr* at one or two copies per cell (Figure 2.4B), and confirmed that no ER membrane alterations were observable by electron microscopy (data not shown). This demonstrates that the structures observed when the Hmg2p^{s} with the helical N-domain is fused GFP or when the Hmg2p^{s} TM domain is fused to GFP (Hmg2p^{s}-GFP* and Hmg2p^{s}-GFP, respectively), were not a result of an intrinsic activity of the cytoplasmic regions.

The ER-anchored HMGR cytoplasmic domain is sufficient to reorganize membranes

As mentioned earlier, the huHMGR cytoplasmic domain forms homodimers and homotetramers. Due to the high conservation of this domain from yeast to humans, it is reasonable to believe that the yeast cytoplasmic domain also forms multimers. To determine if the cytoplasmic domains of yeast HMGR have an intrinsic ability to reorganize membranes, potentially via multimerization, we generated a fusion between Ole1p^{i} and the cytoplasmic domain of Hmg2p (Ole1p^{i}-Hmg2p CD) and expressed it from the *TDH3pr*. In striking contrast to GFP, the cytoplasmic domain of Hmg2p caused a reorganization of membranes when fused to Ole1p^{i}; when present at only one copy, ~72% of the population had visible membrane structures (Figure 2.4A and B).

The cytoplasmic domain of Hmg1p and Hmg2p are 93% identical, so we would expect the Hmg1p cytoplasmic domain to also stimulate a reorganization of ER membranes. When we tested a construct that fused the cytoplasmic domain of Hmg1p to Ole1p^{i} (Ole1p^{i}-Hmg1p CD), we found that they appeared identical to those caused by the Ole1p^{i}-Hmg2p CD fusion (Figure 2.4B and C). The cytoplasmic domain of Hmg1p stimulates ER structures that are both nuclear-associated and cytoplasmic (Figure 2.4C). When a single *TDH3pr*-driven copy was expressed, ~69% of cells had visible ER arrays, and when the

copy number was doubled, the percentage climbed to 77% (Figure 2.4A). These numbers were markedly higher than those achieved with the full-length Hmg1p. Our findings indicate that interactions via the HMGR cytosolic domain are sufficient to cause scaffolding of ER membranes when anchored to any TM protein.

The Ole1p^{i}-HMGR CD-induced structures are distinct from Hmg1p and Hmg2p

Hmg1p and Hmg2p structures are distinct from each other in both their cellular localization and in their colocalization with Kar2p. Both the Hmg1p and Hmg2p cytoplasmic domain fusions to Ole1p^{i} generate both nuclear associated and cytoplasmic structures. This suggests that the TM domains of Hmg1p and Hmg2p determine the differences in their respective structures. Using our Ole1p^{i}-HMGR cytoplasmic domain fusion proteins, we next examined their localization with respect to Kar2p. We would expect both Ole1p^{i}-Hmg1p CD and Ole1p^{i}-Hmg2p CD to behave similarly if the TM domain determines the characteristics of the structures. Both the Ole1p^{i}-HMGR cytoplasmic domain fusion proteins strongly colocalized with Kar2p (Figure 2.4B). This demonstrates that not only does the TM domain determine if the structures will colocalize with Kar2p, but that there is a feature of the Hmg1p TM domain that restricts structure formation to the nucleus.

The membrane structures generated by both Hmg1p and Hmg2p^{s} are smooth, closely associated stacks of unbranched membranes. We wanted to determine the nature of the structures generated by the Ole1p^{i} fusions to the cytoplasmic domains of Hmg1p and Hmg2p. By immunofluorescence, we cannot determine these features. However, by electron microscopy we observed that the Ole1p^{i}-HMGR cytoplasmic domain fusions generated structures composed of branched networks of membranes (Figure 2.4C and 2.5B). These structures are significantly different from those generated by either Hmg1p or Hmg2p.

In some cells expressing the Ole1p^{i}-HMGR cytoplasmic domain constructs, we saw that these bits of membrane are actually connected tubules that very closely resemble the hexagonal arrays that have been observed in mammalian cells with elevated levels of HMGR [9]. One such panel is shown in Figure 2.5B of Ole1p^{i}-Hmg2p CD. These highly branched networks are remarkably different from the tightly packed stacks of membrane generated by Hmg2p^{s} (Figure 2.5A and B). We also verified that the catalytic activity of HMGR is not required to generate these structures by analyzing Ole1p^{i} fused to the inactive cytoplasmic domain of Hmg2p (data not shown). In addition, we made an N-terminal Hmg2p cytoplasmic domain fusion to Ole1p^{i} (Hmg2p CD-Ole1p^{i}), and observed similarly branched membrane arrays by electron microscopy (data not shown). Together, these findings suggest that while a

Figure 2.5 The Ole1p-HMGR cytoplasmic domain fusions make distinct membrane structures.

Electron micrographs of strains with two *TDH3pr*-driven copies of (A) Ole1p^{i}-Hmg2p CD – inactive Ole1p fused to the cytoplasmic domain of Hmg2p, and (B) Hmg2p^{s} at 20K (top) and 80K (bottom) magnification. Solid arrows indicate stacks of membrane characteristic of Hmg2p. Double arrows indicate tubular membrane arrays generated by Ole1p^{i}-Hmg2p CD fusion constructs.

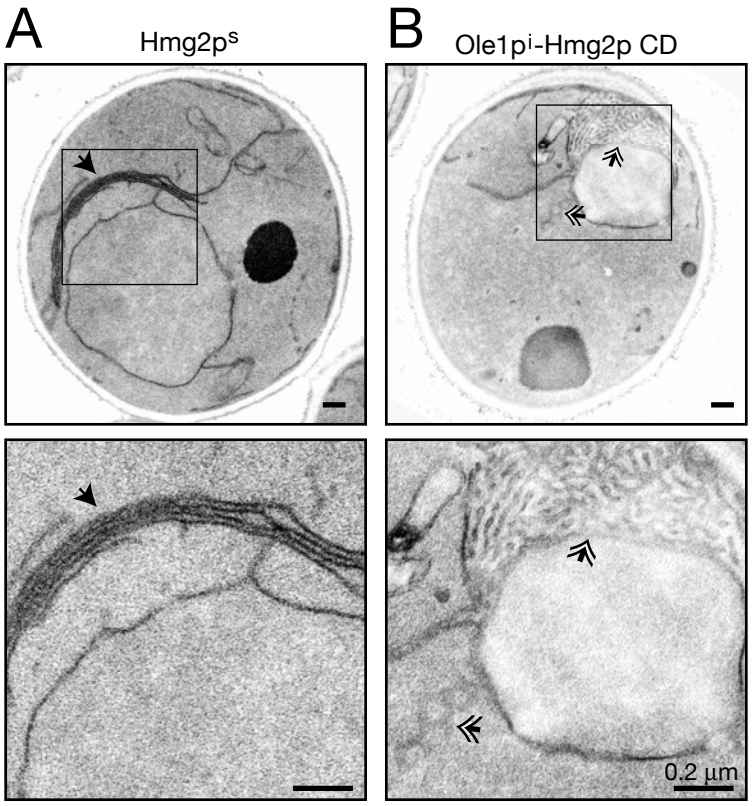
A
Hmg2p^{s}
B
Ole1p^{i}-Hmg2p CD
0.2 µm

cytoplasmic domain is necessary for structures to form, the TM domain plays a critical role in dictating the characteristics of the structures generated.

Screen for Hmg2p Proliferated ER (HPE) genes

Analysis of Hmg1p identified genes that are specifically required for Hmg1p-induced ER structures, and did not affect Hmg2p-induced membrane structures. This suggested that a reciprocal analysis would uncover genes specifically required for Hmg2p-induced structures, which is what we next sought to do. We were particularly interested in determining to what degree these genes would be specifically required for the action of Hmg2p, versus general ER organization. In designing our strategy, we integrated our findings about what is required for Hmg2p to generate its characteristic structures and selected the to use a version of Hmg2p that replaced the multimerization domain with GFP, Hmg2p^{s}-GFP*, to conduct our screen. The protein lacks catalytic activity, which we demonstrated causes a significant stress. It is a stable, optical form of Hmg2p, which allows for facile screening of live cells on plates without the need to use dyes or fix cells. Lastly, the absence of the HMGR multimerization domain removes the independent ability of the cytoplasmic domain to alter ER membranes, as determined with the Ole1p fusion, yet generates characteristic Hmg2p structures with high fidelity. In this way, we hoped to narrow the scope of our screen to genes required for altering ER structure via interactions mediated by the Hmg2p TM domain.

We introduced Hmg2p^{s}-GFP* into the collection of viable yeast nulls. A strain with our Hmg2p^{s}-GFP* coding region under the control of the inducible *GAL1-10pr*, was robotically crossed to the viable haploid null collection (for strategy, see [24]). The entire crossing and selection process was conducted on dextrose plates so that the galactose-dependant Hmg2p^{s}-GFP* expression did not occur during the strain production phase. The resulting array of null haploids harboring our expression plasmid was then patched onto raffinose plates and allowed to grow for 24-48 hours to eliminate the glucose repression, and next patched onto galactose plates to induce Hmg2p^{s}-GFP* expression. After a period of induction on galactose, each null strain was individually examined for alterations or absence of the characteristic Hmg2p^{s}-GFP* structures. We identified 140 candidate nulls with altered Hmg2p^{s}-GFP*-induced structures from this primary screen. Of these nulls, 50 were manually deleted in our strain background and re-tested. We introduced our *TDH3pr* driven Hmg2p^{s}-GFP* into this subset and scored the cells again for lack of characteristic localization of Hmg2p^{s}-GFP*.

The genes identified were separated into three distinct classes based on Hmg2p^{s}-GFP* localization, and are listed in Table 2.1, and representative images are depicted in Figure 2.6. The first class, Class I, is composed of two genes, *NEM1* and *SPO7*, and have previously been identified as altering nuclear and ER morphology [25,26]. Hmg2p^{s}-GFP* localization in this class of mutants

Table 2.1: Genes that affect Hmg2p^{s}-GFP* localization

Class I		
Gene	**ORF**	**protein description**
NEM1	YHR004C	controls nuclear growth - negative regulator of phospholipid biosynthetic genes
SPO7	YAL009W	controls nuclear growth - negative regulator of phospholipid biosynthetic genes
Class II		
Gene	**ORF**	**protein description**
ERG28	YER044C	ER membrane protein - facilitates protein-protein interactions
ERV25	YML012W	member of p24 family - involved in ER to Golgi transport
HMP1	YOR227W	verified ORF of unknown function
HOF1	YMR032W	protein with SH3 domain - involved in cytokinesis and cytoskeletal dynamics
COD1/SPF1	YEL031W	ER localized P-type ATPase
Class III		
Gene	**ORF**	**protein description**
*BNR1 / BNI1**	YIL159W / YNL271C	formins - involved in budding and actin dynamics
HMP2	YMR293C	verified ORF of unknown function
*PSD1***	YNL169C	mitochondrial phosphatidyl serine decarboxylase - phosphatidyl choline biosynthesis
VMA2	YBR127C	subunit B of V-ATPase - proton pump found throughout endomembrane system

** double knockout evaluated*

*** identified through overlapping ORF, YNL170W*

Figure 2.6 HPE genes fall into three distinct classes.

Live cell imaging of Hmg2p^{s}-GFP* localization in four different strains is shown. Cells imaged have a single integrated copy of Hmg2p^{s}-GFP*. Wild type is shown for reference, and the representative Classes are depicted as follows: *nem1*Δ for Class I, *hof1*Δ for Class II, and *hpe2*Δ for Class III. Arrows indicate distinct structures.

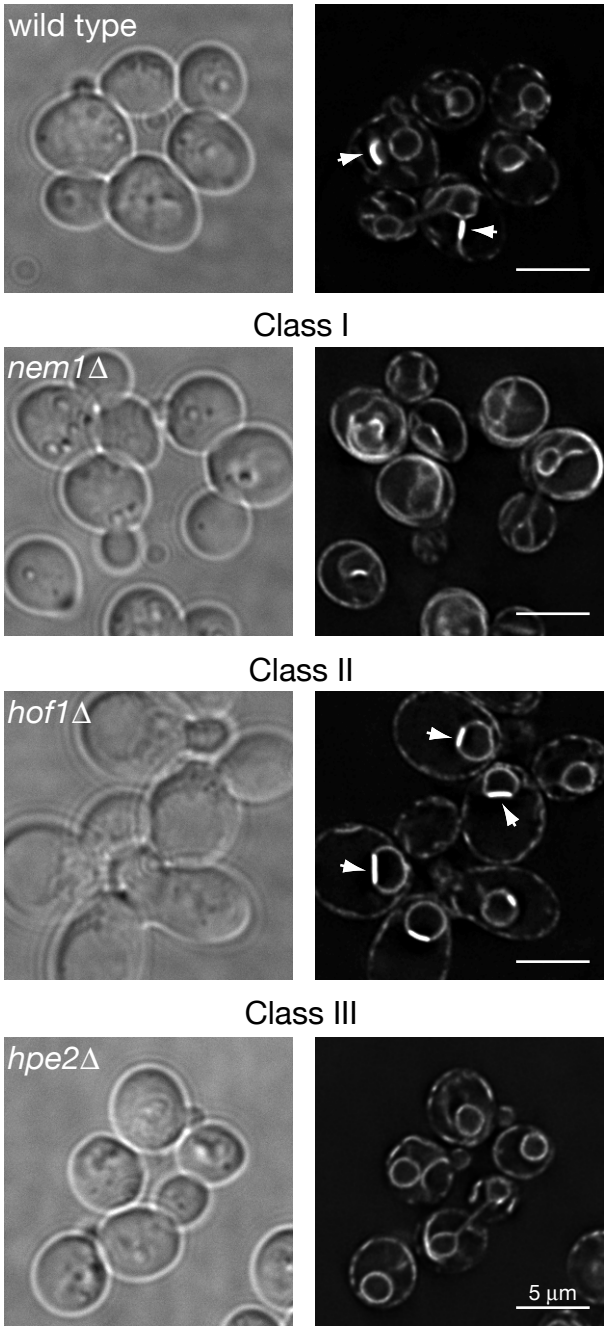
wild type
Class I
nem1Δ
Class II
hof1Δ
Class III
hpe2Δ
5 µm

is distributed widely throughout the ER, with few areas of intense localization. Unlike wild type cells that expressed high levels of Hmg2p^{s}-GFP* had a very spotty or punctate distribution of Hmg2p^{s}-GFP*, Class I nulls had a very even, smooth-looking distribution of Hmg2p^{s}-GFP* (Figure 2.6), The next class of null strains, Class II, all similarly generated Hmg2p^{s}-GFP*-induced stacks of membranes that were completely nuclear-associated, reminiscent of Hmg1p-induced karmellae (Figure 2.6). Membrane stacks were not observed away from the nucleus in any of these Class II nulls when Hmg2p^{s}-GFP* was overexpressed. Finally, Class III nulls did not have any observable structures in >95% of the cells. Instead, Hmg2p^{s}-GFP* localization was generally uniform throughout the ER, and looked very similar to the distribution of any number of ER proteins in *S. cerevisiae*, including Kar2p. We confirmed by flow cytometry that the lack of structures observed in the null strains examined was not due to a decrease in Hmg2p^{s}-GFP* expression (data not shown). These genes are the first identified to alter the morphology of the structures generated by Hmg2p.

Class II and III genes are specifically required for Hmg2p^{s}-GFP* structures

The genes that we identified in this screen were selected based on the localization of Hmg2p^{s}-GFP* in the null. As mentioned earlier, the Class I genes have previously been identified as independently altering both nuclear and ER membranes even without Hmg2p overexpression. We were seeking

genes specifically required for Hmg2p^{s}-GFP* structure formation, and therefore wanted to identify, and eliminate from our study, genes that were required for general ER morphology and distribution. We examined the ER in strains lacking Hmg2p^{s}-GFP*, using the ER membrane protein Sec63p and the ER lumenal protein KGFP*. Only the Class I nulls caused aberrant localization of these markers compared to wild type (data not shown). Analysis of the Class II and Class III nulls revealed that they all had an ER distribution that was indistinguishable from wild type by analysis of these two ER markers (data not shown). This suggests that our screen was effective in identifying genes that affect Hmg2p^{s}-GFP* structures, and not general ER morphology.

After determining that the Class II and III genes did not obviously alter general ER morphology, we wanted to determine if these genes only affected Hmg2p-induced structures, or if they also affected Hmg1p-dependant proliferations. To test this, we introduced a karmellae-forming GFP-tagged Hmg1p into these strains. This Hmg1p construct has the last 67 amino acids of the cytoplasmic domain replaced with GFP and has been previously reported to generate karmellae (called Hmg1^{mem}:Hmg1$^{525\text{-}987}$:GFP [13]).When we compared the localization profiles of Hmg1pΔ67-GFP in the Class II and Class III nulls, we found that none affected karmellae formation (data not shown). This GFP fusion of Hmg1p still has much of the multimerization domain intact, therefore, we cannot rule out the possibility that structures observed in our null

strains are due to multimerization via the cytoplasmic domain. We further examined if the genes that we identified altered the localization of an independent proliferant, P450CmA1 from *Candida maltosa* in these strains and again found no perturbation in Class II or Class III strains (data not shown). This suggests that the genes that we identified are not generally required by all means of ER membrane reorganization, but are specifically required to generate the characteristic structures of Hmg2p.

Correctly folded TM domain of Hmg2p is required for separation from Kar2p

We wanted to further investigate the roles of these genes in Hmg2p-induced membrane organization. To do this, we selected the Class II gene, *COD1/SPF1*, which was previously identified in a screen for genes that allow constitutive degradation of Hmg2p [27]. In the *cod1/spf1* null strain, Hmg2p^{s}-GFP* induces distinct nuclear-associated stacks of membrane (Figure 2.7A and B). Previous work in our lab has demonstrated that the membrane topology of Hmg2p in a *cod1/spf1*Δ strain is altered, via a limited proteolysis assay [28]. Therefore, we hypothesized that the localization of Hmg2p^{s}-GFP* in the Class II null strains might be due to altered Hmg2p membrane topology. To test this, we performed an Hmg2p limited proteolysis assay on the Class II null strains, and found that only the *cod1/spf1*Δ strain has a trypsin digestion pattern indicative of an altered TM domain (data not shown). This suggested that the

Figure 2.7 Proper topology of the TM domain of Hmg2p is required for discrete localization from Kar2p.

(A) Live cell imaging of Hmg2p^{s}-GFP* in a *cod1/spf1* null strain. *TDH3pr*-driven Hmg2p^{s}-GFP* is present at one copy per cell. (B) Electron micrograph of structures observed in *cod1/spf1* null strain with two copies of *TDH3pr*-driven Hmg2p^{s}-GFP*. (C) Immunofluorescence of Kar2p with Hmg2p^{s}-GFP in a *cod1/spf1* null strain, and with 6myc-Hmg2p-GFP in a *hrd1* null strain. Nucleus is labeled with DAPI. Arrows indicate characteristic structures in each panel.

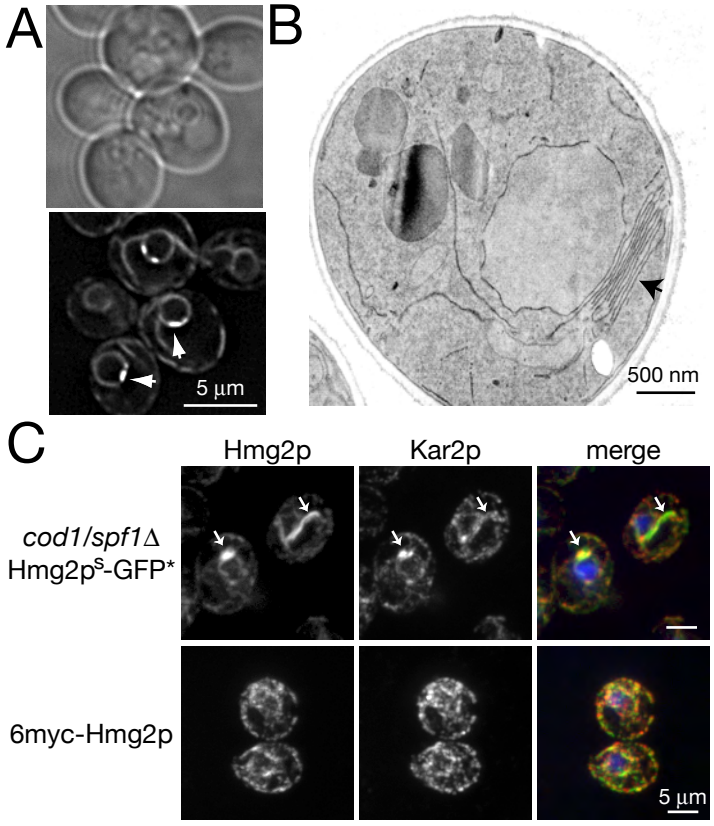
A
B
5 µm
500 nm
C
Hmg2p
Kar2p
merge
cod1/spf1Δ
Hmg2p^S-GFP*
6myc-Hmg2p
5 µm

localization pattern of Hmg2p-GFP* in the Class II null strains is not a result of altered Hmg2p TM topology, per se.

We next examined another feature of Hmg2p overexpression; the separation of Hmg2p and Kar2p. The *cod1/spf1* null strain exhibited extensive colocalization between Kar2p and either Hmg2p^{s}-GFP* or Hmg2p^{s} (Figure 2.7C). However, upon inspection of the rest of the Class II nulls, we did not find significant colocalization between Kar2p and Hmg2p^{s} (data not shown), indicating that this is also not a general feature of the Class II nulls.

Other labs have demonstrated that *cod1/spf1* null strains have a myriad of altered ER functions, including but not limited to upregulated UPR, altered Ca^{2+} homeostasis, and defects in glycoprotein processing and ERAD (for examples, see[29-31]). We wanted to distinguish if the colocalization observed in the *cod1/spf1* null strain was due to the altered topology of the TM region of Hmg2p, or some other altered ER function. To do this we examined the localization of Kar2p with respect to a misfolded variant of Hmg2p (6myc-Hmg2p-GFP), which has been studied in our laboratory [32]. Because this protein is misfolded, and therefore constitutively degraded by the HRD-pathway, we used the *hrd1* null background for our immunofluorescence analysis to ensure adequate protein levels. We did not observe any Hmg2p-induced ER structures when this protein was overexpressed (Figure 2.7C). In addition, we observed that there was a significant amount of colocalization

between 6myc-Hmg2p and Kar2p. These findings indicate that proper folding of the TM domain is one necessary criterion for maintaining separation between Hmg2p and Kar2p.

Discussion:

Despite the striking ER reorganization that occurs when HMGR levels are elevated within cells, the molecular mechanisms at play in generating this intracellular response have largely eluded researchers. We have uncovered requirements for making characteristic Hmg2p-induced structures, and our findings are summarized in Table 2.2. In addition to identifying elements within Hmg2p that are required for generating its structures, we have identified other genes that are required for this process.

Hmg1p and Hmg2p

Although Hmg1p and Hmg2p are very similar proteins, cells respond differently to elevated levels of these isozymes. In fact, expression levels of these isozymes from the same *TDH3pr* are different. Analysis of myc-tagged Hmg1p and Hmg2p revealed that Hmg1p is expressed at a lower level than Hmg2p^{s}, which has been observed previously with GFP-tagged versions of these two proteins [20]. Much of the analyses with Hmg1p by other groups have been conducted using the strong, inducible *GAL1-10pr*, whereas our analysis here was conducted with the constitutive *TDH3pr*. Our direct comparison of the expression from the *TDH3pr* to that of the *GAL1-10pr*, demonstrated that *TDH3pr*-driven expression is half as strong as *GAL1-10pr*.

Table 2.2: Summary of proteins analyzed in this study

Protein Overexpressed	Protein Description	Membrane structure observed			Co-localization with Kar2p
		Nuclear stacks	Cytosolic stacks	Branched arrays	
Hmg1p	full-length, active Hmg1p	yes	no	no	yes
Hmg2p^{s}	full-length, active Hmg2p with K6R stabilizing mutation	yes	yes	no	no
Hmg2p^{si}	stable, inactive Hmg2p	yes	yes	no	no
Hmg2p^{s} TM	stable transmembrane domain and linker region of Hmg2p	no	no	no	no
Hmg2p^{s}-GFP	stable transmembrane domain and linker region of Hmg2p fused to GFP	yes	yes	no	no
Hmg2p^{s}-TM*	stable Hmg2p TM domain, linker and helical N-domain	no	no	no	no
Hmg2p^{s}-GFP*	stable Hmg2p TM domain, linker and helical N-domain fused to GFP	yes	yes	no	no
6myc-Hmg2p-GFP	Hmg2p-GFP* with 6myc tag in first lumenal loop – causes gross misfolding of TM domain	no	no	no	yes
Ole1p^{i}	Ole1p with H161 and H166A inactivating mutations	no	no	no	yes
Ole1p^{i}-GFP	inactive Ole1p fused to GFP	no	no	no	yes
Ole1p^{i}-GFP*	inactive Ole1p fused to the Hmg2p linker region, helical N-domain and GFP	no	no	no	yes
Ole1p^{i}-Hmg2p CD	inactive Ole1p fused to the Hmg2p linker region and cytoplasmic domain	no	no	yes	yes
Ole1p^{i}-Hmg1p CD	inactive Ole1p fused to the Hmg2p linker region and cytoplasmic domain	no	no	yes	yes

Restructuring the ER

There are multiple sufficient conditions for reorganizing ER membranes with Hmg2p (Figure 2.8 and Table 2.2). By fusing the HMGR cytoplasmic domain to an independent ER anchored protein that does not otherwise alter membranes (Ole1p^{i}-Hmg2p CD and Ole1p^{i}-Hmg1p CD), we found that striking membrane reorganization occurred (Figure 2.8C). This is most likely through a multimerization of the HMGR cytoplasmic domain, although we did not directly test this. Although both the Hmg1p and Hmg2p cytosolic domains caused a profound alteration in membrane structure when tethered to an independent TM protein, this condition is not sufficient to generate the characteristic Hmg1p and Hmg2p stacks of membrane (Table 2.2). The structures generated by cytoplasmic domain interactions might be considered analogous to organized smooth ER (OSER) formation by GFP observed in mammalian cells [23].

Elevated Hmg2p expression induced strips and whorls of membranes when the multimerization domain was replaced with GFP, or when the entire cytoplasmic domain was replaced with GFP (Hmg2p^{s}-GFP* and Hmg2p^{s}-GFP, respectively), indicating that the cytoplasmic domain of Hmg2p is not required to generate these structures. One concern was that the structures we were observing in our Hmg2p-GFP fusions were a result of weak homotypic interactions between cytoplasmic GFPs. However, we found that fusing GFP to

Figure 2.8 Summary of the combinations of the two sufficient conditions for structure formation by HMGR.

(A) Full-length Hmg2p molecules multimerize via the catalytic domain, and through intermolecular attractions between the catalytic domains (here the N domain) and transmembrane regions. (B) Hmg2p-GFP* is shown. Interactions occur between the transmembrane domain of Hmg2p and the N domain. (C) Ole1p^{i}-Hmg2p CD fusion proteins associate via the catalytic domains of Hmg2p. (D) Ole1p^{i}-GFP* proteins do not form structures. Neither GFP nor the N-domain of the Hmg2p CD interacts with themselves, each other, or the transmembrane region of Ole1p^{i}.

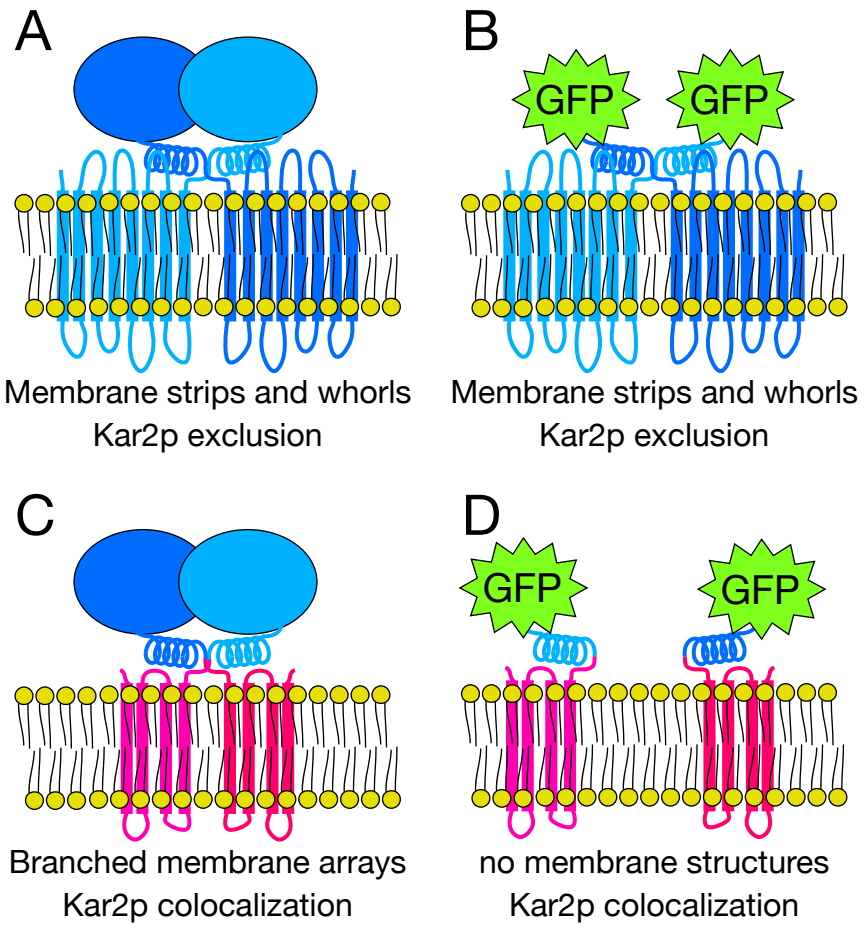
A
B
GFP
GFP
Membrane strips and whorls
Kar2p exclusion
Membrane strips and whorls
Kar2p exclusion
C
D
GFP
GFP
Branched membrane arrays
Kar2p colocalization
no membrane structures
Kar2p colocalization

Ole1p was not sufficient to reorganize membranes, as was the case with the HMGR cytoplasmic domains (Figure 2.8D). In addition, the TM domain of Hmg2p^{s} alone was not sufficient to reorganize membranes. Therefore, we propose that there is an intermolecular interaction that occurs between the TM domain of one Hmg2p and the cytoplasmic helical N-domain of a second Hmg2p (Figure 2.8A and B). The lack of structure formation by 6myc-Hmg2p-GFP, which is the Hmg2p TM, linker, and helical N-domain fused to GFP and a grossly misfolded TM domain due to the insertion of the 6myc tag, supports this model. We do not know if any folded cytoplasmic domain would facilitate this interaction or if there is a shared feature between GFP and the cytosolic domain of Hmg2p. These findings illustrate another parallel between Hmg2p and Hmg1p, in that TM and cytoplasmic domains both contribute to structure formation.

The TM domain

The structures generated in response to overexpressed Hmg1p and Hmg2p have distinctive features associated with them. Both generate smooth, unbranched membranes that are closely associated into stacks. The Ole1p^{i}-HMGR cytoplasmic domain arrays are highly branched, bearing little resemblance to either Hmg1p or Hmg2p-induced stacks. Additionally, Hmg1p and Hmg2p have distinct localization profiles with respect to Kar2p. Simply, Hmg1p-induced structures colocalize with Kar2p whereas those generated by

Hmg2p do not. Both of the Ole1p^{i} fusions to the Hmg1p and Hmg2p cytosolic domains resulted in membrane arrays that colocalize with Kar2p. These findings suggest that the TM domain dictates this inclusion/exclusion from the resultant structures.

Hmg2p overexpression results in the formation of ER structures, and these structures exclude Kar2p, which could make these regions that lack Kar2p unique subdomains of the ER. This Kar2p exclusion could be a feature of the ER structures or of the Hmg2p, or both. Our findings with Hmg2p variants that do not generate ER structures revealed that surprisingly, it is a feature of the TM domain of Hmg2p.

Increased expression of the Hmg2p TM domain alone is not sufficient to reorganize membranes, however, it is sufficient to maintain the discrete localization between itself and Kar2p. Precisely what features of the TM domain are required are not known at this point. However, we observed extensive colocalization between Kar2p and Hmg2p in a *cod1/spf1* null and between Kar2p and 6myc-Hmg2p, two independent situations in which the Hmg2p TM domain is grossly misfolded. Therefore, there might be a structural component of the TM domain that is required to maintain separation from Kar2p, and potentially other ER components. The mechanism by which Hmg2p is spatially maintained away from Kar2p within the continuous membrane network of the ER will be interesting to uncover.

New genes involved in Hmg2p membrane reorganization

Identifying the features of Hmg2p enabled us to design our screen using a version of Hmg2p with the minimal determinants for generating its characteristic structures. Our co-culture analysis revealed that the catalytic activity of Hmg2p, which is not required for Hmg2p-structure formation, imposes a significant stress on the cells. Surprisingly, the membrane reorganization that occurs in response to elevated levels of Hmg2p, revealed by the inactive Hmg2p, Hmg2p^{si}, caused only a very small, albeit reproducible, growth defect. This cellular effect was one of the first indications that there may be genes required for generating the cellular response to elevated levels of Hmg2p.

Utilizing the yeast haploid array enabled us to conduct a facile visual morphological screen. Rather than examine the membranes directly, we scored the localization of an optical reporter, Hmg2p^{s}-GFP*, as an indicator of membrane structures. In this way, we have successfully identified genes involved in Hmg2p-induced membrane reorganization. These genes are specifically required for the formation of Hmg2p^{s}-GFP* membrane structures. We were not surprised to discover that full-length Hmg2p^{s} is distributed normally in many of the new mutants identified. We knew that the membrane-anchored cytoplasmic domain of HMGR is sufficient to alter ER structure when anchored to the ER via an independent TM protein (Figure 2.8B). Therefore,

identifying mutants that affected both the cytosolic domain interactions and the interactions involving the TM domain was unlikely. Our goal was to identify genes that are required for the Hmg2p-specific structures, and this screen has identified several.

Among the genes that were uncovered were two that have been previously identified as required for general ER morphology, *NEM1* and *SPO7*. In our initial screen, we identified *NEM1*, and based on the known role of this protein in ER and nuclear morphology, tested its binding partner, *SPO7*. These genes did not fit our stringent criteria as genes that were specifically required for Hmg2p-induced structures, as opposed to being involved in general ER morphology. However, all of the other genes identified were specifically required for Hmg2ps-GFP*-induced ER alterations.

Those genes that are specifically required for Hmg2p-induced ER structures fell into two distinct classes, Class II and Class III, categorized using the localization of Hmg2p^{s}-GFP* by live cell imaging. Class III nulls no not have observable membrane structures. On the other hand, Class II nulls appear to generate nuclear-associated membrane arrays, similar to those caused by Hmg1p observed in both live cell imaging and immunofluorescence.

Interestingly, we did not uncover any of the VPS genes, which are necessary for karmellae formation by Hmg1p [15]. In fact, none of the Class II or III genes have been previously implicated in ER morphology. Of particular

interest is the *PSD1* gene. Psd1p is an enzyme that generates phosphatidylethanolamine by decarboxylating phosphatidylserine (for review, see [33]). In fact, yeast rely heavily on the methylation pathway, which utilizes Psd1p, for generating the majority of cellular phosphatidylethanolamine and phosphatidylcholine. In our screen, the ORF, *YNL170W* was identified as an interesting candidate. However, upon closer examination, we found that it overlapped with *YNL169C*, the ORF of *PSD1*. By generating non-overlapping deletions of each of these coding regions, we were able to determine that the loss of *PSD1* was responsible for the interesting phenotype we observed. This is the first phospholipid biosynthetic enzyme identified in Hmg2p-induced structure formation. In addition to this phospholipid biosynthetic gene, we also uncovered other ER proteins, including *ERG28* and *COD1/SPF1*. Unraveling how this gene, and the others contribute to specific ER morphology induced by Hmg2p overexpression will be exciting.

Methods:

Strains, Recombinant DNA Methods, and Media - Yeast strains RHY471 (*MATα ade2-101 met2 lys2-801 his3Δ200 ura3-52*) and RHY2863 (*MATa ade2-101 met2 lys2-801 his3Δ200 ura3-52 trp1Δ::hisG leu2Δ*) were the parents for all strains in these experiments, except for RHY3013 which was used for the genetic screen. RHY3013 is derived from Y3656 (*MATα lys2Δ0 ura3Δ leu2Δ0 his3Δ0 met15Δ0 can1Δ::MFA1pr-HIS3-Mfalpha1pr-LEU2*) [24]. Plasmids were constructed using standard DNA techniques. Specific oligo sequences and plasmid construction methods will gladly be provided upon request. Strains were gown at 30°C in indicated media.

Electron Microscopy - Cells were prepared for EM as described by [34]. Briefly, cells were grown to $0.65 \leq OD_{600} \geq 1.0$ in YPD, fixed with 4% glutaraldehyde, postfixed with 2% potassium permanganate, en bloc stained with 1% uranyl acetate, dehydrated and embedded in Spurr's resin. Eighty nm thick sections were cut and post-stained with Sato lead before visualizing on a JEOL 1200 KeV microscope.

Western Blot - Whole cell lysates were prepared via a general TCA method. Two to 10 OD_{600} units of cells were collected and resuspended in 900 µl water. 100% TCA was added before a 30 minute incubation on ice. Cells were pelleted, washed twice with acetone and resuspended in 100 µl of TCA

boiling buffer (50mM Tris pH 7.5, 1mM EDTA, 1% SDS, 6M urea). Beads were added prior to vortexing for 5 minutes. Lysates were heated to 50°C for 10 minutes prior to a 5-minute spin at 13K in a microfuge. Supernatant was transferred to a new tube and protein was quantitated using the Bradford method. 10 μg of protein was loaded onto either 8 or 14% SDS-PAGE gels, run electrophoretically, transferred onto nitrocellulose and placed in TBST (10 mM Tris, pH 8.0, 140 mM NaCl, 0.05% Tween 20) with 2% Carnation nonfat dried milk (2% TBSTM). Blots were then incubated with either α-myc 9E10 1:500, rabbit α-Hmg2p loop 1,2 (1:650), or rabbit α-PGK (1:10000) washed, and probed with goat anti-mouse HRP or goat anti-rabbit HRP (Jackson Immunologicals) 1:12,500, rinsed with ddH_2O, and scanned on a Typhoon phosphorimager after ECL plus exposure (GE Health).

Co-culture Fitness Assays - Isogenic strains that differed in only the gene expressed from the same constitutive promoter (*TDH3*) at the *URA3* locus were compared in this assay. Single colonies were grown in synthetic complete liquid media lacking uracil to log phase, $0.1 \leq OD_{600} \geq 0.5$. The cultures were adjusted to an $OD_{600} = 0.05$ and 1 ml of each culture (one bright and one dark) was added to the same tube and thoroughly mixed to generate the co-culture. A 300 μl aliquot of each co-culture was then removed for analysis by flow cytometry. The co-cultures were then diluted to $OD_{600} = 5 \times 10^{-5}$, final volume

2.5 ml, and allowed to grow for about 24 hours. Then the cell density was determined, a sample analyzed by flow cytometry, and the culture diluted again for the next day. Log phase growth was maintained at all times.

Immunofluorescence - The protocol for immunofluorescence was adapted from [35]. Briefly, 6-10 ml of cells were grown in YPD to $0.5 < OD_{600} > 1.0$. Formaldehyde was added to 4%, and cells were fixed for 1 hour at room temperature. Cells were washed twice in 1 ml IF Buffer (1mM $KHPO_4$ pH 7.4, 1.2M sorbitol) and resuspended in 200 μl IF Buffer with 10 μg/ml zymolyase 100T. Cells were incubated at 30°C for 20-25 minutes to spheroplast cells, followed by one wash with 1ml IF Buffer, then a second wash with 1ml PBS. Cells were resuspended in 1 ml PBS an adhered to poly-L-lysine coated pre-printed slides (Carlson Scientific). Cells were blocked with 1% BSA/ 0.5% Tween in PBS for 1 hour, primary antibodies were added for 1 hour at the following dilutions 9E10 ascites (myc): 1:750 and anti-Kar2p: 1:1500. Wells were washed 5x 5 minutes in block solution, and secondary antibodies were added at 1:500 dilution for 40 minutes (Invitrogen Probes, goat α-rabbit Alexa Fluor 595 and goat α-mouse Alexa Fluor 488). Wells were washed as before, coated with Vectashield containing DAPI (Vector Labs), covered with a coverslip, and sealed with nail polish. Images were captured on a Leica DM6000 spinning disk confocal unit.

Genetic Screen - Strain RHY3013 expressed Hmg2p^{s}-GFP* from the inducible *GAL1-10* promoter, which was integrated at the *ADE2* locus and marked with the nourseothricin (CloNAT) resistance gene, NatMX. This strain was crossed robotically to the haploid null collection as described [24]. Colonies were grown on glucose then patched onto raffinose for 24 hours, followed by patching onto galactose plates for 18 hours prior to scoring. Knockout strains that mislocalized Hmg2p^{s}-GFP* were noted as interesting candidates.

Live Cell Imaging - Cells were grown to log phase $0.3 < OD_{600} > 0.6$ in appropriate synthetic complete media, pelleted for 3 minutes at 6K RPM in a tabletop microcentrifuge, and resuspended in 50 μl of PBS. Cells were then visualized on a DeltaVision microscope equipped with appropriate filter sets.

Table 2.3: Strains used in Chapter 2. Unless specified otherwise, all genes are expressed from the *TDH3* promoter. Parent strains are in bold.

Strain	Genotype	Plasmid
RHY471	***MATα ade2-101, ura3-52, met2, lys2-801, his3Δ200***	none
RHY2739	*ade2-101::ADE2::GAL1-10pr::1MYC-HMG2 K6R*	pRH1571
RHY2740	*ade2-101::ADE2::GAL1-10pr::1MYC-HMG1*	pRH1584
RHY3326	*ura3-52::URA3::6MYC-HMG2-GFP, hrd1::KanMX*	pRH1694
RHY2863	***MATa ade2-101, ura3-52, met2, lys2-801, his3Δ200, trp1::hisG, leu2Δ***	none
RHY6433	*ura3-52::URA3::1MYC-HMG2 K6R*	pRH2218
RHY6531	*ade2-101::ADE2::1MYC-HMG1*	pRH1593
RHY6908	*ade2-101::ADE2::3MYC-OLE1-GFP* H161A, H166A*	pRH2416
RHY6906	*ade2-101::ADE2::3MYC-OLE1-GFP H161A, H166A*	pRH2411
RHY6907	*ade2-101::ADE2::3MYC-OLE1-CD1 H161A, H166A*	pRH2414
RHY6904	*ade2-101::ADE2::3MYC-OLE1-CD2 H161A, H166A*	pRH2406
RHY6123	*ura3-52::URA3::3MYC-OLE1 H161A, H166A*	pRH1828
RHY6334	*ade2-101::ADE2::1MYC-HMG2 K6R, D711N, E920Q*	pRH2108
RHY6333	*ura3-52::URA3::1MYC-HMG2Δ618-1045 K6R (HMG2 TM)*	pRH2251
RHY6934	*ade2-101::ADE2::1MYC-HMG2Δ672-1045 K6R (HMG2 TM*)*	pRH2429
RHY5590	*ura3-52::URA3::HMG2-GFP* K6R*	pRH2171
RHY6933	*ade2-101::ADE2::HMG2-GFP K6R*	pRH2427
RHY6131	*ura3-52::URA3::GFP*	pRH1743
RHY6128	*ura3-52::URA3::HMG2Δ1-527 (CD of HMG2)*	pRH2229
RHY6129	*ura3-52::URA3::HMG2Δ1-527, E711Q, D920N (inactive CD of HMG2)*	pRH2134
RHY6085	*ura3-52::URA3*	pRH313
RHY6442	*ade2-101::ADE2::1MYC-HMG2 K6R, ura3-52::URA3::1MYC-HMG2 K6R*	pRH2218, pRH1576
RHY6635	*ade2-101::ADE2::1MYC-HMG1, ura3-52::URA3::1MYC-HMG1*	pRH945, pRH1593
RHY6921	*ade2-101::ADE2::3MYC-OLE1-GFP* H161A, H166A, ura3-52::URA3::3MYC-OLE1-GFP* H161A, H166A*	pRH2416, pRH2413
RHY6922	*ade2-101::ADE2::3MYC-OLE1-GFP H161A, H166A, ura3-52::URA3::3MYC-OLE1-GFP H161A, H166A*	pRH2411, pRH2415
RHY6927	*ade2-101::ADE2::3MYC-OLE1-CD1 H161A, H166A, ura3-52::URA3::3MYC-OLE1-CD1 H161A, H166A*	pRH2414, pRH2418
RHY6928	*ade2-101::ADE2::3MYC-OLE1-CD2 H161A, H166A, ura3-52::URA3::3MYC-OLE1-CD2 H161A, H166A*	pRH2406, pRH2407

Table 2.3: Strains used in Chapter 2, continued.

Strain	Genotype	Plasmid
RHY6543	*ade2-101::ADE2::3MYC-OLE1 H161A, H166A, ura3-52::URA3::3MYC-OLE1 H161A, H166A*	pRH1828, pRH2107
RHY6409	*ade2-101::ADE2::1MYC-HMG2 K6R, D711N, E920Q, ura3-52::URA3::HMG2 K6R, D711N, E920Q*	pRH2108, pRH2232
RHY6372	*ade2-101::ADE2::1MYC-HMG2Δ618-1045 K6R (HMG2 TM), ura3-52::URA3::1MYC-HMG2Δ618-1045 K6R (HMG2 TM)*	pRH2251, pRH2264
RHY6943	*ade2-101::ADE2::1MYC-HMG2Δ672-1045 K6R (HMG2 TM*), ura3-52::URA3::1MYC-HMG2Δ672-1045 K6R (HMG2 TM*)*	pRH2429, pRH2430
RHY6194	*ade2-101::ADE2::HMG2-GFP* K6R, ura3-52::URA3::HMG2-GFP* K6R*	pRH2171, pRH1738
RHY6942	*ade2-101::ADE2::HMG2-GFP K6R, ura3-52::URA3::HMG2-GFP K6R*	pRH2427, pRH2428
RHY5609	*ura3-52::URA3::HMG2-GFP* K6R, nem1Δ::KanMX*	pRH2171
RHY5594	*ura3-52::URA3::HMG2-GFP* K6R, hof1Δ::KanMX*	pRH2171
RHY5599	*ura3-52::URA3::HMG2-GFP* K6R, hpe2Δ::KanMX*	pRH2171
RHY6034	*ura3-52::URA3::HMG2-GFP* K6R, cod1/spf11Δ::KanMX*	pRH2171
RHY6195	*ade2-101::ADE2::HMG2-GFP* K6R, ura3-52::URA3::HMG2-GFP* K6R, cod1/spf1Δ::KanMX*	pRH2171, pRH1738
Y3656	***MATα lys2Δ0 ura3Δ leu2Δ0 his3Δ0 met15Δ0 can1Δ::MFA1pr-HIS3-Mfalpha1pr-LEU2***	none
RHY3013	*ADE2::NatMX::GAL1-10pr::Hmg2p^{s}-GFP**	pRH2978

Acknowledgements:

Amy Tong generated the yeast haploid array containing the *GAL1-10pr* driven Hmg2p^{s}-GFP* expression plasmid. Ying Jones acquired all of the electron microscopy images. I thank Scott Emr for use of the DeltaVision microscope, and Gentry Patrick for use of the Leica DM6000 microscope. Thanks also to Robert Rickert and Michael David for FACScalibur flow cytometer access and to Tracy Johnson and Maho Niwa for use of the Typhoon Phosphorimager. I also thank Randy Hampton and Alicia Bicknell for critical reading of this chapter.

Chapter 2 is a manuscript in preparation that will be submitted for publication.

References:

1. Wiest DL, Burkhardt JK, Hester S, Hortsch M, Meyer DI, Argon Y: **Membrane biogenesis during B cell differentiation: most endoplasmic reticulum proteins are expressed coordinately**. *J Cell Biol* 1990, **110**:1501-1511.

2. Wright R, Basson M, D'Ari L, Rine J: **Increased amounts of HMG-CoA reductase induce "karmellae": a proliferation of stacked membrane pairs surrounding the yeast nucleus**. *J Cell Biol* 1988, **107**:101-114.

3. Black VH: **The development of smooth-surfaced endoplasmic reticulum in adrenal cortical cells of fetal guinea pigs**. *Am J Anat* 1972, **135**:381-417.

4. Menzel R, Kargel E, Vogel F, Bottcher C, Schunck WH: **Topogenesis of a microsomal cytochrome P450 and induction of endoplasmic reticulum membrane proliferation in Saccharomyces cerevisiae**. *Arch Biochem Biophys* 1996, **330**:97-109.

5. Jones AL, Fawcett DW: **Hypertrophy of the agranular endoplasmic reticulum in hamster liver induced by phenobarbital (with a review on the functions of this organelle in liver)**. *J Histochem Cytochem* 1966, **14**:215-232.

6. Federovitch CM, Ron D, Hampton RY: **The dynamic ER: experimental approaches and current questions**. *Curr Opin Cell Biol* 2005, **17**:409-414.

7. Istvan ES, Palnitkar M, Buchanan SK, Deisenhofer J: **Crystal structure of the catalytic portion of human HMG-CoA reductase: insights into regulation of activity and catalysis**. *Embo J* 2000, **19**:819-830.

8. Sisson JK, Fahrenbach WH: **Fine structure of steroidogenic cells of a primate cutaneous organ**. *Am J Anat* 1967, **121**:337-367.

9. Chin DJ, Luskey KL, Anderson RG, Faust JR, Goldstein JL, Brown MS: **Appearance of crystalloid endoplasmic reticulum in compactin-resistant Chinese hamster cells with a 500-fold increase in 3-hydroxy-3-methylglutaryl-coenzyme A reductase**. *Proceedings of the National Academy of Sciences of the United States of America* 1982, **79**:1185-1189.

10. Basson ME, Thorsness M, Rine J: **Saccharomyces cerevisiae contains two functional genes encoding 3- hydroxy-3-methylglutaryl-coenzyme A reductase**. *Proc Natl Acad Sci U S A* 1986, **83**:5563-5567.

11. Koning AJ, Roberts CJ, Wright RL: **Different subcellular localization of Saccharomyces cerevisiae HMG-CoA reductase isozymes at elevated levels**

corresponds to distinct endoplasmic reticulum membrane proliferations. *Molecular Biology of the Cell* 1996, **7**:769-789.

12. Parrish ML, Sengstag C, Rine JD, Wright RL: **Identification of the sequences in HMG-CoA reductase required for karmellae assembly**. *Molecular Biology of the Cell* 1995, **6**:1535-1547.

13. Profant DA, Roberts CJ, Koning AJ, Wright RL: **The role of the 3-hydroxy 3-methylglutaryl coenzyme A reductase cytosolic domain in karmellae biogenesis**. *Molecular Biology of the Cell* 1999, **10**:3409-3423.

14. Profant DA, Roberts CJ, Wright RL: **Mutational analysis of the karmellae-inducing signal in Hmg1p, a yeast HMG-CoA reductase isozyme**. *Yeast* 2000, **16**:811-827.

15. Koning AJ, Larson LL, Cadera EJ, Parrish ML, Wright RL: **Mutations That Affect Vacuole Biogenesis Inhibit Proliferation of the Endoplasmic Reticulum in Saccharomyces cerevisiae**. *Genetics* 2002, **160**:1335-1352.

16. Wright R, Parrish ML, Cadera E, Larson L, Matson CK, Garrett-Engele P, Armour C, Lum PY, Shoemaker DD: **Parallel analysis of tagged deletion mutants efficiently identifies genes involved in endoplasmic reticulum biogenesis**. *Yeast* 2003, **20**:881-892.

17. Loertscher J, Larson LL, Matson CK, Parrish ML, Felthauser A, Sturm A, Tachibana C, Bard M, Wright R: **Endoplasmic reticulum-associated degradation is required for cold adaptation and regulation of sterol biosynthesis in the yeast Saccharomyces cerevisiae**. *Eukaryot Cell* 2006, **5**:712-722.

18. Hampton RY: **ER-associated degradation in protein quality control and cellular regulation**. *Curr Opin Cell Biol* 2002, **14**:476-482.

19. Gardner RG, Hampton RY: **A 'distributed degron' allows regulated entry into the ER degradation pathway**. *Embo Journal* 1999, **18**:5994-6004.

20. Hampton RY, Koning A, Wright R, Rine J: **In vivo examination of membrane protein localization and degradation with green fluorescent protein**. *Proceedings of the National Academy of Sciences of the United States of America* 1996, **93**:828-833.

21. Osterberg M, Kim H, Warringer J, Melen K, Blomberg A, von Heijne G: **Phenotypic effects of membrane protein overexpression in Saccharomyces cerevisiae**. *Proc Natl Acad Sci U S A* 2006, **103**:11148-11153.

22. Basson ME, Moore RL, O'Rear J, Rine J: **Identifying mutations in duplicated functions in Saccharomyces cerevisiae: recessive mutations in HMG-CoA reductase genes**. *Genetics* 1987, **117**:645-655.

23. Snapp EL, Hegde RS, Francolini M, Lombardo F, Colombo S, Pedrazzini E, Borgese N, Lippincott-Schwartz J: **Formation of stacked ER cisternae by low affinity protein interactions**. *J Cell Biol* 2003, **163**:257-269.

24. Tong AH, Evangelista M, Parsons AB, Xu H, Bader GD, Page N, Robinson M, Raghibizadeh S, Hogue CW, Bussey H, et al.: **Systematic genetic analysis with ordered arrays of yeast deletion mutants**. *Science* 2001, **294**:2364-2368.

25. Santos-Rosa H, Leung J, Grimsey N, Peak-Chew S, Siniossoglou S: **The yeast lipin Smp2 couples phospholipid biosynthesis to nuclear membrane growth**. *Embo J* 2005, **24**:1931-1941.

26. Siniossoglou S, Santos-Rosa H, Rappsilber J, Mann M, Hurt E: **A novel complex of membrane proteins required for formation of a spherical nucleus**. *Embo J* 1998, **17**:6449-6464.

27. Cronin SR, Khoury A, Ferry DK, Hampton RY: **Regulation of HMG-CoA reductase degradation requires the P-type ATPase Cod1p/Spf1p**. *Journal of Cell Biology* 2000, **148**:915-924.

28. Shearer AG, Hampton RY: **Structural control of endoplasmic reticulum-associated degradation: effect of chemical chaperones on 3-hydroxy-3-methylglutaryl-CoA reductase**. *J Biol Chem* 2004, **279**:188-196.

29. Cronin SR, Rao R, Hampton RY: **Cod1p/Spf1p is a P-type ATPase involved in ER function and Ca2+ homeostasis**. *J Cell Biol* 2002, **157**:1017-1028.

30. Vashist S, Frank CG, Jakob CA, Ng DT: **Two distinctly localized p-type ATPases collaborate to maintain organelle homeostasis required for glycoprotein processing and quality control**. *Mol Biol Cell* 2002, **13**:3955-3966.

31. Suzuki C: **Immunochemical and mutational analyses of P-type ATPase Spf1p involved in the yeast secretory pathway**. *Biosci Biotechnol Biochem* 2001, **65**:2405-2411.

32. Hampton RY, Gardner RG, Rine J: **Role of 26S proteasome and HRD genes in the degradation of 3-hydroxy-3-methylglutaryl-CoA reductase, an integral endoplasmic reticulum membrane protein**. *Molecular Biology of the Cell* 1996, **7**:2029-2044.

33. Voelker DR: **Phosphatidylserine decarboxylase**. *Biochim Biophys Acta* 1997, **1348**:236-244.

34. Wright R: **Transmission electron microscopy of yeast**. *Microsc Res Tech* 2000, **51**:496-510.

35. Pringle JR, Adams AE, Drubin DG, Haarer BK: **Immunofluorescence methods for yeast**. *Methods Enzymol* 1991, **194**:565-602.

Chapter 3:

Hmg2p-induced membrane proliferation

Abstract:

The endoplasmic reticulum (ER) is large, plastic organelle that can undergo dramatic changes in shape and size. Increased demand on any of the ER functions, including protein folding, lipid biosynthesis, and drug detoxification can bring about these changes. HmgCoA reductase (HMGR) is an ER localized enzyme that converts mevalonate to HMG-CoA, as key step in sterol biosynthesis. Elevated levels of this protein cause a profound change in ER structure that is often referred to as ER proliferation. However, the distinction between ER membrane proliferation and ER membrane reorganization has not been clearly delineated. In this work, we differentiate between Hmg2p-induced ER reorganization and Hmg2p-induced membrane proliferation by directly examining phospholipid abundance in cells. Our analysis reveals that only the full-length, enzymatically active Hmg2p causes an increase in phospholipid abundance when overexpressed. Furthermore, we demonstrate that Hmg2p-induced membrane proliferation is coordinated with a change in phospholipid composition, both of which require the phospholipid biosynthetic enzyme Psd1p. Specifically, Hmg2p overexpression causes a decrease in phosphatidylserine levels and an increase in phosphatidylcholine levels.

Introduction:

The endoplasmic reticulum (ER) is a highly dynamic and plastic organelle. As the site of protein folding, lipid biosynthesis, and drug detoxification, the demands on the ER are high and constantly changing. Occurrences of altered ER morphology and expansion have been noted in response to a variety of cellular situations ranging from B-cell differentiation, which proliferates the rough ER, to single protein overexpression, which induces hypertrophy of the smooth ER.

Despite the wide array of circumstances in which changes in ER need and/or morphology are observed, there is a scarcity of quantitative analysis regarding the expansion of ER membranes. The ER, being such a prominent organelle, has been the focus of many microscopic studies, which have dominated the membrane proliferation field. Although these analyses are valuable, they have limited ability to expand the understanding of the underlying mechanisms involved in mediating these physiological occurrences. In many cases, it has been assumed that the striking arrays of ER are indicative of increased phospholipid content.

There are means of directly altering the expression of phospholipid biosynthetic enzymes, which increases cellular phospholipids. The yeast lipin, Smp2p negatively regulates transcription of phospholipid biosynthetic genes

when phosphorylated by the Nem1p/Spo7p complex [1]. Cells lacking any of these three components are reported to proliferate nuclear and smooth ER membranes, as observed by microscopy, however the extent of phospholipid increase in these cells has not yet been determined. In these cells, mRNA transcripts of key phospholipid biosynthetic genes, such as *INO1*, are elevated when transcriptional regulation by Smp2p is abolished [1,2], which suggests an increase in cellular phospholipids. Furthermore, the upregulation of *INO1* transcripts in this case is not dependant on unfolded protein response (UPR), a conserved signaling pathway that responds to accumulation of misfolded proteins that has been implicated in ER proliferation.

There are also many cases in which increased expression of single membrane proteins causes a striking change in ER membranes. Phenobarbital treatment in animal models causes a profound increase in smooth ER membranes, presumably due to elevated expression of the drug-detoxifying gene, cytochrome P450 (CYP450) [3,4]. In yeast, CYP450 overexpression has been reported to increase total cellular phospholipids ~1.3-fold, by direct analysis of phospholipid content. This phospholipid increase occurs normally in the absence of the UPR. However, the UPR is required for upregulation of *INO1* mRNA that occurs when CYP450 levels are elevated [5]. This calls into question whether or not mRNA quantitation can be used as a reliable indicator of phospholipid biosynthesis.

Increased expression of HMG-CoA Reductase (HMGR), the essential enzyme that converts mevalonate to HMG-CoA in sterol biosynthesis, causes a striking alteration of ER membranes. Changes in ER morphology that occur in response to elevated expression of HMGR have been observed since the 1950's, when smooth ER elaborations were first documented in the fetal adrenal glands [6]. At the time, however, it was not known that HMGR levels were elevated in these cell types. Tissue culture lines have since been generated to overexpress HMGR, which phenocopies the ER arrays observed in natural cell types, such as adrenal cortical cells [7]. This ability to proliferate membranes in response to HMGR is conserved, and occurs upon increased expression of HMGR in yeast, enabling genetic studies [8,9].

The term proliferation is used to describe the morphological alterations observed via light and electron microscopy when HMGR levels are elevated. However, a biochemical analysis of phospholipid content has never been conducted to distinguish whether these changes are due to actual increases in phospholipids or rearrangement of existing membranes. For example, analysis of a multimerizing GFP in mammalian cells by Snapp and colleagues demonstrated that fusion of a multimerizing protein to a transmembrane protein is sufficient to dramatically reorganize ER structure, but not necessarily to increase phospholipid abundance [10].

In addition, little is understood regarding the molecular mechanisms that govern these changes in ER morphology. Extensive studies in mammalian systems have demonstrated close coordination between sterol, fatty acid and phospholipid biosynthesis through transcriptional regulation mediated by the sterol regulatory element binding proteins (SREBPs) (for reviews, see [11,12]). However an analogous signaling pathway to that of the mammalian SREBP has yet to be uncovered in yeast. In fact, until recently (Chapter 2), no lipid biosynthetic genes have been shown to play a role in HMGR proliferation in yeast.

In this study, we examine cases in which Hmg2p, one of the yeast HMGR isozymes, can proliferate membranes. We have determined that although increased expression of many Hmg2p variants can alter ER membrane structures, only the full-length, enzymatically active protein stimulates an increase in phospholipids. Contrary to widely-held views in the field, we found many instances of dramatic alteration in ER morphology that were not accompanied by an increase in phospholipids. When full-length Hmg2p is overexpressed, the increase in phospholipids is coordinated with an alteration of phospholipid composition, suggesting a role for the lipid biosynthetic enzyme, Psd1p in the cellular response to Hmg2p overexpression. This is the first evidence for an Hmg2p-induced signaling response in yeast, and couples membrane proliferation to sterol biosynthesis.

Results:

Phospholipid and cell volume quantitation

In setting out to quantitate phospholipids, we found that choice of normalization was varied in the literature. Although DNA quantity, optical density (OD), and protein are common denominators for normalizing phospholipids, we used cell number (determined empirically for every culture in each assay) to normalize our data. In this way, variables such as cell size, granularity, and shape did not affect our analysis. For example, if we normalized to protein or OD with cells that overexpress Ole1p (see below), our equation would not factor in the change in cell size, thus phospholipids would not be reported to increase accurately.

The volume analysis of cells was important in interpreting changes in phospholipid amount that occurred. Because small changes in radius result in large volume changes, precise measurements were required. As opposed to radius or diameter measurements via optical means, and subsequent volume calculations, we measured cell size using a Multisizer^{TM} 3 Coulter Counter®. This method directly measures particle (cell) volume.

Before analyzing Hmg2p overexpression, we wanted to generate a baseline for the magnitude of expected increases in total cellular phospholipids, using some conditions with known effects on lipid pathways, since little

quantitative analysis has been conducted in yeast under conditions of membrane proliferation. We began by examining genetic conditions in which phospholipid increases seemed most probable. First we examined cells in which phospholipid biosynthetic genes were directly upregulated. We then examined cells with increased production of fatty acids – essential components of phospholipids.

Cells lacking *NEM1* have increased intracellular phospholipids

Cells lacking the Nem1p phosphatase are defective in down-regulating transcription of phospholipid biosynthetic genes [1]. In our strain background, *nem1* null cells have a similar morphology to that reported by Siniossoglou and colleagues [2]: cells have an abnormal nucleus and extended nuclear-associated strips of membranes (Figure 3.1A). However, direct quantitation of total phospholipid content in *nem1* null strains has not been reported. We directly measured phospholipids and found that *nem1* null cells had twice the amount of total phospholipid per cell than that of the corresponding wild type strain (Figure 3.1B). It is assumed that this increase in phospholipids is localized to the nuclear and ER membranes, however we could not discount the possibility that cell size might also be affected. By directly analyzing cell volume, we found that *nem1* null cells are comparable in size to wild type cells (Figure 3.1C).

Figure 3.1 Altering fatty acid or phospholipid synthesis has different effects on cells.

(A) Electron micrographs of representative cells as labeled: cells lacking *NEM1* (*nem1*Δ), expressing two copies of *TDH3pr*-driven enzymatically active Ole1p (Ole1p) or inactive Ole1p (Ole1p^{i}), and a wild type strain are shown. Membrane stacks are indicated with arrows, N - nucleus. (B) Phospholipid quantitation of a nem1 null strain, and strains expressing two copies of *TDH3pr*-driven enzymatically active Ole1p (Ole1p) or inactive Ole1p (Ole1p^{i}), compared to an isogenic wild type strain. Averages and standard errors are shown, n=3. ** - p-value < 0.005 (C) Cell volume of strains in B compared to an isogenic wild type strain. Averages and standard errors are shown, n=3. ** - p-value < 0.005

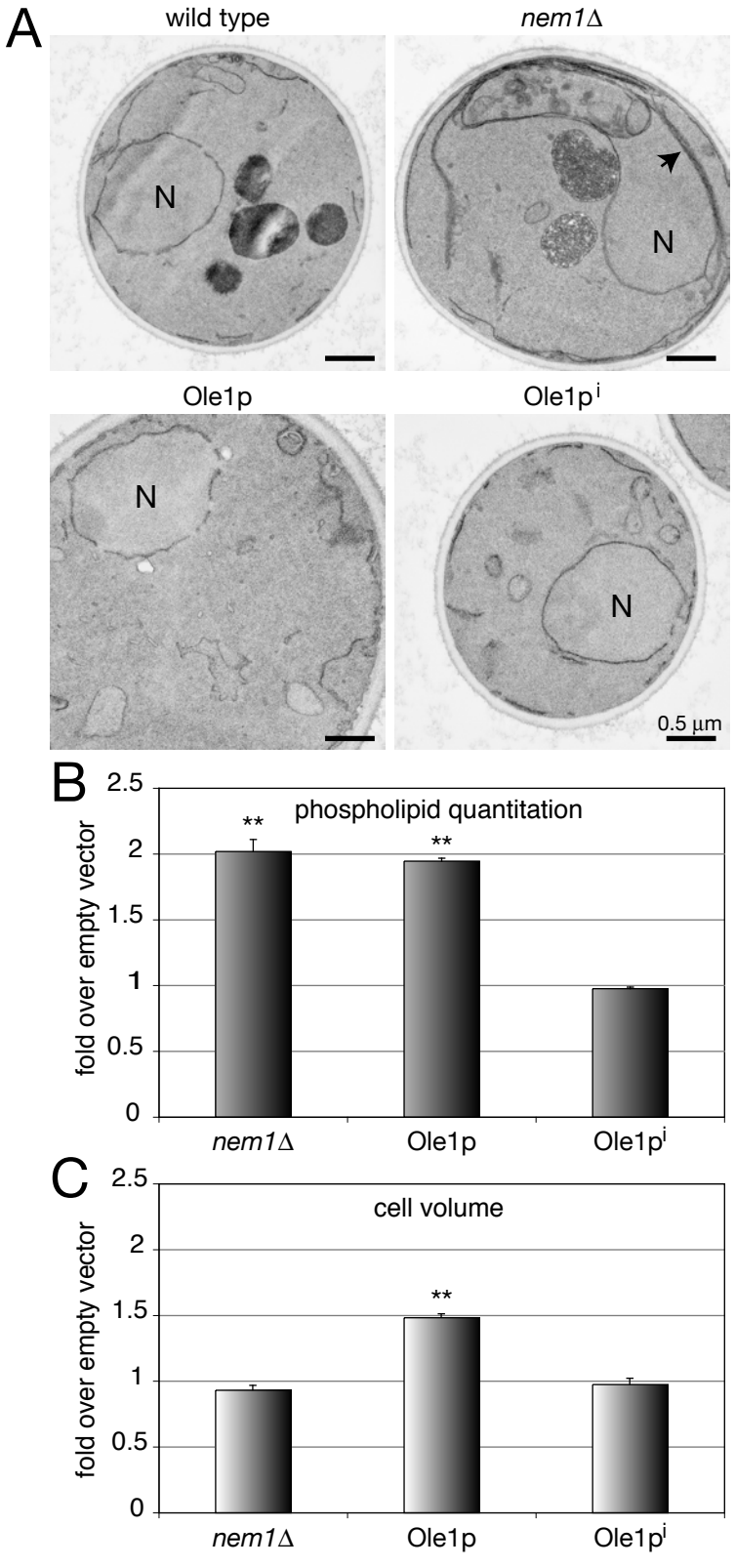
A
wild type
nem1Δ
N
N
Ole1p
Ole1p^i
N
N
0.5 μm
B
phospholipid quantitation
fold over empty vector
2.5
2
1.5
1
0.5
0
**
**
nem1Δ
Ole1p
Ole1p^i
C
cell volume
fold over empty vector
2.5
2
1.5
1
0.5
0
**
nem1Δ
Ole1p
Ole1p^i

Elevated Ole1p activity causes an increase in cell size

In mammalian cells, there is a close coordination between fatty acid, phospholipid, and sterol biosynthesis, so we posited that in yeast, increasing expression of a key enzyme in fatty acid biosynthesis could also affect cellular membranes. The essential Δ9 desaturase in yeast, Ole1p, is highly regulated at the level of transcription and mRNA stability (for review, see [13]). To test if increased expression of Ole1p would visibly alter cellular membranes, we expressed the *OLE1* ORF from the strong, constitutive *TDH3* promoter (*TDH3pr*), and introduced two copies of this plasmid into yeast cells. Upon inspection of these Ole1p overexpressing strains, it was clear that cell size was markedly increased (Figure 3.1A). Our volume analysis indicated that strains with elevated Ole1p activity were 1.5 times larger than wild type cells (Figure 3.1C). We determined that cells expressing Ole1p from the *TDH3pr* had twice as much phospholipid per cell than a comparable wild type strain (Figure 3.1B).

We verified that both the changes in cell size and increase in total cellular phospholipids were due to increased Ole1p activity by similarly expressing Ole1p with the H161A and H166A inactivating mutations (Ole1p^{i}). By microscopy, the strain expressing the inactive Ole1p appeared to be similar in size to the isogenic wild type strain (Figure 3.1A), which was confirmed by volume analysis (Figure 3.1C). As expected, the increase in phospholipids was also not observed when Ole1p^{i} was overexpressed (Figure 3.1B). These results

illustrate the importance of cell size when examining increases in cellular phospholipids, which validates our methodology for quantitating phospholipids.

Elevated HMGR expression increases total cellular phospholipids

We next evaluated the effect of elevating HMGR on total cellular phospholipids. *S. cerevisiae* has two isozymes of HMGR, Hmg1p and Hmg2p, both of which cause profound alteration of ER membranes when overexpressed (Figure 3.2A and [14]). Hmg1p is an extremely stable protein. Conversely, Hmg2p undergoes regulated ER-associated degradation (ERAD) (for review, see [15]). However, mutating K6 to arginine prevents Hmg2p from entering the ERAD pathway [16]. This modification allowed maximal expression of Hmg2p. Accordingly, the stabilizing K6R mutation was used throughout this work, referred to as Hmg2p^{s}.

To evaluate the effect that HMGR overexpression has on cellular phospholipids, we introduced one or two copies of our *TDH3pr* expression plasmids into yeast. Our quantitation of phospholipids in these strains indicated that, when present at two copies per cell, *TDH3pr*-driven Hmg1p and Hmg2p^{s} increase cellular phospholipids by 1.2 and 1.5 fold respectively, compared to wild type (Figure 3.2B). Previous reports have demonstrated that Hmg1p is 40% less abundant than Hmg2p when overexpressed under identical conditions (Chapter 2, and [17]). This difference in protein abundance might explain the difference in total phospholipid quantity observed. When we compared the

Figure 3.2 Increased expression of HMGR causes an increase in cellular phospholipids.

(A) Electron micrographs of cells with two integrated copies of *TDH3pr*-driven Hmg1p or Hmg2p^{s}. Membrane stacks are indicated with arrows, N- nucleus. (B) Phospholipid quantitation of strains with one (1x TDH3pr) or two (2x TDH3pr) integrated plasmids expressing *TDH3pr*-driven Hmg1p or Hmg2p^{s} compared to an isogenic wild type strain. Averages and standard errors are shown, n=3. * p-value = 0.098
(C) Cell volume of strains with two integrated copies of Hmg1p or Hmg2p^{s} compared to an isogenic wild type strain. Averages and standard errors are shown, n=3.

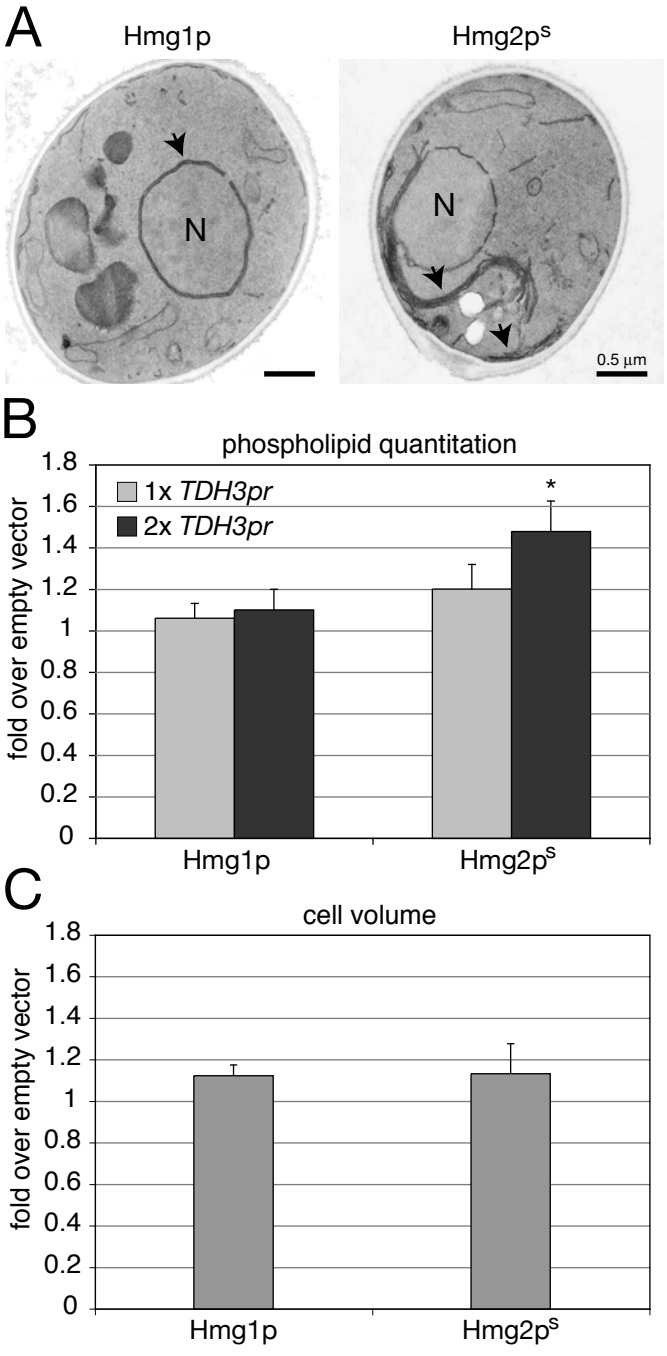
A
Hmg1p
Hmg2p^s
N
N
0.5 µm
B
phospholipid quantitation
1x TDH3pr
2x TDH3pr
*
fold over empty vector
1.8
1.6
1.4
1.2
1
0.8
0.6
0.4
0.2
0
Hmg1p
Hmg2p^s
C
cell volume
fold over empty vector
1.8
1.6
1.4
1.2
1
0.8
0.6
0.4
0.2
0
Hmg1p
Hmg2p^s

volume of cells with increased expression of Hmg1p or Hmg2p^{s} to a wild type strain, we observed that the volume was only slightly elevated in both cases (Figure 3.2C). However, unlike the phospholipid increase, which appeared to be dependant on level of protein expressed, the cell volume was comparable for the strains overexpressing Hmg1p or Hmg2p^{s}. This suggests that the increase in phospholipids was most likely not due to increased cell size.

Hmg2p enzyme activity is necessary to increase phospholipids

In our previous work, we examined the features of Hmg2p necessary to alter ER membranes (Chapter 2). To determine if the requirements for membrane proliferation by Hmg2p were the same as for ER membrane reorganization, we tested several Hmg2p variants. The enzymatic activity of Hmg2p is not required to reorganize membranes (Chapter 2, and Figure 3.3A). Introducing two conservative point mutations (E711Q and D920N) into the coding region of Hmg2p^{s} completely eliminates enzymatic function. However overexpression of this inactive Hmg2p (Hmg2p^{si}) still causes stacks and whorls of membrane to form (Figure 3.3A). In fact, partially (Hmg2p^{s}-GFP*) or completely (Hmg2p^{s}-GFP) replacing the catalytic domain with GFP, still allows ER structures to form (Figure 3.3A). Our previous studies have shown that the structure formation by the Hmg2p-GFP fusions is not a feature of the GFP (Chapter 2).

Figure 3.3 Catalytic activity of Hmg2p is not required to reorganize membranes, but is required to increase cellular phospholipids.

(A) Electron micrographs of cells with two integrated copies of *TDH3pr*-driven Hmg2p^{s} (stable Hmg2p), Hmg2p^{si} (stable, inactive Hmg2p), Hmg2p^{s}-GFP* (Hmg2p^{s} with last 375 aa of catalytic domain replaced with GFP), or Hmg2p^{s}-GFP (Hmg2p^{s} with entire catalytic domain replaced with GFP). Membrane stacks are indicated with arrows, N - nucleus. (B) Phospholipid quantitation of strains with two copies of *TDH3pr*-driven Hmg2p^{s}, Hmg2p^{si}, Hmg2p^{s}-GFP*, Hmg2p^{s}-GFP, or Hmg2p CD compared to an isogenic wild type strain. Averages and standard errors are shown, n=3. ** - p-value 0.016

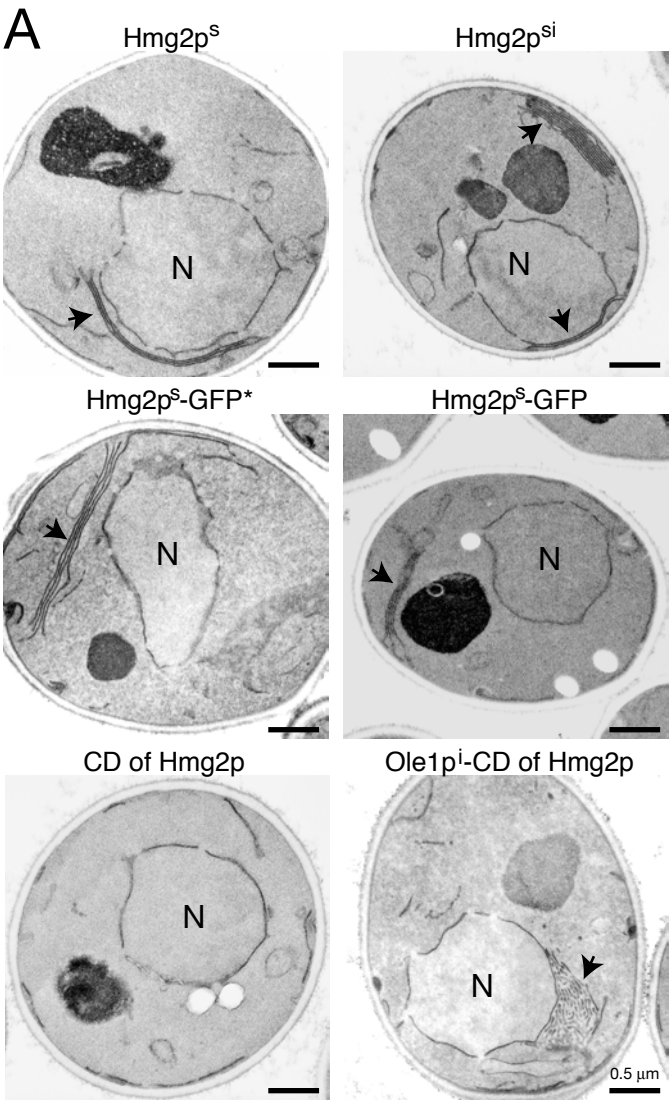
A
Hmg2p^s
Hmg2p^si
Hmg2p^s-GFP*
Hmg2p^s-GFP
CD of Hmg2p
Ole1p^i-CD of Hmg2p
N
0.5 μm
B
phospholipid quantitation
fold over empty vector
0
0.2
0.4
0.6
0.8
1
1.2
1.4
1.6
1.8
**
Hmg2p^s
Hmg2p^si
Hmg2p^s-GFP*
Hmg2p^s-GFP
CD of Hmg2p
Ole1p^i-CD of Hmg2p

When we examined these inactive variants of Hmg2p^{s}, we were surprised to find that no increase in phospholipids was observed (Figure 3.3B). These data demonstrate that striking changes in ER morphology are not necessarily an indication of membrane proliferation. Furthermore, the enzymatic activity of Hmg2p, which is not required to reorganize ER membranes, appeared to be a necessary component in membrane proliferation.

Elevated enzymatic activity of Hmg2p is not sufficient to increase phospholipids

Our results showed that enzymatic activity of overexpressed Hmg2p^{s} was required to increase total cellular phospholipids. To test if increased Hmg2p activity was sufficient, we expressed the soluble enzymatic portion of Hmg2p (CD of Hmg2p) from the strong *TDH3pr* and introduced two copies of this plasmid into cells. It has been previously shown that this soluble domain is enzymatically active [16]. Furthermore, these strains are highly resistant to lovastatin, a potent inhibitor of HMGR (data not shown). By electron microscopy, no ER structures were visible when this soluble protein was expressed (Figure 3.3A), and no increase in total cellular phospholipids was detected (Figure 3.3B). This result demonstrates that increased activity of Hmg2p is not sufficient to increase phospholipids.

We next evaluated if localization of the active catalytic domain of Hmg2p to the surface of the ER was sufficient to increase phospholipids. Our

previous work has demonstrated that anchoring the cytosolic domain of Hmg2p onto a transmembrane protein, such as Ole1p^{i} (Ole1p^{i}-CD of Hmg2p), causes a drastic rearrangement of the ER (Figure 3.3A and Chapter 2). When we examined effects of expressing this fusion protein on total cellular phospholipids however, no increase was observed (Figure 3.3B). These results confirm that increased Hmg2p activity is not sufficient to increase total cellular phospholipids, even when present at the surface of the ER.

Full-length, active Hmg2p^{s} is required to increase phospholipids

We evaluated if full-length active Hmg2p^{s} was required to increase phospholipids. One possibility was that increased HMGR catalytic activity and increased HMGR protein levels were two separate requirements. If this were the case, then co-expression of an inactive Hmg2p with the soluble catalytic domain of Hmg2p would be sufficient to increase membranes. We tested different combinations of *TDH3pr*-driven variants of Hmg2p, and engineered strains that had two expression plasmids for each protein. However, neither expression of Hmg2p^{s} TM (truncated immediately prior to the catalytic domain) or Hmg2p^{si} co-expressed with the soluble CD of Hmg2p increased total cellular phospholipids (data not shown). These data strongly suggest that elevated expression of the full-length active Hmg2p is necessary to increase phospholipids, implying that both the TM domain and catalytic activity have critical roles and that both these activities must reside within the same protein.

Proliferants Hmg2p^{s} and P450Cm1 do not stimulate the UPR

The unfolded protein response (UPR) is a signaling cascade that senses and responds to unfolded proteins in the ER (for review see [18]). Upon activation, the ER localized kinase, Ire1p, initiates splicing of *HAC1* mRNA, which then is translated into an active transcription factor to upregulate UPR target genes, such as *KAR2*, via unfolded protein response elements (UPREs) present in promoters.

The UPR has been implicated in proliferating ER membranes, particularly as a necessary part of B cell differentiation [19,20]. Upregulation of the UPR has also been reported by increased expression by the *Candida albicans* cytochrome P450 protein (P450Cm1) in *S. cerevisiae* as determined by *KAR2* mRNA transcript levels [5]. These studies showed that elevated expression of CYP450Cm1 increases total cellular phospholipids ~1.3 fold, which we independently confirmed (data not shown). Interestingly, the increase in phospholipid by increased CYP450Cm1 does not require the UPR. An extensive study by Larson and colleagues demonstrated that neither Hmg1p nor Hmg2p overexpression induces the UPR, as measured by *KAR2* mRNA levels [21].

We directly tested for induction of the UPR in response to elevated expression of the proliferants Hmg2p^{s} and CYP450Cm1 in two distinct assays, using CPY*, a misfolded protein known to induce the UPR, as a positive

control. In the first assay, we analyzed *HAC1* mRNA splicing. The second assay determines transcriptional activation by active Hac1p using a 4xUPRE::GFP reporter, and is quantitated by flow cytometry (described in [22]). We used the inducible *GAL1-10* promoter to express our proteins. Cells were grown in raffinose to eliminate glucose repression, and galactose was added to 4% for times indicated and we verified expression of our induced proteins by western blot (Figure 3.4A). Surprisingly, only expression of the misfolded protein, CPY*, caused transcriptional activation of the 4xUPRE::GFP reporter gene (Figure 3.4A). Direct examination of *HAC1* mRNA splicing was consistent with the GFP reporter, demonstrating that neither Hmg2p^{s} nor CYP450Cm1 stimulate *HAC1* splicing (Figure 3.4A). These data demonstrate that the induced expression of the proliferants, Hmg2p and CYP450Cm1 do not induce the UPR.

Neither the UPR nor autophagy affects the Hmg2p-induced increase in phospholipids

Menzel and colleagues clearly demonstrated that the phospholipid increase by CYP450Cm1 occurs in the absence of a functional UPR (*ire1*Δ strain) [5]. However, we did not know if the UPR had a role in Hmg2p-induced membrane proliferation. We introduced our Hmg2p^{s} expression plasmids into *ire1* null strains to test if the UPR was required to increase total cellular phospholipids and found that, like CYP450Cm1, it is not (Figure 3.4B). This

Figure 3.4 Neither the UPR nor autophagy affect phospholipid increases by Hmg2p.
(A) Expression of Hmg2p^{s}, P450Cm1, and CPY* from the *GAL1-10pr*, and corresponding effects on 4xUPRE::GFP induction, and *HAC1* splicing at times indicated. Cells were grown in raffinose and galactose was added to 4% for times indicated. Representative western blots indicating protein expression levels of *GAL1-10pr*-driven Hmg2p^{s}, P450Cm1, and CPY*, quantitation of 4xUPRE::GFP expression by flow cytometry, and corresponding northern blot of *HAC1* and *ACT1* mRNA levels are shown. The spliced form of *HAC1* is indicated with arrowhead. (B) Phospholipid quantitation of *ire1* and *atg8* null strains with two integrated copies of *TDH3pr*-driven Hmg2p^{s} or corresponding empty vector, compared to an isogenic wild type strain. Averages and standard errors are shown, n=3. ** p-value < 0.05

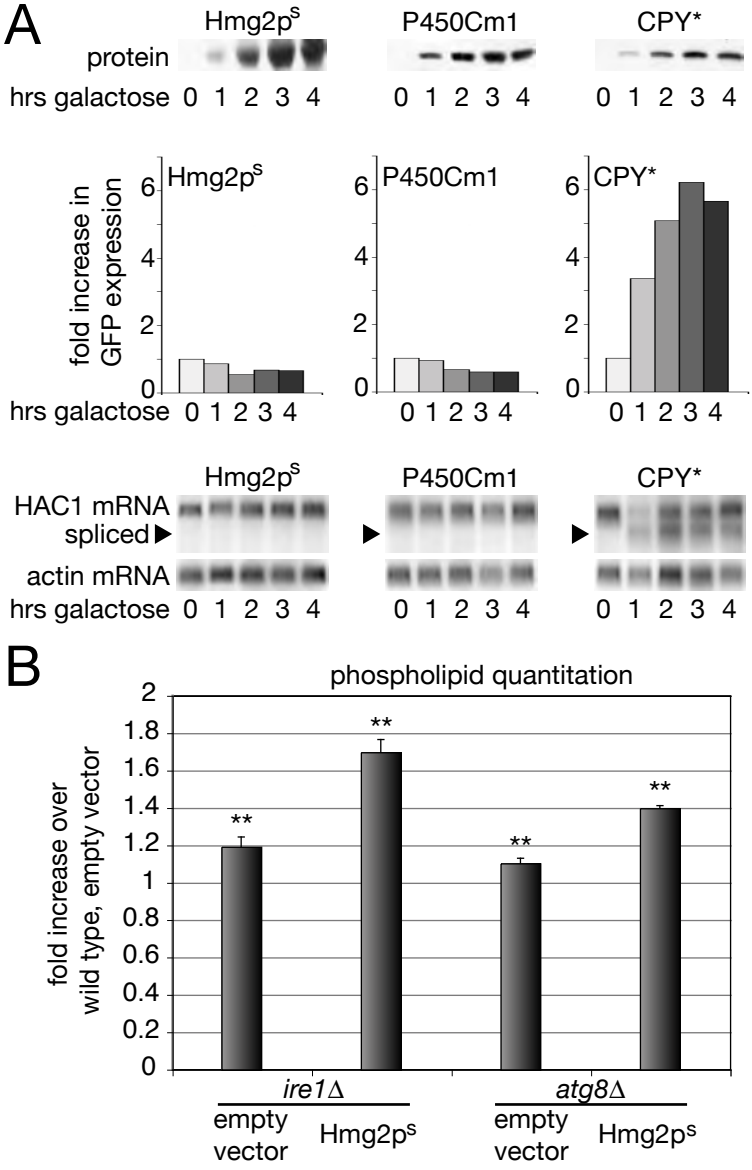
A
Hmg2p^S
P450Cm1
CPY*
protein
hrs galactose 0 1 2 3 4
fold increase in GFP expression
HAC1 mRNA spliced
actin mRNA
B
phospholipid quantitation
fold increase over wild type, empty vector
ire1Δ
atg8Δ
empty vector
Hmg2p^S

demonstrates that the increase in phospholipids by Hmg2p occurs independently of the UPR.

A recent report by Bernales and colleagues implicated autophagy in counterbalancing membrane expansion by the UPR [23]. To test if autophagy played such a role in membrane proliferation by Hmg2p, we introduced our Hmg2p^{s} expression plasmids into *atg8* null cells, which cannot form autophagosomes. The lack of an intact autophagy pathway did not enhance or change the increase in phospholipids caused by elevated Hmg2p^{s} expression (Figure 3.4B).

***PSD1* is required for formation of Hmg2p-induced ER structures**

In our previous work, we conducted a screen to identify genes required for Hmg2p-induced structure formation, using Hmg2p^{s}-GFP*. Although elevated levels of this protein does not increase cellular phospholipids, it generates characteristic stacks and whorls of membrane similarly to the full-length, active Hmg2p^{s} (Figure 3.3A). Despite the lack of phospholipid increase by Hmg2p^{s}-GFP*, our screen identified genes involved in phospholipid biosynthesis, one of which was *PSD1*, the major phosphatidylserine (PtdSer) decarboxylase enzyme in yeast (for review, see [24]). Cells lacking this mitochondrial enzyme do not form Hmg2p^{s}-GFP* membrane stacks and whorls, when grown in synthetic complete media (Figure 3.5A). Interestingly, when *psd1* null cells expressing Hmg2p^{s}-GFP* are grown in YPD, a very rich

Figure 3.5 *PSD1* is required to form Hmg2p-induced ER structures.

(A) Live cell imaging of Hmg2p^{s}-GFP* expressed from the *TDH3pr* in wild type or *psd1* null cells grown in synthetic complete media. Arrows indicate membrane structures. The contrast was increased in the *psd1*Δ panel to demonstrate that no bright foci that would be indicative of structures are observed. (B) Electron micrographs of *TDH3pr*-driven Hmg2p^{s}-GFP*, present at two copies per cell, in a *psd1* null strain grown in YPD. Panel on left shows a cytoplasmic strip, and panel on right show cytoplasmic whorl. Arrows indicate membrane structures, N - nucleus.

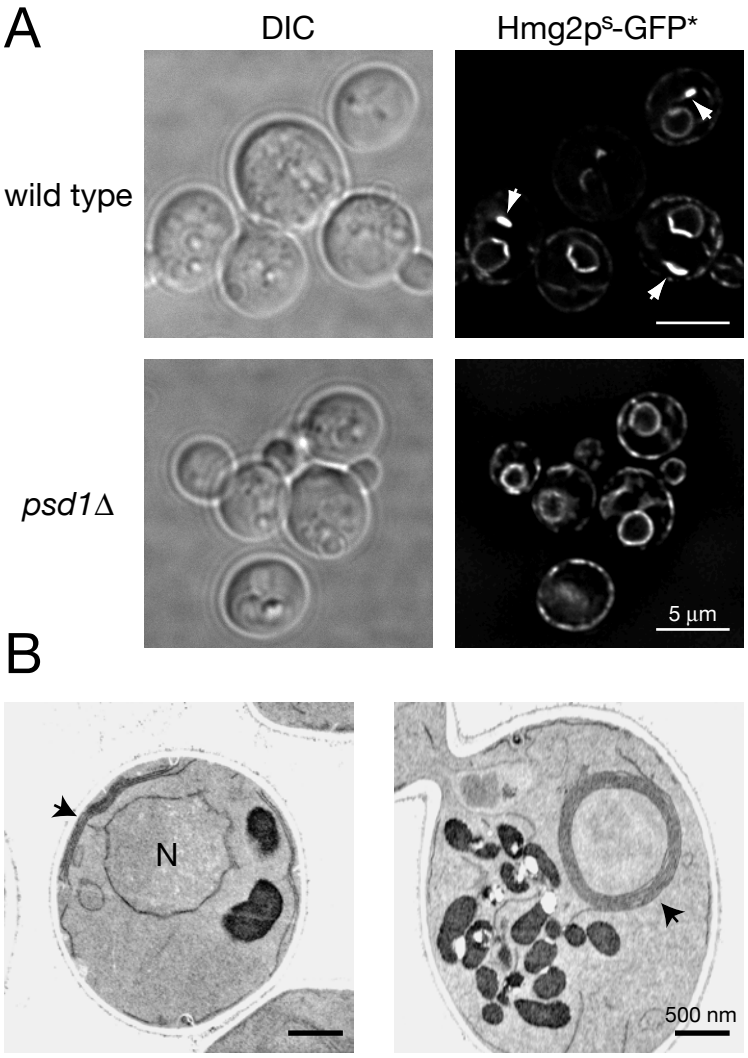
A
DIC
Hmg2p^{s}-GFP*
wild type
*psd1*Δ
5 μm
B
N
500 nm

media, stacks and whorls of membrane form (Figure 3.5B), which was also confirmed by live cell imaging (data not shown). Furthermore, *psd1* null cells overexpressing full-length, active Hmg2p^{s} cannot be transferred from synthetic complete solid media to synthetic complete liquid culture. Under these conditions, the cells cannot enter into logarithmic growth, however this effect is not observed when inoculating into YPD (data not shown).

Hmg2p overexpression significantly alters phospholipid composition

We next examined the effects of Hmg2p^{s} overexpression on the phospholipid composition of cells. An analysis of cells overexpressing Hmg2p^{s} revealed that the phospholipid composition is significantly altered (Figure 3.6A). Total PtdCho levels were elevated 20% whereas PtdSer levels were 5-fold lower when Hmg2p^{s} was expressed. Overexpression of inactive Hmg2p (Hmg2p^{si}) did not alter phospholipid composition (data not shown), indicating that the catalytic activity of Hmg2p was necessary for generating this change.

By testing overexpression of enzymatically active Hmg1p or the soluble CD of Hmg2p, we could evaluate if this change in phospholipid composition was simply due to increased sterol pathway products. Despite the high enzymatic activity of both of these proteins, neither generated the magnitude of change caused by Hmg2p^{s} (Figure 3.6A). These data reveal that although increased HMGR activity is required, it is not sufficient to alter phospholipid composition in these cases.

Figure 3.6 Increased Hmg2p expression alters phospholipid composition.

(A) Phospholipid composition of cells with two integrated copies of empty vector, *TDH3pr*-driven Hmg2p^{s}, Hmg1p or the soluble CD of Hmg2p in a wild type strain. (B) Phospholipid composition of *psd1* null strains with or without two integrated copies of *TDH3pr*-driven Hmg2p^{s}. Averages and standard deviations are shown, n=3. Abbreviations are as follows: PE – phosphatidylethanolamine, PC – phosphatidylcholine, PI – phosphatidylinositol, PS – phosphatidylserine.

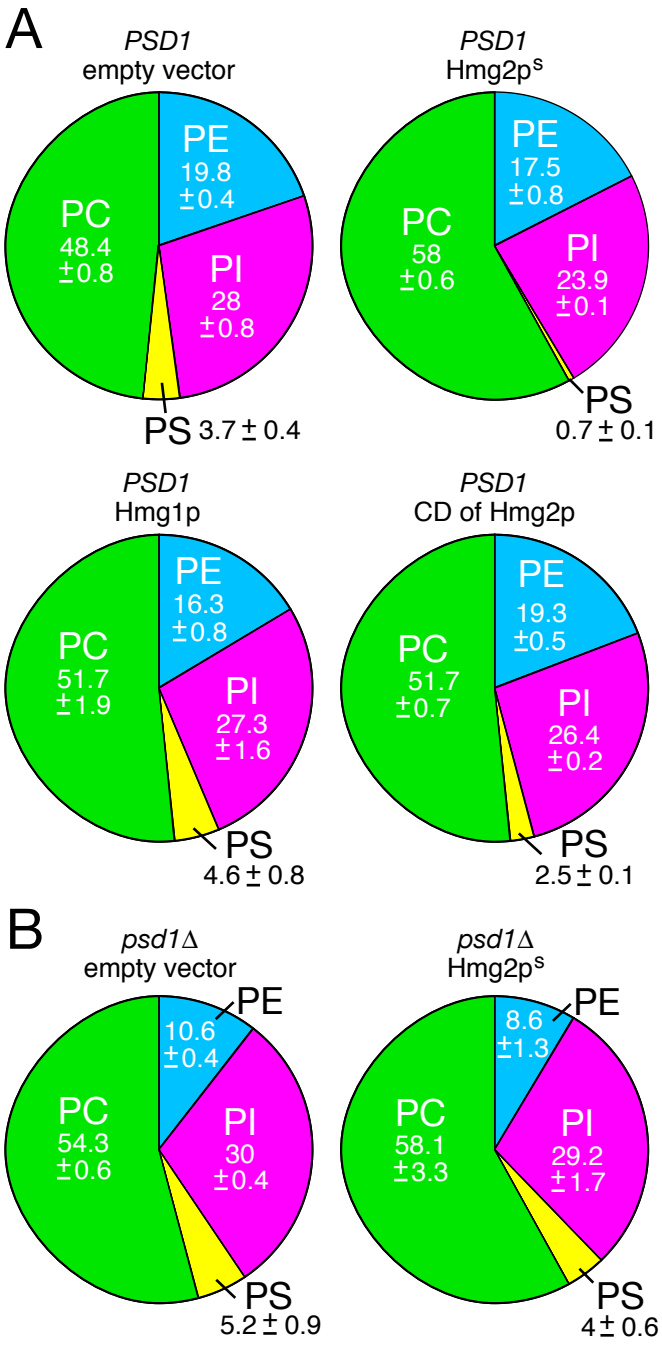
A
PSD1
empty vector
PE
19.8
±0.4
PC
48.4
±0.8
PI
28
±0.8
PS 3.7 ± 0.4
PSD1
Hmg2p^S
PE
17.5
±0.8
PC
58
±0.6
PI
23.9
±0.1
PS
0.7 ± 0.1
PSD1
Hmg1p
PE
16.3
±0.8
PC
51.7
±1.9
PI
27.3
±1.6
PS
4.6 ± 0.8
PSD1
CD of Hmg2p
PE
19.3
±0.5
PC
51.7
±0.7
PI
26.4
±0.2
PS
2.5 ± 0.1
B
psd1Δ
empty vector
PE
10.6
±0.4
PC
54.3
±0.6
PI
30
±0.4
PS
5.2 ± 0.9
psd1Δ
Hmg2p^S
PE
8.6
±1.3
PC
58.1
±3.3
PI
29.2
±1.7
PS
4 ± 0.6

PSD1 is required for Hmg2p^{s}-induced changes in phospholipid composition

The major route of PtdCho synthesis in yeast is through the Kennedy pathway, in which *PSD1* functions (for reviews, see [25,26]). Trotter and Voelker reported that elimination of *PSD1* significantly altered the composition of cellular phospholipids [25], which we independently verified in our strain background (Figure 3.6B). When we compared the phospholipid composition of the *psd1* null strains with and without overexpressed Hmg2p^{s}, the results were surprising. Hmg2p^{s} overexpression in the *psd1* null did not confer any significant change in phospholipid composition compared to the *psd1* null empty vector control (Figure 3.6B), suggesting that *PSD1* is required for Hmg2p^{s}-induced changes in phospholipid composition.

PSD1 is required for the Hmg2p-induced increase in cellular phospholipids

So far, we discovered that *PSD1* is required for both the membrane organization by Hmg2p^{s}-GFP* and for the Hmg2p^{s}-induced change in phospholipid composition. We next asked if *PSD1* was similarly required for the Hmg2p^{s}-induced increase in total cellular phospholipids. To test this, we analyzed the *psd1* null strains with and without overexpressed full-length, active Hmg2p^{s}, and quantitated phospholipids as before. Strains lacking *PSD1* had increased levels of phospholipids, even in the absence of Hmg2p^{s} overexpression (Figure 3.7A). The cell volume of *psd1* null cells was

Figure 3.7 *PSD1* is required for increasing phospholipids in response to Hmg2p overexpression.

(A) Phospholipid quantitation of a *PSD1* strain with two copies of *TDH3pr*-driven Hmg2p^{s} (++), and *psd1* null strains with (++) and without (-) two integrated copies of *TDH3pr*-driven Hmg2p^{s} compared to an isogenic wild type strain. Averages and standard errors are shown, n=3. ** - p-value < 0.05 (B) Cell volume of *psd1* null strains with (++) and without (-) two integrated copies of *TDH3pr*-driven Hmg2p^{s} compared to an isogenic wild type strain. Averages and standard errors are shown, n=3. ** - p-value < 0.05

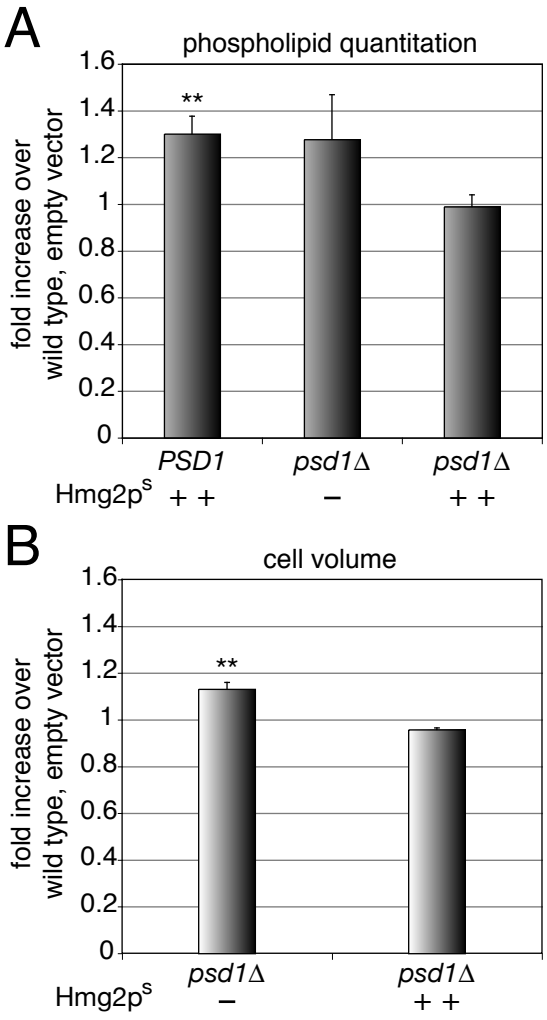
A
phospholipid quantitation
fold increase over wild type, empty vector
1.6
1.4
1.2
1
0.8
0.6
0.4
0.2
0
**
PSD1
psd1Δ
psd1Δ
Hmg2p^s + + – + +
B
cell volume
fold increase over wild type, empty vector
1.6
1.4
1.2
1
0.8
0.6
0.4
0.2
0
**
psd1Δ
psd1Δ
Hmg2p^s – + +

approximately 10% more than a comparable wild type strain (Figure 3.7B), which is similar to the change in cell volume when Hmg2p^{s} or Hmg1p is overexpressed (Figure 3.1C). Interestingly, when Hmg2p^{s} was introduced into the *psd1* null background, no increase in phospholipid quantity or cell volume was observed, when compared to a comparable empty vector, wild type strain (Figure 3.7A and B). Thus *PSD1* is required for the increase in phospholipids caused by Hmg2p^{s} overexpression.

Discussion:

This is the first direct examination of true membrane proliferation caused by HMGR overexpression. Specifically we define membrane proliferation as an increase in the defining molecule of membranes, phospholipids. Accordingly, we directly examined the changes in phospholipid content and composition in cells that overexpress $Hmg2p^{s}$ and found that both are significantly altered. Total cellular phospholipids increased by 50% when Hmg2p was elevated, without a significant change in cell size. Furthermore, PtdCho increased, and PtdSer decreased in response to high Hmg2p levels. Both of these changes required phospholipid biosynthetic enzyme, *PSD1*. Surprisingly, only full-length, active Hmg2p overexpression caused an increase in phospholipid abundance or change in phospholipid composition.

Increasing phospholipids

The abundance of total cellular phospholipid has not been measured in many cases where "phospholipid increases" were reported. Therefore, we sought to determine empirically how much and under what circumstances total phospholipids increased. *NEM1* has previously been reported to negatively regulate transcription of key phospholipid biosynthetic genes [1]. Our analysis of *nem1* null strains revealed a two-fold increase in total phospholipids. This

increase in phospholipids occurred without altering cell size, indicating that phospholipids are twice as concentrated in those cells.

We hypothesized that increasing a highly regulated enzyme involved in fatty acid biosynthesis would also increase total cellular phospholipids. Overexpression of Ole1p, the essential Δ9 desaturase in yeast, confirmed our suspicions. Remarkably, cells with elevated levels of this protein became so enlarged that the haploid cells were as big as diploid cells (data not shown), and had the twice as much phospholipid as comparable wild type cells. The increase in both cell size and phospholipid quantity was dependant on Ole1p enzyme activity. Together, the case of *nem1* null strains and strains with elevated Ole1p expression demonstrate two very different means and manifestations of upregulating cellular phospholipids. These studies help "benchmark" our expectation for the kinds of changes in cellular phospholipids that might be expected in our studies of Hmg2p overexpression.

Membrane structures do not necessarily indicate increased phospholipids

Our analysis of HMGR overexpression revealed that total phospholipids increased by 20% and 50% with Hmg1p and Hmg2p^{s}, respectively. This increase in phospholipids was not due to increased cell size, as was the case with Ole1p overexpression. However, like Ole1p, the increase in phospholipids by Hmg2p was dependant on activity of the protein. These results were surprising given that inactive versions of Hmg2p, including Hmg2p^{s}-GFP* and

Hmg2p^{si}, generate such striking ER structures. This means that the observation of membrane structures per se are not indicative of increases in total phospholipid and should thus be interpreted with care. For example it has recently been reported that the manipulation of the UPR pathway under appropriate circumstances can cause an increase in cellular membrane and thus lipid content [23]. However, these conclusions rest exclusively on the observation of membrane stacks very similar to those caused by Hmg2p^{s}-GFP*. Our work herein demonstrates that without biochemical tests this conclusion cannot be made.

Phospholipid increases by Hmg2p

Finding that only full-length, enzymatically active Hmg2p causes an increase in phospholipids was surprising. We would have expected that all cases of increased HMGR activity would stimulate an increase in phospholipids. However, that was not the case. Expression of the soluble, active catalytic domain had no effect on phospholipids, nor did expression of an active catalytic domain tethered to the ER surface by Ole1p^{i}. Furthermore, co-expression of the inactive Hmg2p with the soluble catalytic domain failed to increase phospholipids. This suggests exciting possibilities regarding how Hmg2p causes an increase in phospholipids. One possibility is that it serves as a platform for other factors to interact.

In the cases where Hmg2p levels were elevated and phospholipids did not increase, such as with inactive Hmg2p variants, there are many scenarios to consider. Although the total cellular phospholipid content was not increased in cells, it was possible that membranes were "borrowed" from other organelles or even that other organelles were "absorbed" into the ER. This would enable ER expansion without increasing cellular phospholipids. Alternately, phospholipid degradation could be increased to keep phospholipid pools constant, which would not be reflected in our assay. In any of these cases, changes in mRNA or protein levels could be occurring. However, microarray and proteomic analysis of strains overexpressing Hmg2p^{s}-GFP* did not indicate any significant alteration in cellular transcripts or protein expression (data not shown). Further analysis into these and other possibilities will be interesting.

***PSD1* is required for Hmg2p effects on cells**

We previously conducted a screen to identify genes required for Hmg2p-induced ER structures using Hmg2p^{s}-GFP* which does not increase phospholipids. However, this screen identified the phospholipid biosynthetic enzyme, *PSD1*. Not only do *psd1* null cells expressing Hmg2p^{s}-GFP* grown in synthetic complete media fail to generate ER structures, but *PSD1* was also required for cells overexpressing full-length, active Hmg2p^{s} to exit stationary phase under specific conditions. These media-specific phenotypes are very interesting and may reveal insights about mechanism. For example, our analysis

of cells grown in minimal media reveals that phospholipid composition is markedly different from cells grown in rich media, such as YPD (data not shown). Yeast extract, one of the main ingredients of YPD, is the water-soluble extract of autolyzed yeast cells and may contain other components in addition to nitrogen, vitamins, carbohydrates and metal ions that can affect, among other things, phospholipid composition. In addition to these media-specific phenotypes, the increase in total cellular phospholipids and the change in composition caused by $Hmg2p^{s}$ overexpression did not occur in the absence of *PSD1*.

The identification of *PSD1* under circumstances in which the Hmg2p variant used did not alter phospholipid content or increase total phospholipids suggests that there is much more to learn. For example, the function of the structures generated by Hmg2p is still a mystery. As is the mechanism by which *PSD1* responds to elevated Hmg2p expression. Further analyses into the mechanisms by which Hmg2p alters ER morphology, changes phospholipid composition, and increases total cellular phospholipids are required.

Coordinating sterol and phospholipid biosynthesis

How yeast coordinate sterol and phospholipid biosynthesis is still unclear. We were surprised to find that elevated expression of the catalytic domain of Hmg2p did not cause any increase in phospholipids in our study, despite the high HMGR activity in that strain. These data suggest that increased

sterol pathway products, in this case, are not sufficient to signal cells to increase phospholipids. Therefore, the precise signal for increasing phospholipids in response to Hmg2p remains to be determined. However, the identification of *PSD1* in the processes of ER reorganization and phospholipid changes by elevated expression of Hmg2p presents a new avenue for identifying these mechanisms. These findings provide the first step in uncovering the mechanisms by which yeast respond to increased levels of HMGR, and coordinate membrane organization, phospholipid biosynthesis and sterol production.

Methods:

Strains, DNA Methods, and Media – Yeast strains RHY471 (*MAT*α *ade2-101 met2 lys2-801 his3*Δ*200 ura3-52*) and RHY2863 (*MATa ade2-101 met2 lys2-801 his3*Δ*200 ura3-52 trp1*Δ*::hisG leu2*Δ) were the parents for all strains in these experiments. Null strains of *nem1*, *ire1*, and *atg8* were generated by PCR amplification of the KanMX knockout cassette from the heterozygous diploid collection (Invitrogen) using standard primers. The *psd1* null was generated using primers oRH3329 (5' GAGGGCAAAAAAGGGAGA AGGACAAGAAAAATCAAAATATTTAACAATAATTGGCTCTTTTTCTG Ccagctgaagcttcgtacgc 3') and oRH3330 (5' GCACCAACAGGAGTCATGCT AAAAAATCCGTACTTCCAACTACCCAACAAAGCAACTCTTTCATTTA GAACGcataggccactagtggatctg 3') that anneal to the pAG25 LoxP CloNAT plasmid (lowercase), that generate a *psd1* deletion that does disrupt the overlapping ORF, YNL170W. All deletions were verified by PCR. Strains were grown in YPD or appropriate synthetic complete media as indicated at 30°C.

Cell growth conditions for phospholipid analyses - Cells were grown in 100 ml YPD for 9-11 doublings prior to harvesting at $0.4 \leq OD_{600} \geq 0.6$. Cells were first pelleted in a KA-10 rotor at 5K RPM, 4°C for 10 minutes. Cells were resuspended in 30 ml ddI H_2O (Mediatech), and 50 µl of cells were removed for determining cells per OD_{600} by hemacytometer. Cells were then pelleted 3 more

times in a clinical centrifuge at 3/4 speed for 5 minutes, and resuspended in H_2O volumes 25 ml and 5 ml, prior to decanting supernatant. Cell pellets were resuspended in the remaining water and OD_{600} readings were taken. Briefly, 10 ODs of cells were collected in 2 ml Eppendorf tubes, and cells were flash frozen in liquid N2, and stored at -80°C until ready to harvest lipids.

Phospholipid Quantitation – Disposable borosilicate glassware (Fisher) and phosphate-free H_2O (Mediatech) was used throughout this protocol. Frozen cells were thawed, volume adjusted to 500 µl with H_2O and 500 µl beads (biosphere) were added. Cells were lysed using a multivortexer alternating 1-minute lysis, 1-minute ice, for six cycles. The lysate was then transferred to a new tube. Two point five ODs of cells (corresponding to 75 µl of lysate) was then used for phospholipid extraction as adapted from [27]. Briefly, 75 µl of lysate was added to 125 µl of water in a glass tube and 4 ml $CHCl_3$: MeOH (2:1) was added. Tubes were vortexed for 1 minute, then spun in a Sorvall SS-34 rotor at 5K RPM, 4°C for 5 minutes. Liquid was transferred to a new tube and 1 ml 0.5N NaCl was added. The two phases were mixed, and spun again. The organic phase was transferred to a new glass tube using a glass Pasteur pipette then dried under a N_2 stream. Phospholipid quantitation was conducted as described by [28]. Briefly, 500 µl of 70% perchloric acid (Sigma) was added to tubes and vortexed before incubating at 200°C for 1.5 hours, covered. Tubes

were cooled and 2.5 ml water was added, followed by 500 μl 2.5% ammonium molybdate, vortexed, then 500 μl 10% freshly prepared ascorbic acid was added and samples were vortexed again. Samples and standards (0-5 μg phosphate) were incubated in boiling water for 10 minutes and allowed to cool. Absorbance readings at 820nm were determined. Each sample was analyzed in duplicate, for a minimum of 3 independent cell preparations.

Phospholipid Composition - Lipids were extracted as described [29], after cells were lysed in a mini-BeadBeater-8 (Biospec Instruments). Total lipids were dried under N_2, resuspended in $CHCl_3$, and injected onto a Zorbax RX-Sil 250 x 4.6 mm (5 μm) column (Agilent Technologies). Glycerophospholipids were separated basically as described [30]. Solution A was $CHCl_3$, MeOH, and ammonium hydroxide (80:19:1), solution B was $CHCl_3$, MeOH, and ammonium hydroxide (60:39:1), and solution C was $CHCl_3$, MeOH, H_2O, ammonium hydroxide (60:34:5:1). Solution A was set at 100% for 3 minutes and then solution B was increased to 100% by 19 minutes and held at 100% for 5 minutes. Solution C was then increased to 100% over 9 minutes and held at 100% for 2 minutes. The column was allowed to re-equilibrate with solution A for 10 minutes before the each injection. Lipids were detected with a PL-ELS 2100 evaporative light scattering detector (Polymer Laboratories, Amherst, MA) with an evaporator temperature of

105°C, nebulizer temperature of 50°C, and a gas (N_2) flow rate of 2 liters per minute. The peaks containing PC, PE, PS, and PI were identified by comparison to known standards (Avanti Polar Lipids). Calibrations for mass amounts were based on external standards.

GFP Reporter Analyses - Cultures were grown into log phase (OD_{600} < 0.5) in appropriate liquid selective media with raffinose as the carbon source. Cultures were diluted back to OD_{600} = 0.1, split into multiple tubes with final volumes of 3 ml for each time point, and galactose was added to 4% at times indicated. A sample was harvested for lysis and western blot and the remainder of the cultures were analyzed for GFP analysis by flow cytometry as described [31].

Isolation of Total RNA - For Northern Blot analysis, raffinose cultures were grown to log phase (OD_{600} < 0.5). Galactose was added to 4% and incubated for the indicated times. 50 ml of cells were collected and pellets were stored at –80°C until processed for RNA and Western blot analysis. Whole-cell RNA was prepared as previously described [32]. Briefly, 700 μl high salt buffer (0.3M NaCl, 20 mM Tris pH 7.6, 10 mM EDTA, 1% SDS) and 700 μl phenol/chloroform/isoamyl alcohol (PCI) were added to the pellets and vortexed in a multivortexer for 1 minute on high. The tubes were incubated at 65°C for 4 minutes, ice for 4 minutes, then the solution was transferred to a 2.0

ml PhaseLoc® tube (Eppendorf) and spun at 14K for 5 minutes. The aqueous phase was transferred to a new tube, 900 μl EtOH was added, and tubes were frozen at -80°C for 20 minutes before a 30 minute spin, 14K, at 4°C. EtOH was removed, pellets were resuspended in 50 μl DEPC-H_2O, and concentrations were determined by spectrometry. All samples were then diluted to 1 μg/μl and stored at -80°C.

Northern Blot Analysis - Northern blot analysis was adapted from [33]. Briefly, 20 μl denaturing mix (64.4% formamide, 8.3% formaldehyde, 100 μg/ml ethidium bromide, 26 mM MOPS, pH 7.0, 6.5 mM NaOAc, 650 μM EDTA) was added to 10 μl of RNA sample, and denatured at 55°C for 15 minutes before adding 2 μl loading dye (50% glycerol, 0.03% xylene blue, 0.03% bromophenol blue, 1 mM EDTA). Samples were loaded onto a 1.5% agarose gel containing 6.7% formaldehyde and run at 100V in buffer E (20 mM MOPS, pH 7.0, 5 mM NaOAc, 500 μM EDTA). Gels were then washed in 10X SSC (1.5 M NaCl, 0.15 M Na Citrate, pH 7.0) for 15 minutes before standard overnight transfer to nitrocellulose using 10X SSC. The membranes were rinsed with 2X SSC for 2 minutes before UV crosslinking (Fisher, FB-UVXL-1000). Membranes were preincubated in 5 ml church buffer (0.5 M Na_2HPO_4, pH 7.2, 1 μM EDTA, 7% SDS) for 1 hour at 65°C. Hybridization probes were generated by random labeling of PCR fragments generated from the complete

coding region of *ACT1* and the 5' region of *HAC1* from genomic DNA using [^{32}P]α-dCTP according to the manufacturer's instructions (Amersham) and added to church buffer. Membranes were incubated overnight at 65°C, washed twice with 2X SSC + 0.1% SDS at room temperature and imaged using a Storm phosporimager.

Western Blot - Whole cell lysates were prepared as described by Gardner et al (1998). Briefly, cell pellets were resuspended in 100 μl SUME (1% SDS, 8 M urea, 10 mM MOPS, pH 6.8, and 10mM EDTA) + protease inhibitors (100 μg/ml N-tosyl-L-phenylalanine chloromethyl ketone, 100 μg/ml pepstatin and 100 μg/ml AEBSF), 100 μl acid washed glass beads was added and the mixture was vortexed at full speed for 3 minutes before addition of 100 μl of 2X urea sample buffer (8 M urea, 4% SDS, 10% ß-mercaptoethanol, 125 mM Tris, pH 6.8). The lysates were then incubated at 55°C for 10 minutes, and then cleared by centrifugation at full speed for 5 minutes. Cellular lysates were blotted using a method adapted from Hampton and Rine (1994). Briefly, 30 μl of sample was loaded onto either 8 or 14% SDS-PAGE gels, run electrophoretically, transferred onto nitrocellulose and placed in TBST (10 mM Tris, pH 8.0, 140 mM NaCl, 0.05% Tween 20) with 2% Carnation nonfat dried milk (2% TBSTM). Blots were then incubated with either α-HA ascites fluid (Covance) 1:2500 or α-myc 9E10 1:500, washed, and probed with goat anti-mouse HRP

1:12,500, rinsed with ddH_2O, and developed with Western Lightning (PerkinElmer).

Electron Microscopy - Cells were prepared for EM as described [34]. Briefly, cells were grown to $0.65 \leq OD_{600} \geq 1.0$ in YPD, fixed with 4% glutaraldehyde, postfixed with 2% potassium permanganate, en bloc stained with 1% uranyl acetate, dehydrated and embedded in Spurr's resin. Eighty nm thick sections were cut and post-stained with Sato lead before visualizing on a JEOL 1200 KeV microscope.

Live Cell Imaging – Cells were grown in appropriate synthetic complete media to $0.4 \leq OD_{600} \geq 0.6$, pelleted at 6K for 3 minutes in a microfuge and resuspended in PBS. Images were acquired on a DeltaVision microscope with appropriate filter sets.

Cell Volume Analysis – Cells were grown to $0.4 \leq OD_{600} \geq 0.6$ in YPD. Formaldehyde was added to 4% and cells were fixed at room temperature for 1 hour. Cells were washed twice with PBS, resuspended in PBS to a final concentration of $10^7 – 10^8$ cells per ml, and stored at 4°C. Cells were analyzed using a Beckman Coulter Counter equipped with a 50 μm aperture. Three hundred events were counted and particles ranging from 5 to 1000 fL were quantitated.

Table 3.1: Strains used in Chapter 3. Unless specified otherwise, all genes are expressed from the *TDH3* promoter. Parent strains are in bold.

Strain	Genotype	Plasmid
RHY471	***MATα ade2-101, ura3-52, met2, lys2-801, his3Δ200***	none
RHY2726	*ade2-101::ADE2::GAL1-10pr::1MYC-HMG2 K6R, ura3-52::URA3::4xUPREpr::GFP*	pRH1579 pRH1571
RHY4733	*ade2-101::ADE2::GAL1-10pr::CPY*-HA, ura3-52::URA3::4xUPREpr::GFP*	pRH1209 pRH1601
RHY2740	*ade2-101::ADE2::GAL1-10pr::CYP450Cm1-HA*	pRH1209 pRH1847
RHY6331	*ade2-101::ADE2, ura3-52::URA3, ire1Δ::KanMX*	pRS402 pRS406
RHY6542	*ade2-101::ADE2::1MYC-HMG2 K6R, ura3-52::URA3::1MYC-HMG2 K6R, ire1Δ::KanMX*	pRH528 pRH1576
RHY6750	*ade2-101::ADE2, ura3-52::URA3, atg8Δ::KanMX*	pRS402 pRS406
RHY6752	*ade2-101::ADE2::1MYC-HMG2 K6R, ura3-52::URA3::1MYC-HMG2 K6R, atg8Δ::KanMX*	pRH2218 pRH1576
RHY2863	***MATa ade2-101, ura3-52, met2, lys2-801, his3Δ200, trp1::hisG, leu2Δ***	none
RHY6191	*ADE2-101::ADE2, URA3-52*	pRS402 pRS406
RHY6190	*ade2-101::ADE2, ura3-52::URA3, nem1Δ::KanMX*	pRS402 pRS406
RHY6544	*ade2-101::ADE2::3MYC-OLE1, ura3-52::URA3::3MYC-OLE1*	pRH2209 pRH2299
RHY6543	*ade2-101::ADE2::3MYC-OLE1 H161A, H166A, ura3-52::URA3::3MYC-OLE1 H161A, H166A*	pRH1828 pRH2107
RHY6123	*ura3-52::URA3::3MYC-OLE1 H161A, H166A*	pRH1828
RHY6433	*ura3-52::URA3::1MYC-HMG2 K6R*	pRH2218
RHY6085	*ura3-52::URA3*	pRH313
RHY6442	*ade2-101::ADE2::1MYC-HMG2 K6R, ura3-52::URA3::1MYC-HMG2 K6R*	pRH2218 pRH1576
RHY7093	*ura3-52::URA3::HMG1*	pRH105-25
RHY7097	*ade2-101::ADE2:HMG1, ura3-52::URA3::HMG1*	pRH105-25 pRH2438

Table 3.1: Strains used in Chapter 3, continued.

Strain	Genotype	Plasmid
RHY6409	*ade2-101::ADE2::1MYC-HMG2 K6R, D711N, E920Q, ura3-52::URA3::HMG2 K6R, D711N, E920Q*	pRH2108 pRH2232
RHY6921	*ade2-101::ADE2::3MYC-OLE1-GFP* H161A, H166A, ura3-52::URA3::3MYC-OLE1-GFP* H161A, H166A*	pRH2416 pRH2413
RHY6194	*ade2-101::ADE2::HMG2-GFP* K6R, ura3-52::URA3::HMG2-GFP* K6R*	pRH2171 pRH1738
RHY6942	*ade2-101::ADE2::HMG2-GFP K6R, ura3-52::URA3::HMG2-GFP K6R*	pRH2427 pRH2428
RHY6533	*ade2-101::ADE2::HMG2Δ1-527 (CD of HMG2), ura3-52::URA3::HMG2Δ1-527 (CD of HMG2)*	pRH2229 pRH1583
RHY6928	*ade2-101::ADE2::3MYC-OLE1-CD2 H161A, H166A, ura3-52::URA3::3MYC-OLE1-CD2 H161A, H166A*	pRH2406 pRH2407
RHY5590	*ura3-52::URA3::HMG2-GFP* K6R*	pRH2171
RHY6240	*ura3-52::URA3::HMG2-GFP* K6R, psd1Δ::NatMX*	pRH2171
RHY7143	*ade2-101::ADE2::HMG2-GFP* K6R, ura3-52::URA3::HMG2-GFP* K6R psd1Δ::NatMX*	pRH2171 pRH1738
RHY7143	*ade2-101::ADE2, ura3-52::URA3, psd1Δ::NatMX*	pRS402 pRS406
RHY6948	*ade2-101::ADE2::1MYC-HMG2 K6R, ura3-52::URA3::1MYC-HMG2 K6R, psd1Δ::NatMX*	pRH2218 pRH1576

Acknowledgements:

Ying Jones acquired all of the electron micrograph images used in this chapter. Will Prinz conducted all of the phospholipid composition analyses. I am grateful to Jim Umen for use of the Multisizer Coulter Counter, and to Scott Emr for use of the DeltaVision microscope. The Niwa laboratory members, particularly Alicia Bicknell, Jenny DuRose, were extraordinarily helpful with RNA preparations and how to do northern blots. I would also like to thank Randy Hampton and Alicia Bicknell for critical reading of this chapter.

References:

1. Santos-Rosa H, Leung J, Grimsey N, Peak-Chew S, Siniossoglou S: **The yeast lipin Smp2 couples phospholipid biosynthesis to nuclear membrane growth**. *Embo J* 2005, **24**:1931-1941.

2. Siniossoglou S, Santos-Rosa H, Rappsilber J, Mann M, Hurt E: **A novel complex of membrane proteins required for formation of a spherical nucleus**. *Embo J* 1998, **17**:6449-6464.

3. Jones AL, Fawcett DW: **Hypertrophy of the agranular endoplasmic reticulum in hamster liver induced by phenobarbital (with a review on the functions of this organelle in liver)**. *J Histochem Cytochem* 1966, **14**:215-232.

4. Staubli W, Hess R, Weibel ER: **Correlated morphometric and biochemical studies on the liver cell. II. Effects of phenobarbital on rat hepatocytes**. *J Cell Biol* 1969, **42**:92-112.

5. Menzel R, Vogel F, Kargel E, Schunck WH: **Inducible membranes in yeast: relation to the unfolded-protein-response pathway**. *Yeast* 1997, **13**:1211-1229.

6. Ross MH, Pappas GD, Lanman JT, Lind J: **Electron microscope observations on the endoplasmic reticulum in the human fetal adrenal**. *J Biophys Biochem Cytol* 1958, **4**:659-661.

7. Chin DJ, Luskey KL, Anderson RG, Faust JR, Goldstein JL, Brown MS: **Appearance of crystalloid endoplasmic reticulum in compactin-resistant Chinese hamster cells with a 500-fold increase in 3-hydroxy-3-methylglutaryl-coenzyme A reductase**. *Proceedings of the National Academy of Sciences of the United States of America* 1982, **79**:1185-1189.

8. Wright R, Rine J: **Transmission electron microscopy and immunocytochemical studies of yeast: analysis of HMG-CoA reductase overproduction by electron microscopy**. *Methods Cell Biol* 1989, **31**:473-512.

9. Koning AJ, Lum PY, Williams JM, Wright R: **DiOC6 staining reveals organelle structure and dynamics in living yeast cells**. *Cell Motil Cytoskeleton* 1993, **25**:111-128.

10. Snapp EL, Hegde RS, Francolini M, Lombardo F, Colombo S, Pedrazzini E, Borgese N, Lippincott-Schwartz J: **Formation of stacked ER cisternae by low affinity protein interactions**. *J Cell Biol* 2003, **163**:257-269.

11. Eberle D, Hegarty B, Bossard P, Ferre P, Foufelle F: **SREBP transcription factors: master regulators of lipid homeostasis**. *Biochimie* 2004, **86**:839-848.

12. Ridgway ND, Byers DM, Cook HW, Storey MK: **Integration of phospholipid and sterol metabolism in mammalian cells**. *Prog Lipid Res* 1999, **38**:337-360.

13. Martin CE, Oh CS, Jiang Y: **Regulation of long chain unsaturated fatty acid synthesis in yeast**. *Biochim Biophys Acta* 2007, **1771**:271-285.

14. Koning AJ, Roberts CJ, Wright RL: **Different subcellular localization of Saccharomyces cerevisiae HMG-CoA reductase isozymes at elevated levels corresponds to distinct endoplasmic reticulum membrane proliferations**. *Molecular Biology of the Cell* 1996, **7**:769-789.

15. Hampton RY: **ER-associated degradation in protein quality control and cellular regulation**. *Curr Opin Cell Biol* 2002, **14**:476-482.

16. Gardner R, Cronin S, Leader B, Rine J, Hampton R, Leder B: **Sequence determinants for regulated degradation of yeast 3-hydroxy-3-methylglutaryl-CoA reductase, an integral endoplasmic reticulum membrane protein**. *Mol Biol Cell* 1998, **9**:2611-2626.

17. Hampton RY, Koning A, Wright R, Rine J: **In vivo examination of membrane protein localization and degradation with green fluorescent protein**. *Proceedings of the National Academy of Sciences of the United States of America* 1996, **93**:828-833.

18. Patil C, Walter P: **Intracellular signaling from the endoplasmic reticulum to the nucleus: the unfolded protein response in yeast and mammals**. *Curr Opin Cell Biol* 2001, **13**:349-355.

19. Shaffer AL, Shapiro-Shelef M, Iwakoshi NN, Lee AH, Qian SB, Zhao H, Yu X, Yang L, Tan BK, Rosenwald A, et al.: **XBP1, downstream of Blimp-1, expands the secretory apparatus and other organelles, and increases protein synthesis in plasma cell differentiation**. *Immunity* 2004, **21**:81-93.

20. Zhang K, Wong HN, Song B, Miller CN, Scheuner D, Kaufman RJ: **The unfolded protein response sensor IRE1alpha is required at 2 distinct steps in B cell lymphopoiesis**. *J Clin Invest* 2005, **115**:268-281.

21. Larson LL, Parrish ML, Koning AJ, Wright RL: **Proliferation of the endoplasmic reticulum occurs normally in cells that lack a functional unfolded protein response**. *Yeast* 2002, **19**:373-392.

22. Cronin SR, Rao R, Hampton RY: **Cod1p/Spf1p is a P-type ATPase involved in ER function and Ca2+ homeostasis**. *J Cell Biol* 2002, **157**:1017-1028.

23. Bernales S, McDonald KL, Walter P: **Autophagy counterbalances endoplasmic reticulum expansion during the unfolded protein response**. *PLoS Biol* 2006, **4**:e423.

24. Voelker DR: **Phosphatidylserine decarboxylase**. *Biochim Biophys Acta* 1997, **1348**:236-244.

25. Carman GM, Kersting MC: **Phospholipid synthesis in yeast: regulation by phosphorylation**. *Biochem Cell Biol* 2004, **82**:62-70.

26. Voelker DR: **Interorganelle transport of aminoglycerophospholipids**. *Biochim Biophys Acta* 2000, **1486**:97-107.

27. Folch J, Lees M, Sloane Stanley GH: **A simple method for the isolation and purification of total lipides from animal tissues**. *J Biol Chem* 1957, **226**:497-509.

28. Rouser G, Fkeischer S, Yamamoto A: **Two dimensional then layer chromatographic separation of polar lipids and determination of phospholipids by phosphorus analysis of spots**. *Lipids* 1970, **5**:494-496.

29. Parks LW, Bottema CD, Rodriguez RJ, Lewis TA: **Yeast sterols: yeast mutants as tools for the study of sterol metabolism**. *Methods Enzymol* 1985, **111**:333-346.

30. Stith BJ, Hall J, Ayres P, Waggoner L, Moore JD, Shaw WA: **Quantification of major classes of Xenopus phospholipids by high performance liquid chromatography with evaporative light scattering detection**. *J Lipid Res* 2000, **41**:1448-1454.

31. Cronin SR, Hampton RY: **Measuring Protein Degradation with Green Fluorescent Protein**. In *Methods in Enzymology, Green Fluorescent Protein.* Edited by Conn PM: Academic Press, Inc.; 1999:58-73. vol 302.]

32. Kohrer K, Domdey H: **Preparation of high molecular weight RNA**. *Methods Enzymol* 1991, **194**:398-405.

33. Sambrook J, Fritsch EF, Maniatis T: *Molecular Cloning* edn 2nd. New York: Cols Sprin Harbor Laboratory Press; 1989.

34. Wright R: **Transmission electron microscopy of yeast**. *Microsc Res Tech* 2000, **51**:496-510.

Chapter 4:

Future Directions

Although in this dissertation I have tried to address some fundamental questions about the effects of Hmg2p on the formation of ER membrane structures and its effects on phospholipids, there is still a great deal more to understand. In this chapter, I will discuss where I envision the field heading, given the data and ideas that I have collected. This is by no means an exhaustive list of what can be done, but rather a focus on the areas of which are of greatest interest to me.

Functional role for structures formed by HMGR

Much of the focus of this work has been to identify the requirements for generating Hmg2p-induced structures. However, very little attention has been given to the functional roles that these structures may have in the cell. Given that HMGR-induced membrane organization is conserved from yeast to mammals, it is reasonable surmise that the structures may be significant to one or more cellular functions.

Are HMGR-induced structures involved in ERAD?

The focus of the Hampton Lab has been to understand ER associated degradation (ERAD), by analyzing the regulated degradation of Hmg2p. Despite the vast amount of study on the regulated degradation of Hmg2p, nothing is known about what role, if any, the structures formed by Hmg2p play in this capacity. To facilitate the study of the regulated degradation of Hmg2p,

strains that have high expression of Hmg2p or one of the GFP-tagged variants of Hmg2p are utilized. Therefore, the platform is already in place to determine if the structures formed by Hmg2p serve any function in its regulated degradation. Immunofluorescence studies could be conducted to determine if the ubiquitin ligase, Hrd1p, is present in the Hmg2p-induced structures, which would then set the foundation for further inquiry.

With such high levels of Hmg2p in the cell, it is possible that the ERAD machinery has an upper limit on the number of proteins that can be processed at any given time. There are cases when Hmg2p accumulates in the cell, as with lovastatin treatment. When misfolded proteins accumulate in the cytoplasm, it has been shown by a number of groups that aggregates form (for review see [1]). The structures generated by Hmg2p could be a way of sequestering the excess protein with which the cell is not able to destroy.

Another alternative is that the Hmg2p-induced structures could protect Hmg2p from degradation. Some of the Hmg2p variants that I generated do not induce the formation of membrane arrays. Therefore, it could be determined if a non-structure forming Hmg2p variant (without the stabilizing K6R mutation) is protected when structures are generated with Hmg2p^{s}. For example, Hmg2p^{s}-GFP* generates structures and does not enter the ERAD pathway. Introducing the Hmg2p TM variant (which does not induce membrane stacks, and is conveniently myc-tagged) into this strain would allow the evaluation of this

protein in the presence of Hmg2p-induced structures. Immunofluorescence would show if Hmg2p TM enters into the structures generated by Hmg2p^{s}-GFP*, and based on these results, a simple analysis of the degradation rate would demonstrate if the structures serve to segregate Hmg2p from the degradation machinery of the ER.

Are HMGR-induced structures sterol production sites?

HMGR catalyzes the rate-limiting step in sterol biosynthesis. It would be foolish to study the structures generated by this protein without considering its highly conserved enzymatic function. There are many instances of differentiated cell types that have developed specialized ER structures to address cellular need, such as the sarcoplasmic reticulum of smooth muscle cells [2,3]. The fact that HMGR-induced membrane arrays are such a prominent feature of sterol producing cells makes this possibility seem likely [4,5].

The structures formed by HMGR could have evolved over time to allow efficient production of sterols and other mevalonate pathway products. A simple survey of the proteins enriched in the structures generated by Hmg2p would provide preliminary data regarding the function of these Hmg2p-induced subdomains. Furthermore, it makes sense, from a functional standpoint, that all of the enzymes involved in sterol production be in close proximity to each other. Support for this idea is provided by the *erg28* null strain. Although *ERG28* has no known enzymatic role in sterol production, it has been shown to

be important in facilitating protein-protein interactions with known enzymes of the sterol biosynthetic pathway [6]. Loss of *ERG28* causes an increase in lovastatin sensitivity, presumably due to a defect in sterol production. Furthermore, our studies showed that *ERG28* is one of the genes that is required for Hmg2p^{s}-GFP* structure formation. It will be interesting to determine how these HMGR-induced structures are involved in sterol synthesis, and specifically the role of Erg28p in their formation.

Are HMGR-induced structures the site of lipid droplet formation?

One topic that was not previously addressed is that of lipid droplets. Lipid droplets are the site of excess phospholipid and sterol storage in the form of triacylglycerides (TAGs) and sterol esters (STEs), respectively (for reviews see [7,8]). TAG and STE formation occurs at the ER surface and it is hypothesized that lipid droplets emerge from the ER, although this has not been demonstrated. Lipid particles are encapsulated by a lipid monolayer and have a mere 16 resident proteins [9]. In cells that do not have lipid particles, ergosterol synthesis is impaired and the proteins that would normally be found in lipid particles are localized to the ER [10], demonstrating the close association between these two cellular entities.

Lipid particles are assayed very easily using a lipophilic dye, Nile Red. This dye stains all neutral lipids red, however, qualities of lipid particles cause them to fluoresce an intense green color when stained with the dye. Hence,

crude quantitation of lipid particles can be ascertained by flow cytometry using the channel settings for GFP. These Nile Red stained lipid particles are obvious by fluorescence imaging (Figure 4.1) and can be quantitated this way as well.

Work by Polakowski and colleagues has indicated that lipid particles increase when HMGR activity is elevated in cells [11] and I confirmed these findings (Figure 4.2). I also found that treatment of these cells with lovastatin causes a rapid reduction in lipid particles (Figure 4.2). Given that HMGR catalyzes the rate-limiting step in sterol biosynthesis, which is directly inhibited by lovastatin, these results are not surprising. Despite the obvious relationship between HMGR activity and lipid particle abundance, study of the interplay between these two components has not occurred.

I was surprised to discover that when full-length Hmg2p^{s} is expressed in cells, the amount of lipid particles is greater than if Hmg1p or only the soluble catalytic domain is expressed (Figure 4.2). Lovastatin resistance is similar when these proteins are overexpressed, so I would expect that the abundance of lipid particles to also be similar when comparing these strains. However, I have shown in Chapter 2 that the number of cells with Hmg1p-induced structures is markedly lower than the number of cells with Hmg2p^{s}-induced structures, and that the soluble catalytic domain does not induce any structure formation. These findings might suggest a potential role for the HMGR-induced structures in sterol biosynthesis and ultimately, lipid particle formation.

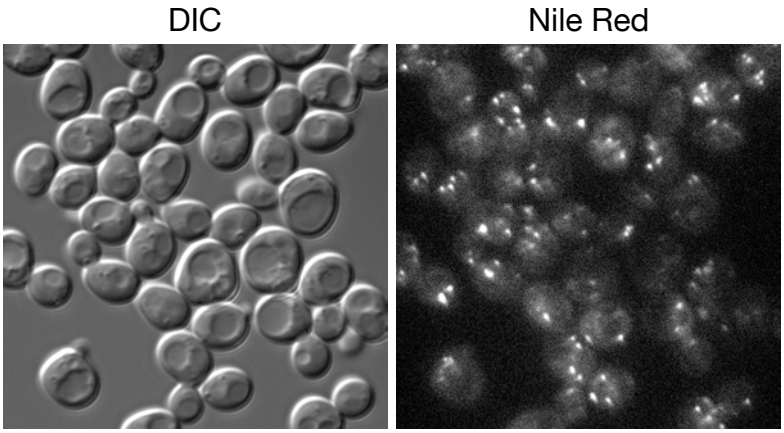

Figure 4.1 Lipid particles are stained with Nile Red
Wild type cells stained with Nile Red.

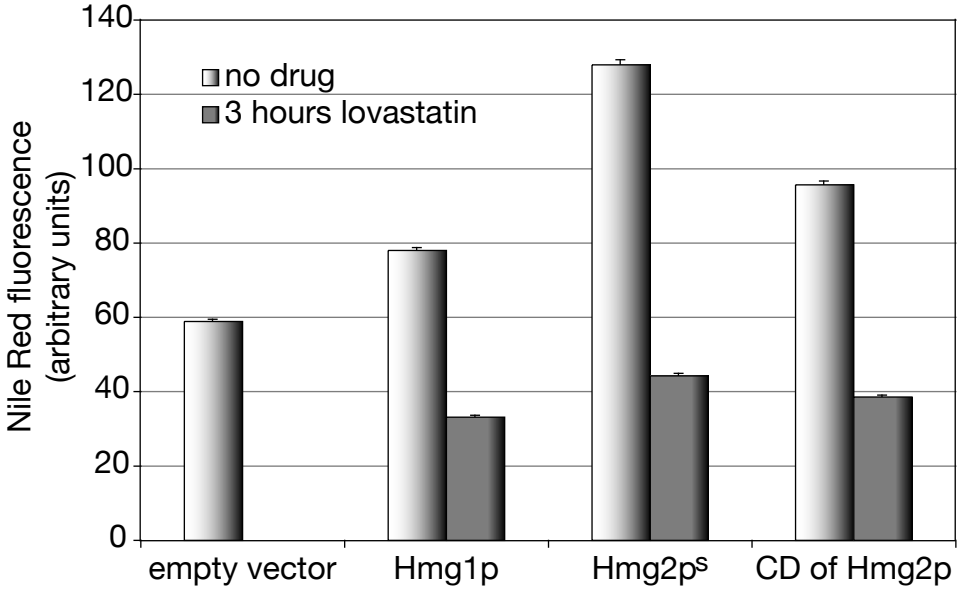

Figure 4.2 Lipid particles decrease during lovastatin treatment
Cells expressing two *TDH3pr*-driven copies of empty vector, Hmg1p, Hmg2p , or the soluble catalytic domain of Hmg2p are shown with and without lovastatin treatment for 3 hours. Nile Red fluorescence was quantitated via flow cytometry. Means and standard errors are shown.

As mentioned earlier, the site of lipid particle formation has not been empirically determined. It is my belief that HMGR-induced structures are a primary site of lipid particle formation. Strains that overexpress Hmg2p may provide the ideal platform to address this question. Lovastatin treatment inhibits HMGR enzyme function, thus blocking the mevalonate pathway, and causes a marked decrease in cellular lipid particles (Figure 4.2). Upon release from lovastatin, lipid particles rapidly form in cells (data not shown). By analyzing cells with high levels of $Hmg2p^{s}$ upon release from lovastatin treatment it may be possible to observe the formation of lipid particles via electron microscopy.

Some obvious questions result from incorporating our knowledge about Hmg2p and its effects on cells in the context of sterol production and lipid particles. For example, are cells that do not form lipid particles viable when HMGR activity is increased by expressing either the full-length protein or the soluble catalytic domain? Do HPE mutants have any defects in lipid particle formation? It will be interesting to see how these two seemingly separate fields begin to merge.

What are the effects of the HPE genes on sporulation?

Although this is not discussed elsewhere, at one point I began crossing the various HPE genes to one another to determine epistasis. However, I found that sporulation was impaired when I crossed the different mutants to each

other. For example, if a *cod1/spf1* null strain is crossed to a strain harboring the *pie1-1* mutation, tetrads do not form at all. This was the most extreme case that I observed, but I did not explore this in great detail. A careful analysis of the sporulation phenotypes when crossing the mutant strains to one another could provide valuable insights into the function of these genes.

Does the UPR increase phospholipids?

Although this question is not as germane to the analysis of Hmg2p, it is very relevant to understanding ER membrane dynamics. The UPR is a conserved signaling pathway that responds to misfolded proteins by inducing the transcription of target genes by activation of XBP1 (mammalian systems) or *HAC1* (yeast). This pathway is required for the differentiation of a lymphocyte into an antibody-producing B-cell [12,13]. It remains to be determined if UPR induction is sufficient to increase ER membranes. It is a widely-held belief that it is, however I firmly believe that it is highly debatable and in need of careful, well-controlled analysis.

The UPR and membrane expansion in yeast

Cox and colleagues analyzed the inositol auxotropy phenotype of UPR-deficient strains [14], demonstrating that *INO1* mRNA levels are elevated upon tunicamycin treatment, which is used to induce the UPR. They further showed that induction of HMGR expression in UPR-deficient strains was lethal, which

was later shown to be an artifact [15]. This analysis was the seed for the belief that the UPR causes an increase in ER membranes, despite the lack of quantitative proof. A microarray analysis was conducted to determine the transcriptional targets of the UPR in yeast, which uncovered a wide array of genes, including some involved in phospholipid synthesis that further supported these beliefs [16]. The most recent analysis in yeast was by Bernales and colleagues, which quantitated ER expansion solely on quantitation of membranes observed in transmission electron microscopy sections [17], which can be misleading (see Chapter 3). In this study, the UPR was induced by 8 mM DTT treatment (1-2mM DTT induces the UPR robustly) or by forced expression of the active *HAC1* transcription factor.

The UPR and membrane expansion in fibroblasts

A similar study of forced expression of the active XBP1 transcription factor in mammalian cells demonstrated that it induces increased synthesis of phosphatidylcholine and phosphatidylethanolamine, suggesting an increase in ER membranes [18]. Furthermore, the extent of ER increase was calculated based on analysis of single transmission electron microscopy sections, like the study in yeast. While this and the follow-up study [19] both clearly demonstrate that changes in phospholipid composition occurs, the total abundance of phospholipid in these cases has not been reported, which would definitively show if membrane expansion is occurring. I would also like to know if the

overall size of these cells is altered upon forced XBP1 expression. Although these studies are very suggestive of an UPR-mediated increase in phospholipids, the results are not conclusive.

My insights on the UPR and membrane expansion in yeast

It is important to note that constitutive expression of active XBP1 in mammalian cells or active Hac1p in yeast is lethal, as is an 8 mM dose of DTT to yeast. I have independently tested the effects of treating cells with 8 mM DTT, and my preliminary analysis suggests that there are UPR-independent mechanisms for increasing phospholipids (Figure 4.3A). Furthermore, I have found that loss of *ATG8* does not further increase total phospholipid abundance upon DTT treatment when compared to wild type strains under similar treatment conditions (Figure 4.3A), bringing into question the role of ER-phagy in UPR-mediated membrane increases [17,20]. When cell size is taken into account in cases where cells are treated with such high DTT concentrations, the matter of determining what membranes are increasing becomes even more complex (Figure 4.3B). Careful analysis of the capacity of the UPR, being defined as the *IRE1*-mediated transcriptional activation of genes via *HAC1*, to increase ER membranes should be done. I think the results will be both interesting and surprising.

It is my prediction that the increases in membranes that occur upon DTT treatment are a result of one of two things. The first possibility, which I favor, is

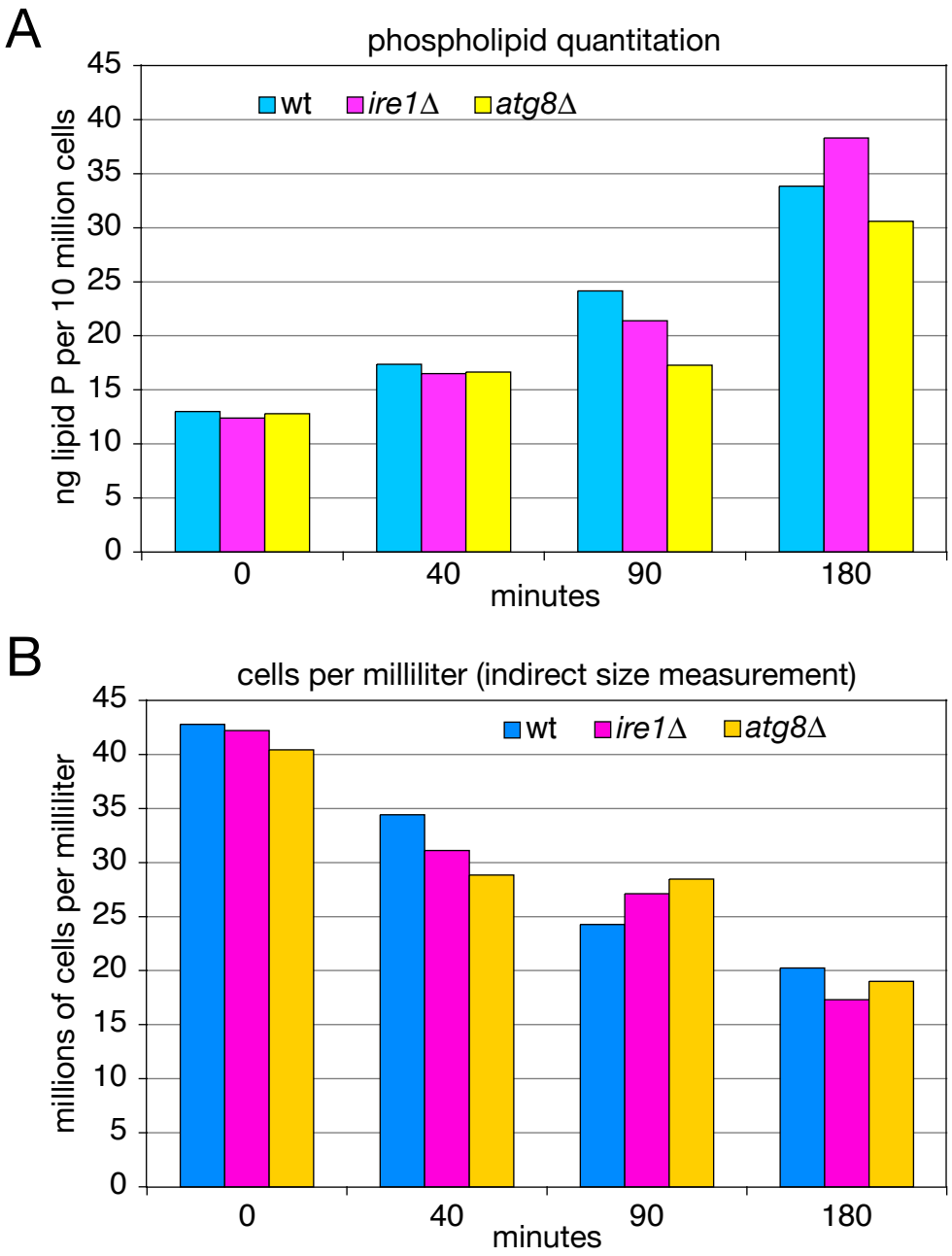

Figure 4.3 Phospholipid abundance and cell size are affected by DTT treatment in an *IRE1*-independent manner.

Cells were treated with 8 mM DTT for times indicated. *ire1* null strains lack a functional UPR, and *atg8* null strains lack autophagic pathways. (A) Phospholipid quantitation of wild type, *ire1*Δ, and *atg8*Δ cells. (B) Cell density per milliliter was determined for each of the time points. The number of cells per milliliter is inversely proportional to cell size.

that DTT treatment causes membranes to increase in a manner consistent with drug detoxification and/or cell death. The membrane structures observed could be part of how the cells try to survive or even be part of the apoptotic response of yeast. As previously mentioned the cases where expansions of membrane are observed are extreme and result in cellular lethality. The second possibility is that DTT triggers a new, uncharacterized branch of the UPR that is *IRE1* and *HAC1*-independent. Induced expression of the misfolded protein CPY* strongly induces the UPR in yeast, and it would be interesting to see how phospholipids change in response to that stimulus.

Closing remarks

There is so much to be learned about how Hmg2p overexpression affects ER membranes and the mechanisms through which this occurs. Further integrating this knowledge into how other single-protein proliferants, such as CYP450Cm1, exert their effects on the cells will be interesting. Do they all work through a similar mechanism or do they each have independent ways of altering the phospholipids of the cell? How conserved are these mechanisms across species? What is the role of the UPR in membrane proliferation? These are interesting questions that I hope will be answered in time.

Methods:

Nile Red Staining – Nile Red (Invitrogen Probes) was dissolved in EtOH and kept as a 10 mg/ml stock at 4°C, in the dark. The solution looks very fibrous, but should not be filtered. Cells were grown in YPD to log phase, and 1 OD_{600} was pelleted and resuspended in PBS with 10 μg/ml Nile Red. Cells were then pelleted and resuspended in PBS without Nile Red and either viewed with FITC filters on a Nikon Optiphot II, or analyzed on a flow cytometer using GFP settings. For lovastatin treatment, 25 mg/ml lovastatin was added to 100 μg/ml for 3 hours prior to Nile Red staining.

UPR Induction and Phospholipid Quantitation – Cells were grown to log phase in YPD. A 1 M DTT stock solution was freshly prepared, and added to 8 mM for times indicated. Cells were harvested and analyzed for total phospholipid abundance as described in Chapter 3. For each time point, a sample of cells was analyzed to determine cell density, as an indirect measure of cell volume. Cells were sonicated at 15% for 10 seconds prior to quantitation via hemacytometer.

Table 4.1: Strains used in Chapter 4. Parent strains are in bold.

Strain	Genotype	Plasmid
RHY471	***MATα ade2-101, ura3-52, met2, lys2-801, his3Δ200***	none
RHY3195	*ire1Δ::KanMX*	none
RHY4064	*atg8Δ::KanMX*	none
RHY2863	***MATa ade2-101, ura3-52, met2, lys2-801, his3Δ200, trp1::hisG, leu2Δ***	none
RHY6191	*ADE2-101::ADE2, URA3-52*	pRS402 pRS406
RHY6442	*ade2-101::ADE2::1MYC-HMG2 K6R, ura3-52::URA3::1MYC-HMG2 K6R*	pRH2218 pRH1576
RHY6533	*ade2-101::ADE2::HMG2Δ1-527 (CD of HMG2), ura3-52::URA3::HMG2Δ1-527 (CD of HMG2)*	pRH2229 pRH1583
RHY6635	*ade2-101::ADE2::1MYC-HMG1, ura3-52::URA3::1MYC-HMG1*	pRH945 pRH1593

References:

1. Johnston JA, Ward CL, Kopito RR: **Aggresomes: a cellular response to misfolded proteins**. *J Cell Biol* 1998, **143**:1883-1898.

2. Sitia R, Meldolesi J: **Endoplasmic reticulum: a dynamic patchwork of specialized subregions**. *Mol Biol Cell* 1992, **3**:1067-1072.

3. Sorrentino V: **Molecular determinants of the structural and functional organization of the sarcoplasmic reticulum**. *Biochim Biophys Acta* 2004, **1742**:113-118.

4. Black VH: **The development of smooth-surfaced endoplasmic reticulum in adrenal cortical cells of fetal guinea pigs**. *Am J Anat* 1972, **135**:381-417.

5. Sisson JK, Fahrenbach WH: **Fine structure of steroidogenic cells of a primate cutaneous organ**. *Am J Anat* 1967, **121**:337-367.

6. Mo C, Bard M: **Erg28p is a key protein in the yeast sterol biosynthetic enzyme complex**. *J Lipid Res* 2005, **46**:1991-1998.

7. Daum G, Wagner A, Czabany T, Athenstaedt K: **Dynamics of neutral lipid storage and mobilization in yeast**. *Biochimie* 2007, **89**:243-248.

8. Wagner A, Daum G: **Formation and mobilization of neutral lipids in the yeast Saccharomyces cerevisiae**. *Biochem Soc Trans* 2005, **33**:1174-1177.

9. Athenstaedt K, Zweytick D, Jandrositz A, Kohlwein SD, Daum G: **Identification and characterization of major lipid particle proteins of the yeast Saccharomyces cerevisiae**. *J Bacteriol* 1999, **181**:6441-6448.

10. Sorger D, Athenstaedt K, Hrastnik C, Daum G: **A yeast strain lacking lipid particles bears a defect in ergosterol formation**. *J Biol Chem* 2004, **279**:31190-31196.

11. Polakowski T, Stahl U, Lang C: **Overexpression of a cytosolic hydroxymethylglutaryl-CoA reductase leads to squalene accumulation in yeast**. *Appl Microbiol Biotechnol* 1998, **49**:66-71.

12. Shaffer AL, Shapiro-Shelef M, Iwakoshi NN, Lee AH, Qian SB, Zhao H, Yu X, Yang L, Tan BK, Rosenwald A, et al.: **XBP1, downstream of Blimp-1, expands the secretory apparatus and other organelles, and increases protein synthesis in plasma cell differentiation**. *Immunity* 2004, **21**:81-93.

13. Zhang K, Wong HN, Song B, Miller CN, Scheuner D, Kaufman RJ: **The unfolded protein response sensor IRE1alpha is required at 2 distinct steps in B cell lymphopoiesis**. *J Clin Invest* 2005, **115**:268-281.

14. Cox JS, Chapman RE, Walter P: **The unfolded protein response coordinates the production of endoplasmic reticulum protein and endoplasmic reticulum membrane**. *Mol Biol Cell* 1997, **8**:1805-1814.

15. Larson LL, Parrish ML, Koning AJ, Wright RL: **Proliferation of the endoplasmic reticulum occurs normally in cells that lack a functional unfolded protein response**. *Yeast* 2002, **19**:373-392.

16. Travers KJ, Patil CK, Wodicka L, Lockhart DJ, Weissman JS, Walter P: **Functional and genomic analyses reveal an essential coordination between the unfolded protein response and ER-associated degradation**. *Cell* 2000, **101**:249-258.

17. Bernales S, McDonald KL, Walter P: **Autophagy counterbalances endoplasmic reticulum expansion during the unfolded protein response**. *PLoS Biol* 2006, **4**:e423.

18. Sriburi R, Jackowski S, Mori K, Brewer JW: **XBP1: a link between the unfolded protein response, lipid biosynthesis, and biogenesis of the endoplasmic reticulum**. *J Cell Biol* 2004, **167**:35-41.

19. Sriburi R, Bommiasamy H, Buldak GL, Robbins GR, Frank M, Jackowski S, Brewer JW: **Coordinate regulation of phospholipid biosynthesis and secretory pathway gene expression in XBP-1(S)-induced endoplasmic reticulum biogenesis**. *J Biol Chem* 2007, **282**:7024-7034.

20. Bernales S, Schuck S, Walter P: **ER-phagy: selective autophagy of the endoplasmic reticulum**. *Autophagy* 2007, 3:285-287.

Appendix 1:

Mapping the *PIE1* locus

The UV screen: Mapping the *pie1-1* locus

We conducted a UV mutagenesis screen, which is described in great detail in the Masters Thesis of Thomas Cunningham. Briefly, cells with a single integrated copy of *TDH3pr*-driven Hmg2p^{s}-GFP* (Hmg2p with stabilizing K6R mutation, and GFP replacing last 375 amino acids of catalytic domain), were plated and mutagenized. Colonies were grown at 30°C and each colony was scored visually for aberrant Hmg2p^{s}-GFP* localization. In this way, several potential candidate mutants were identified.

pie1-1 phenotype

Our next goal was to identify the mutant ORFs responsible for the phenotypes. Upon examining the strains further, we determined which phenotypes were caused by single ORFs. Among these was the strain harboring the *pie1-1* mutation. The localization of Hmg2p^{s}-GFP* in this strain was particularly interesting. When grown in log phase, the cells had very few observable structures compared to wild type (Figure A1.1). However, as the cells became denser in the culture ($OD_{600} > 0.3$ in minimal selective media), the cells began to look more wild type. Even in early log phase, the phenotype was not 100% penetrant. This suggested that the phenotype observed was either the result of slow kinetics, or growth phase dependant.

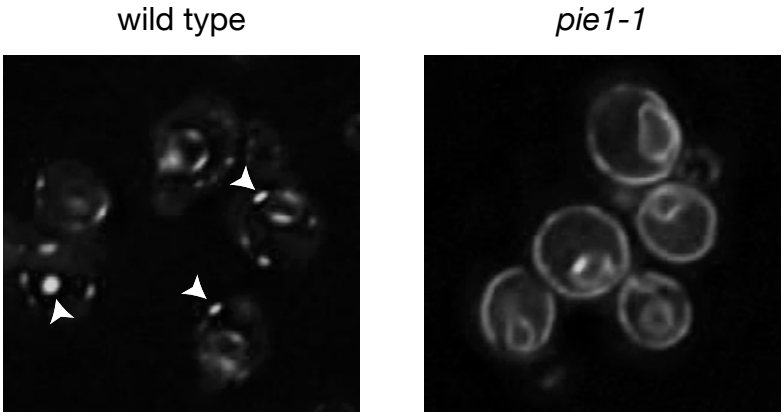

Figure A1.1 *PIE1* is required for Hmg2p^{s}-GFP*-induced structures
Fluorescence microscopy images of wild type and *pie1-1* cells expressing *TDH3pr*-driven Hmg2p^{s}-GFP*. Structures are indicated with arrowheads.

We identified a secondary phenotype attributable to the *pie1-1* mutation. These strains were temperature sensitive, meaning that they could not grow at 35°C. We found that both the temperature sensitivity and the aberrant Hmg2p^{s}-GFP* localization phenotypes were recessive, which would allow us to clone the gene by complementation. The temperature sensitive phenotype would allow cloning of the gene to occur via selection rather than screening for rescue of the wild type Hmg2p^{s}-GFP* localization. We could simply score for the ability to grow at higher temperatures.

***pie1-1*, the gene that wouldn't be rescued**

To clone the *pie1-1* gene, we tried several approaches. First, we tried rescuing the temperature sensitivity by transforming in the "B" Rose library [1]. This library was generated by Sau3A partial digestion of yeast genomic DNA, which was subsequently cloned into YCp50. Upon transforming the cells with the library, we allowed various times of growth at 30°C and room temperature before transferring plates to 35°C. We also tried replica plating from plates grown at 30°C or room temperature to 35°C. Despite many efforts with this library, we could not identify any plasmids that rescued the temperature sensitive phenotype of the *pie1-1* mutant.

One possibility was that the region of DNA that would rescue was not present in the Rose library, so we tried a different one. This time we used the

Hirsch library [2], which was constructed in a way similar to that of the Rose library. However, again, we were unsuccessful in rescuing the temperature sensitive phenotype. Scoring for rescue of the visual phenotype would be extremely labor intensive, especially since we had no idea if a plasmid that could rescue was part of either library, so we opted for a more traditional method of cloning – mapping.

***PIE1* is on chromosome XIII**

Although mapping a gene sounds dreadful, there are many wonderful tools that are now available that make the process very facile. To identify on which chromosome our gene of interest was located, we used the set of strains designed by Wakem and Sherman [3]. The method is very simple: the 16 mapping strains (one for each chromosome) are engineered to have sites recognized by a 2μm recombinase located very near the centromere of a chromosome and are marked with *URA3*. These strains are cir- because they lack the recombinase that specifically recognizes these sites. However, most laboratory strains are cir+, which means that when the mapping strains are crossed to wild type strains, recombination can occur, which results in loss of the designated chromosome. To ensure loss of the chromosomes, diploids are plated on 5-FOA plates, which are lethal to strains with a functional *URA3*. The resultant strains are haplo-insufficient for that particular chromosome. Therefore, the resulting diploid strain that is still harboring the mutant

phenotype is haplo-insufficient for the chromosome on which the gene of interest is located.

In Figure A1.2, we show the resulting diploids from crossing the *pie1-1* strain to all of the mapping strains that were readily available. At 35°C, the diploid that is haplo-insufficient for chromosome XIII fails to grow. This demonstrates that *pie1-1* is located on that chromosome.

***pie1-1* is centromerically linked**

The article "Getting Started with Yeast" was particularly valuable as a reference in mapping, and I highly recommend it [4].

Now that we determined on which chromosome *pie1-1* was located, we were faced with determining where exactly on the chromosome that was. First, we asked if *pie1-1* was centromerically linked. This was done by examining the segregation of the *pie1-1* mutant in relation to a known centromerically linked marker, in this case *TRP1* (Figure A1.3A). We examined the tetrads that had both the *pie1-1* and *trp1::hisG* markers segregating, and found that *pie1-1* appears to be centromerically linked, which was very lucky. Using the numbers from our tetrad analysis, we were able to determine approximately how closely linked *pie1-1* was to the centromere, in this case approximately 53Kb away (Figure A1.3B).

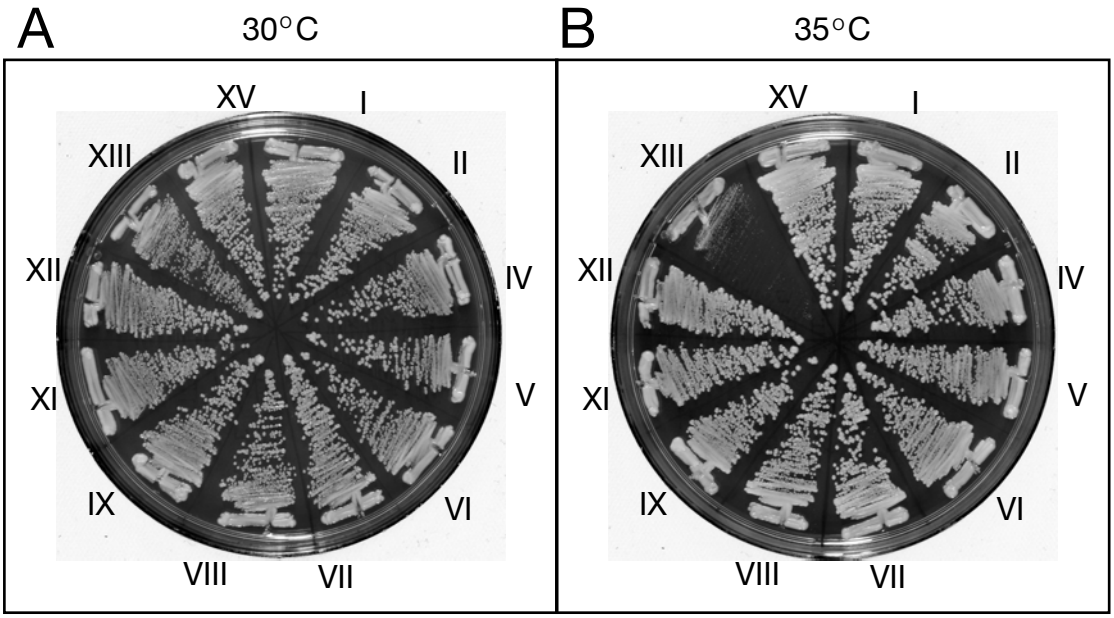

Figure A1.2 The *pie1-1* locus is located on chromosome XIII

Images of 5-FOA plates with the haplo-insufficient yeast for the chromosomes indicated. The *pie1-1* strain was crossed to each of the chromosomal mapping strains. The resulting diploids were plated onto 5-FOA, to induce loss of the chromosome indicated, and grown for 2 days at (A) 30°C or (B) 35°C.

A

pie1-1, TRP1* x *PIE1, trp1::hisG

	PD	NPD	TT
	pie1, TRP1	***pie1, trp1***	***pie1, trp1***
	pie1, TRP1	***pie1, trp1***	***pie1, TRP1***
	PIE1, trp1	***PIE1, TRP1***	***PIE1, trp1***
	PIE1, trp1	***PIE1, TRP1***	***PIE1, TRP1***
Random Assortment	1	1	4
Linkage	> 1	< 1	0
Centromeric Linkage	1	1	< 4
Observed	**1**	**1**	**1**

B

$$\text{cM}' = \left(\frac{100}{2}\right)\left(\frac{\text{TT}}{\text{PD} + \text{NPD} + \text{TT}}\right) = \left(\frac{100}{2}\right)\left(\frac{10}{9 + 9 + 10}\right) = \textbf{18 cM (53Kb)}$$

Figure A1.3 *pie1-1* is centromerically linked

(A) Tetrad analysis of *pie1-1* and *TRP1* segregation. The three possible tetrad combinations for the two markers are drawn out. Expected values for PD : NPD : TT for random assortment, linkage, and centromeric linkage and the observed ratio are shown. (B) Formula for calculating map distance, including values from analysis in A. Abbreviations are as follows: PD – parental ditype, NPD – nonparental ditype, TT – tetratype, cM – centimorgan, and Kb – kilobases.

pie1-1 is on the left arm of chromosome XIII

Our next goal was to determine on which side of the centromere *pie1-1* was located. We selected two genes, *USA1* and *MSN2*, both located on chromosome XIII, and already marked with drug resistance markers in our strain collection. We would expect to see less recombination between the two loci that were closer together, indicating linkage. Upon dissecting these tetrads, we found that *pie1-1* was more closely linked to *USA1* than *MSN2* (Figure A1.4A). This indicated that our gene of interest was located on the left arm of chromosome XIII.

Zeroing in on *pie1-1*

To determine the exact location of the *PIE1* locus, three-factor mapping was necessary. This technique is useful to determine if the gene of interest is between two other loci, based on the segregation of the three different markers with respect to one another, which is illustrated in Figure A1.4B and C. This analysis demonstrates that the *PIE1* locus is located in between the *GAL80* and *USA1* loci. This is because recombination never occurred between *GAL80* and *PIE1*, but recombination did occur between *GAL80* and *USA1*, and between *USA1* and *PIE1*. Finer resolution of the location of *PIE1* could be achieved by dissecting more tetrads. The region of chromosome XIII between the *PIF1* and *USA1* loci is illustrated in Figure A1.5, as depicted by the Saccharomyces Genome Database (SGD).

Figure A1.4 *PIE1* is located between *GAL80* and *USA1*

(A) *PIE1* was mapped with respect to the *USA1* and *MSN2* loci, located on the left and right arms of chromosome XIII, respectively. PD, NPD and TT scores for each cross are shown. (B) Three locus mapping with *PIE1*, *USA1* and *PIF1*, which are all located in the left arm of chromosome XIII. Segregation of markers is shown. (C) Three locus mapping with *PIE1*, *USA1*, and *GAL80*, which are all located on the left arm of chromosome XIII. Segregation of markers is shown. Centromeres are indicated with blue circle, and relative locations of known genes are marked.

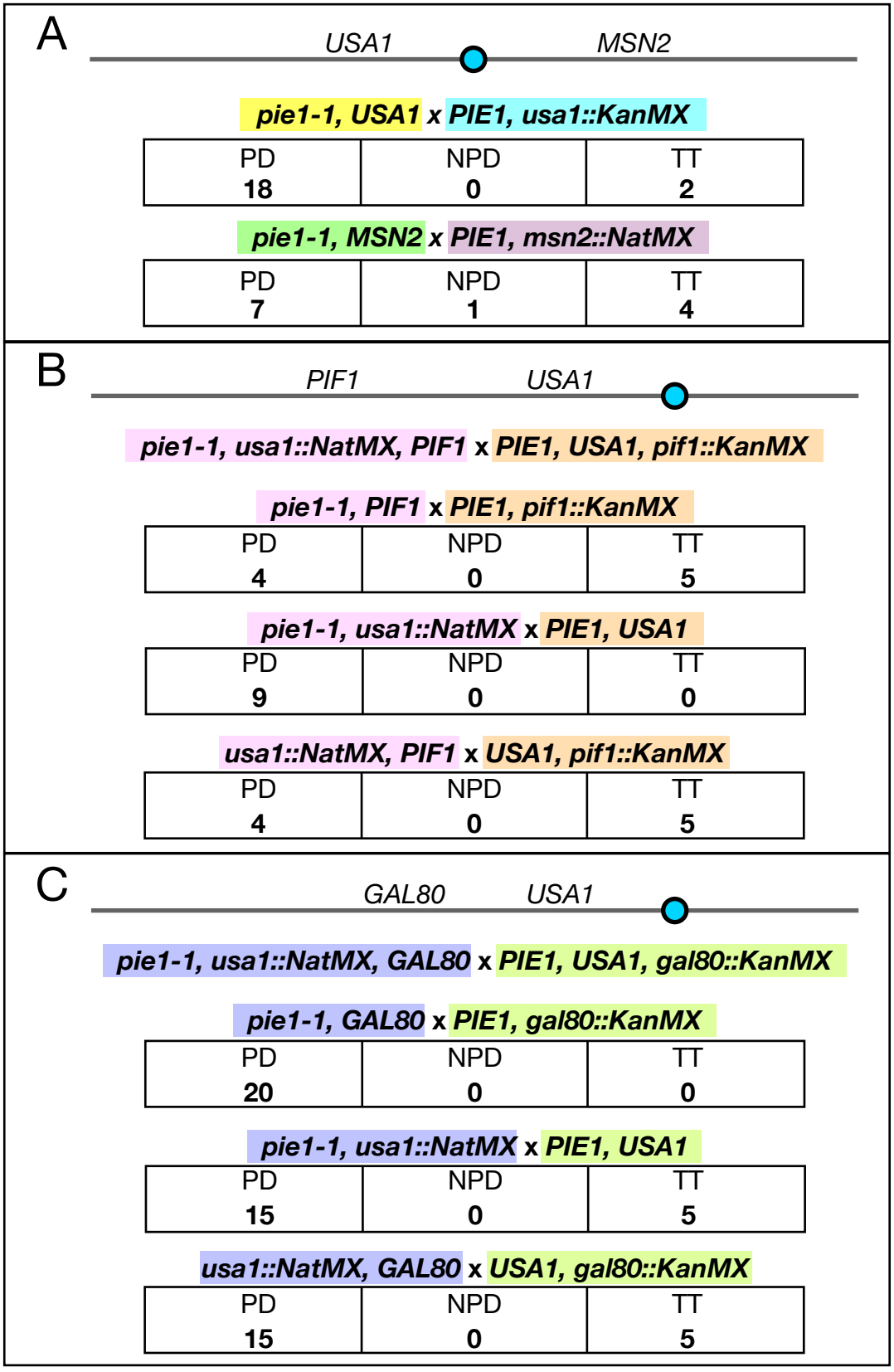
A
USA1
MSN2
pie1-1, USA1 x PIE1, usa1::KanMX
PD 18
NPD 0
TT 2
pie1-1, MSN2 x PIE1, msn2::NatMX
PD 7
NPD 1
TT 4
B
PIF1
USA1
pie1-1, usa1::NatMX, PIF1 x PIE1, USA1, pif1::KanMX
pie1-1, PIF1 x PIE1, pif1::KanMX
PD 4
NPD 0
TT 5
pie1-1, usa1::NatMX x PIE1, USA1
PD 9
NPD 0
TT 0
usa1::NatMX, PIF1 x USA1, pif1::KanMX
PD 4
NPD 0
TT 5
C
GAL80
USA1
pie1-1, usa1::NatMX, GAL80 x PIE1, USA1, gal80::KanMX
pie1-1, GAL80 x PIE1, gal80::KanMX
PD 20
NPD 0
TT 0
pie1-1, usa1::NatMX x PIE1, USA1
PD 15
NPD 0
TT 5
usa1::NatMX, GAL80 x USA1, gal80::KanMX
PD 15
NPD 0
TT 5

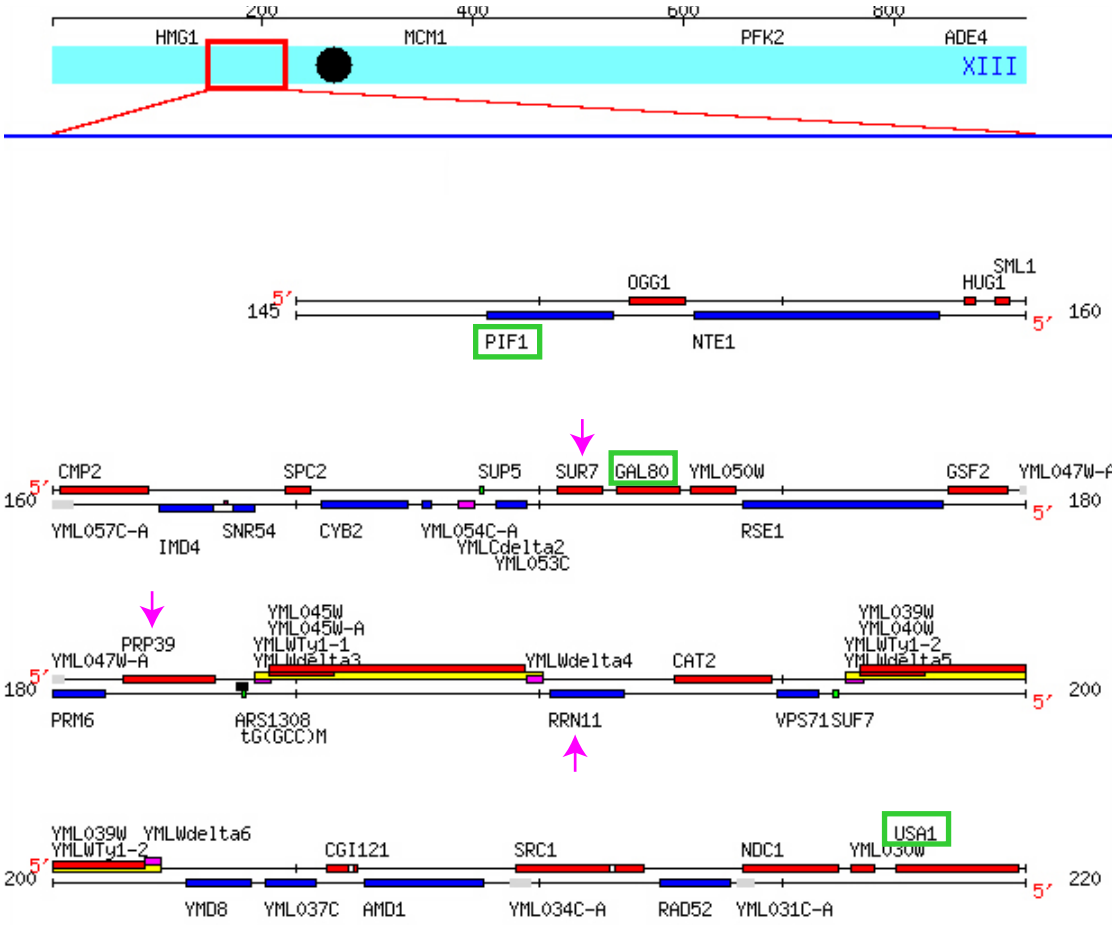

Figure A1.5 Region of chromosome XIII between *PIF1* and *USA1*
Genes used to map *PIE1* are enclosed in green rectangles. Names of ORFs are indicated. Coding regions that read left to right are in red (and yellow), and those that read right to left are blue. Hypothetical ORFs are gray. Genes that I think are likely candidates are indicated with arrows. Adapted from SGD.

My best guesses

Aside from the fact that there are many uncharacterized ORFs in this area, there are a great deal of potentially interesting genes. First, this gene is most certainly not any of the genes identified in the screen in Chapter 2, so regardless of its identity, it will be a new gene implicated in Hmg2p structure formation. I have learned that Psd1p activity decreases as cells become more dense in culture and that changes in phospholipid composition due to Psd1p are difficult, if not impossible to observe above OD_{600} 0.5 when grown in YPD. Because of the growth-phase-dependant Hmg2p^{s}-GFP* localization phenotype of *pie1-1*, I am hopeful that this gene will reveal more about the mechanism in which *PSD1* is involved.

If I were to select 3 genes for win, place and show, then I would select : *PRP39*, *RRN11* and *SUR7*. Both *PRP39* and *RRN11* are essential genes, meaning that they were not analyzed in the haploid deletion collection, so that makes both of them likely candidates. *PRP39* is involved in mRNA splicing and *RRN11* is a protein required for rDNA transcription by RNA polymerase I. Although these are not my favorite genes, I would not be surprised if either of them were *PIE1*. *SUR7* is a gene that affects sporulation and sphingolipid content. Although it is also not in the region that I predict *PIE1* to be located, it is immediately upstream of *GAL80*, making it a strong possibility. If I were to be biased about what gene I want it to be, this would be my choice.

Next steps

If the identification of *PIE1* were to continue, then more tetrads would need to be analyzed to narrow down the region in which *PIE1* was located. Once the region is sufficiently small, crosses could be conducted between the mutant *pie1-1* strain, and the candidate null strains from the haploid null collection, for those genes that are not essential. If none of the non-essential candidates rescue, then the essential genes could be subcloned into an appropriate plasmid and transformed into the *pie1-1* strain to determine if the phenotype can be complemented.

This gene seems to be very interesting and I do hope that someone will take the initiative to determine the identity of *PIE1* and uncover its role in Hmg2p structure formation and membrane proliferation.

Table A1.1: Strains used in Appendix 1. Unless specified otherwise, all genes are expressed from the *TDH3* promoter.

Strain	Genotype	Plasmid
RHY471	*MATα ade2-101, ura3-52, met2, lys2-801, his3Δ200*	none
RHY2701	*MATα, ade2-101, met2, lys2-801, his3Δ200, ura3-52::URA3::Hmg2p^{s}-GFP* K6R*	pRH671
PMY3	*MATα, ade2-101, met2, lys2-801, his3Δ200, ura3-52::URA3::Hmg2p^{s}-GFP* K6R, pie1-1*	pRH671
FOA3	*MATα, ade2-101, met2, lys2-801, his3Δ200, ura3-52, pie1-1*	none
A3 (RHY4640)	*MATα, ade2-101::ADE2::Hmg2p^{s}-GFP* K6R, met2, lys2-801, his3Δ200, ura3-52, pie1-1*	pRH1738
RHY1719	*MATa ade2-101, ura3-52, met2, lys2-801, his3Δ200, trp1::hisG*	none
RHY2977	*MATa ade2-101::ADE2, ura3-52::URA3::Hmg2p^{s}-GFP* K6R, met2, lys2-801, his3Δ200, trp1::hisG*	pRH671 pRH1613
RHY4394	*MATa ade2-101::ADE2::Hmg2p^{s}-GFP* K6R, leu2Δ, ura3-52, met2, lys2-801, his3Δ200, trp1::hisG*	pRH1738
RHY5631	*MATα, ade2-101, met2, lys2-801, his3Δ200, ura3-52::URA3::4xUPRE::GFP, usa1Δ::KanMX*	pRH1209
RHY6634	*MATα, ade2-101, met2, lys2-801, his3Δ200, ura3-52, trp1::hisG, leu2Δ, usa1Δ::KanMX*	none
RHY6651	*MATα, ade2-101, met2, lys2-801, his3Δ200, ura3-52, trp1::hisG, leu2Δ, usa1Δ::NatMX, pie1-1*	none
RHY3460	*MATα, ade2-101, met2, lys2-801, his3Δ200, ura3-52::URA3::HMG1-GFP, msn2Δ::NatMX*	pRH475
Clone509 (RHY6632)	*MATa, ura3Δ0, leu2Δ0, his3Δ1, met15Δ0 pif1Δ::KanMX*	none
Clone520 (RHY6633)	*MATa, ura3Δ0, leu2Δ0, his3Δ1, met15Δ0 gal80Δ::KanMX*	none
B-7588 (RHY5751)	*MATa, met2, ura3-52, trp1-289, leu2,112, cir0, CHR1::URA3*	none
B-7170 (RHY5752)	*MATa, met2, ura3-52, trp1-289, leu2,112, cir0, his3Δ1, CHR2::URA3*	none
B-7589 (RHY5754)	*MATa, met2, ura3-52, trp1-289, leu2,112, cir0, his3Δ1, CHR4::URA3*	none
B-7590 (RHY5755)	*MATa, met2, ura3-52, trp1-289, leu2,112, cir0, his3Δ1, CHR5::URA3*	none

Table A1.1: Strains used in Appendix 1, continued.

Strain	Genotype	Plasmid
B-7591 (RHY5756)	*MATa, met2, ura3-52, trp1-289, leu2,112, cir0, his3Δ1, CHR6::URA3*	none
B-7173 (RHY5757)	*MATa, met2, ura3-52, trp1-289, leu2,112, cir0, his3Δ1, CHR7::URA3*	none
B-7174 (RHY5758)	*MATa, met2, ura3-52, trp1-289, leu2,112, cir0, his3Δ1, CHR8::URA3*	none
B-7175 (RHY5759)	*MATa, met2, ura3-52, trp1-289, leu2,112, cir0, his3Δ1, CHR9::URA3*	none
B-178 (RHY5761)	*MATa, met2, ura3-52, trp1-289, leu2,112, cir0, his3Δ1, CHR11::URA3*	none
B-7595 (RHY5762)	*MATa, met2, ura3-52, trp1-289, leu2,112, cir0, CHR12::URA3*	none
B-7255 (RHY5763)	*MATa, met2, ura3-52, trp1-289, leu2,112, cir0, CHR13::URA3*	none
B-7180 (RHY5765)	*MATa, met2, ura3-52, trp1-289, leu2,112, cir0, his3Δ1, CHR15::URA3*	none

Acknowledgements:

I would like to acknowledge the amazing efforts of Thomas Cunningham and Moncia Rodriguez in conducting the UV screen. That process was very tedious and their contributions are appreciated. Both Thomas Cunningham and Shirine Benhenda worked tirelessly to clone the *pie1-1* gene using various libraries, and conducted some of the crosses in evaluating the *pie1-1* phenotypes. I am indebted to Tricia Laurenson and Lorraine Pillus for all their time and expertise regarding gene mapping. I also would like to thank Jasper Rine for sending us the cir0 mapping strains, and Scott Emr for use of the DeltaVision microscope, and for the *pif1* and *gal80* null strains.

References:

1. Rose MD, Novick P, Thomas JH, Botstein D, Fink GR: **A Saccharomyces cerevisiae genomic plasmid bank based on a centromere-containing shuttle vector**. *Gene* 1987, **60**:237-243.

2. Hirsch HH, Schiffer HH, Muller H, Wolf DH: **Biogenesis of the yeast vacuole (lysosome). Mutation in the active site of the vacuolar serine proteinase yscB abolishes proteolytic maturation of its 73-kDa precursor to the 41.5-kDa pro-enzyme and a newly detected 41-kDa peptide**. *Eur J Biochem* 1992, **203**:641-653.

3. Wakem LP, Sherman F: **Chromosomal assignment of mutations by specific chromosome loss in the yeast Saccharomyces cerevisiae**. *Genetics* 1990, **125**:333-340.

4. Sherman F: **Getting started with yeast**. *Methods Enzymol* 2002, **350**:3-41.